PAN AFRICAN UNIVERSITY

Institute for Basic Sciences, Technology and Innovation

Development of Self-Compacting Translucent Concrete Incorporating Recycled Glass Aggregate for Sustainable Construction

AWETEHAGN TUAUM GEBREMARIAM

A thesis submitted in partial fulfillment of the requirement of the Degree of Master of Science in Civil Engineering (Structural Engineering) in the Pan African University Institute for Basic Sciences, Technology and Innovation

April 2018

Development of Self-Compacting Translucent Concrete Incorporating Recycled Glass Aggregate for Sustainable Construction

AWETEHAGN TUAUM GEBREMARIAM

Master of Science in Civil Engineering

(Structural Engineering)

PAN AFRICAN UNIVERSITY

Institute for Basic Sciences, Technology and Innovation

DECLARATION

This thesis is my original work and has not been presented for a degree or any other award in any other university.

Signature ……...…….. Date ……

Awetehagn Tuaum Gebremariam

This thesis has been submitted for examination with our approval as University Supervisors.

Signature …….…….. Date ……

Eng. Prof. Stanley Muse Shitote

Rongo University, Rongo, Kenya

Signature …….. Date ……....……

Eng. Prof. Walter Odhiambo Oyawa

Commission for University Education, Nairobi, Kenya

DEDICATION

I dedicate this thesis to Almighty God for his love and protection. I also dedicate my thesis to my beloved parents, Tuaum Gebremariam Teklu and Meazu Tesfay Gebreyesus, and my loving grandfather's Tesfay Gebreyesus and Abrihet Tessema for their kindness and endless support.

Awetehagn Tuaum Gebremariam

ACKNOWLEDGEMENT

First and foremost I wish to thank the Almighty God for giving me the opportunity and strength to carry out this work. I am greatly indebted to my supervisors Eng. Prof. Stanley Muse Shitote and Eng. Prof. Walter Odhiambo Oyawa for their guidance, advice, direction, support and constructive criticisms throughout the thesis work. I also render my sincere thanks to my beloved family and friends for their continuing encouragement, love, and support.

My profound gratitude and deep regards also goes to African Union Commission (AUC) and Japan International Cooperation Agency (JICA) for funding this research through Africa-ai-Japan Project (African Union -*african innovation* - JKUAT and PAUSTI Network Project).

Finally, I would like to thank the materials laboratory, transportation laboratory, soil laboratory and electrical laboratory technicians of the Jomo Kenyatta University of Agriculture and Technology (JKUAT) for their immense support and logistic facilitations.

PUBLICATIONS RESULTING FROM THIS RESEARCH

Tuaum, A., Shitote, S. and Oyawa, W. (2018). Experimental Study of Self-Compacting Mortar Incorporating Recycled Glass Aggregate. *Buildings*, vol. 8 (2), MDPI, Basel, Switzerland. DOI:10.3390/buildings8020015.

Tuaum, A., Shitote, S. and Oyawa, W. (2018). Experimental Evaluation on Light Transmittance Performance of Translucent Concrete. *International Journal of Applied Engineering Research*, vol. 13 (2), Research India Publications, India. pp. 1209-1218.

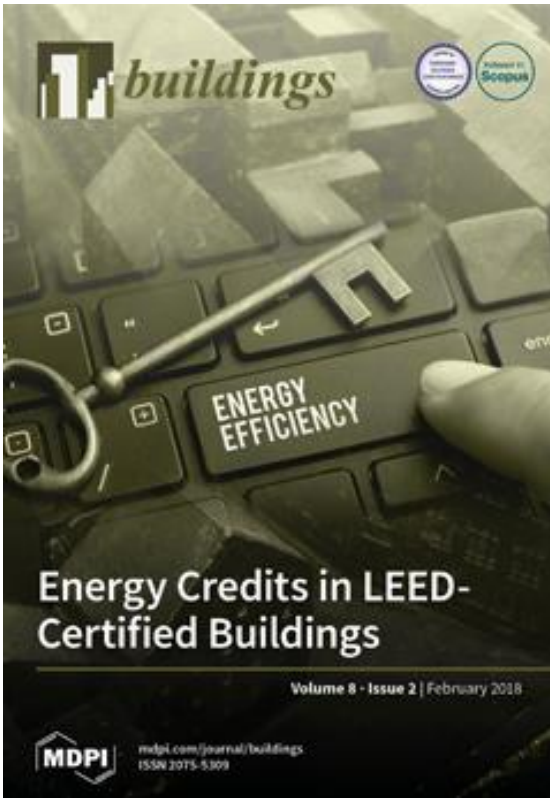

ABSTRACT

Worldwide, artificial lighting consumes around 19% of the total delivered electricity. The electric lighting demand has constantly been increasing with the increase in the population, urbanization, and construction of high-rise buildings. The production of electricity contributes to the increase in the greenhouse gas emissions. Translucent concrete is an innovative solution towards significantly reducing the need for artificial lighting by allowing transmission of natural light into building's interior environment when the translucent concrete is used as structural façades and architectural walls. The overall objective of this research was developing translucent concrete incorporating recycled glass aggregate as substitution of natural fine aggregate using self-compacting mortar (SCM). The use of recycled glass aggregate (RGA) in SCM aims to reverse the adverse environmental effects of waste glass, conserve natural resources and as a viable solution towards sustainable solid waste disposal and management.

Limestone powder (LP) was used as filler that constitutes 20% – 30% of the powder volume to reduce the amount of cement. The SCM mixes were designed and evaluated based on Japanese mix design method and EFNARC, respectively. The light transmittance performance of plastic optical fiber (POF) based translucent concrete was evaluated using an electrical circuit test setup with a light dependent resistor (LDR). Structural performance of translucent concrete panels/ façades was also examined to assess ductility and failure mechanism under flexural loading.

The experimental test results showed that the slump flow of SCM mixes decreased and V-funnel flow time increased when the content of recycled glass aggregate (RGA) increased. The bulk density, compressive strength, flexural strength, water absorption and sorptivity of SCM mixes were decreased as RGA content increased. Moreover, the accelerated mortar bar test results showed that the expansion due to alkali-silica reaction (ASR) of SCM mixes increased as the content of RGA increased although the expansion of all mixes was within the acceptable limit and potentially innocuous. The bulk density of translucent concrete was found to decrease marginally with increases the volume ratio of plastic optical fibers (POF). It was also clearly observed that all the translucent concrete specimens exhibited compressive and flexural strength of lower than the reference concrete. On average, the 28 days compressive and flexural strength was 8% – 24% lower for the translucent concrete than for the reference concrete. The light transmittance test showed that the light transmittance performance of the translucent concrete significantly depends on the percentage volume of optical fibers incorporated. The inclusion of POF improves the ductility and flexural toughness of concrete panels. The flexural toughness and toughness factor were 11% – 22% higher in translucent concrete panels than in the reference concrete panel.

Generally, at replacement ratio up to 30%, recycled glass aggregate is viable for production of SCM and translucent concrete with good workability, sufficient strength, and durability. The translucent concrete panels/ façade developed in this study are apt for application in load bearing and non-load bearing architectural walls of green buildings, underground stations, in structural walls of banks, prisons, and museums to increase security and supervision as well as safety.

Keywords: recycled glass aggregate, self-compacting mortar, translucent concrete, light transmittance, sustainable construction, energy, solid waste management.

ABSTRAIT

Dans le monde entier, l'éclairage artificiel consomme environ 19% de l'électricité totale livrée. La demande d'éclairage électrique a constamment augmenté avec l'augmentation de la population, l'urbanisation et la construction de bâtiments de grande hauteur. La production d'électricité contribue à l'augmentation des émissions de gaz à effet de serre. Le béton translucide est une solution innovante permettant de réduire considérablement le besoin d'éclairage artificiel en permettant la transmission de la lumière naturelle dans l'environnement intérieur du bâtiment lorsque le béton translucide est utilisé comme façades structurelles et murs architecturaux. L'objectif global de cette recherche était de développer du béton translucide en incorporant des granulats de verre recyclés en remplacement des granulats fins naturels à l'aide d'un mortier auto-compactant (SCM). L'utilisation d'agrégats de verre recyclé (RGA) dans SCM vise à inverser les effets environnementaux négatifs des déchets de verre, conserver les ressources naturelles et comme une solution viable pour l'élimination et la gestion durable des déchets solides.

La poudre de calcaire (LP) a été utilisée comme charge qui constitue 20% - 30% du volume de poudre pour réduire la quantité de ciment. Les mélanges SCM ont été conçus et évalués sur la base de la méthode de mélange japonaise et de l'EFNARC, respectivement. Les performances de transmission de la lumière du béton translucide à base de fibre optique plastique (POF) ont été évaluées en utilisant une configuration de test de circuit électrique avec une résistance dépendant de la lumière (LDR). La performance structurelle des panneaux/ façades en béton translucide a également été examinée pour évaluer le mécanisme de ductilité et de rupture sous charge de flexion.

Les résultats des essais expérimentaux ont montré que le flux d'affaissement des mélanges de SCM diminuait et que le temps d'écoulement de l'entonnoir en V augmentait lorsque la teneur en agrégat de verre recyclé (RGA) augmentait. La densité apparente, la résistance à la compression, la résistance à la flexion, l'absorption d'eau et la sorptivité des mélanges SCM ont diminué à mesure que la teneur en RGA augmentait. De plus, les résultats des tests accélérés de mortier montrent que l'expansion due à la réaction alcali-silice (ASR) des mélanges SCM augmente à mesure que la teneur en RGA augmente, bien que l'expansion de tous les mélanges soit dans la limite acceptable et potentiellement inoffensive. La densité apparente du béton translucide a diminué de façon marginale avec l'augmentation du rapport volumique des fibres optiques plastiques (POF). Il a également été clairement observé que tous les échantillons de béton translucide présentaient une résistance à la compression et à la flexion inférieure au béton de référence. En moyenne, la résistance à la compression et à la flexion de 28 jours était inférieure de 8% à 24% pour le béton translucide par rapport au béton de référence. L'essai de transmission de la lumière a montré que les performances de transmission de la lumière du béton translucide dépendent de manière significative du pourcentage de volume des fibres optiques incorporées. L'inclusion de POF améliore la ductilité et la ténacité à la flexion des panneaux de béton. Le coefficient de ténacité et de ténacité à la flexion était de 11% à 22% plus élevé dans les panneaux de béton translucide que dans le panneau de béton de référence.

Généralement, au taux de remplacement jusqu'à 30%, l'agrégat de verre recyclé est viable pour la production de SCM et de béton translucide avec une bonne ouvrabilité, une résistance suffisante et une durabilité. Les panneaux/ façades en béton translucide développés dans cette étude peuvent être utilisés dans les murs porteurs et non porteurs des bâtiments verts, des stations de métro, des murs structurels des banques, des prisons et des musées pour augmenter la sécurité et la sécurité.

Mots-clés: agrégat de verre recyclé, mortier auto-compactant, béton translucide, transmittance de la lumière, construction durable, énergie, gestion des déchets solides.

TABLE OF CONTENTS

DECLARATION i
DEDICATION ii
ACKNOWLEDGEMENT iii
PUBLICATIONS RESULTING FROM THIS RESEARCH iv
ABSTRACT v
ABSTRAIT vi
TABLE OF CONTENTS vii
LIST OF TABLES xi
LIST OF FIGURES xii
LIST OF ABBREVIATIONS AND ACRONYMS xv
CHAPTER ONE 1
INTRODUCTION 1
1.1 Background to the study 1
1.2 Statement of the Problem 6
1.3 Objectives 8
1.3.1 Main Objective 8
1.3.2 Specific Objectives 8
1.4 Justification of the study 9
1.5 Scope and Limitations of the study 10
1.5.1 Scope of the study 10
1.5.2 Limitations of the study 11
1.6 Thesis Layout 11
CHAPTER TWO 13
LITERATURE REVIEW 13
2.1 Self-Compacting Mortar/Concrete 13
2.1.1 Mix Design Methods of Self-compacting Mortar/Concrete 13
2.1.1.1 Japanese Mix Design Method (General purpose mix design method) 13
2.1.1.2 CBI mix design method 14
2.1.1.3 LCPC mix design method 14
2.1.2 Principles to achieve Self-compactibility 15
2.1.2.1 Using superplasticizer 15
2.1.2.2 High paste volume 15
2.1.2.3 Limiting aggregate content 16
2.1.2.4 Using viscosity modifying agents (VMA) 16

2.1.3 Guidelines for Self-compacting Mortar/Concrete 16
2.1.3.1 Japanese SCC Guideline 17
2.1.3.2 European SCC Guideline 17
2.1.4 Properties of Self-compacting Mortar/Concrete 18
2.1.4.1 Fresh Properties of Self-compacting Mortar/Concrete 18
2.1.4.2 Hardened properties of self-compacting concrete 19
2.1.4.3 Durability of self-compacting concrete 19
2.1.5 Effect of Recycled Glass Aggregate on Self-Compacting Concrete/Mortar 20
2.1.6 The Influence of Chemical and Mineral Admixtures on Concrete 24
2.1.7 Advantages and Disadvantages of Self-compacting Mortar/Concrete 26
2.1.8 Application of Self-compacting Mortar/Concrete 27
2.2 Translucent Concrete 28
2.2.1 Mechanical Properties of Translucent Concrete 28
2.2.2 Light Transmittance Performance of Translucent Concrete 31
2.2.3 Advantage and Disadvantages of Translucent Concrete 32
2.2.4 Application of Translucent Concrete 33
2.3 Summary of Literature Review 33
2.4 Conceptual Framework 35
CHAPTER THREE 36
MATERIALS AND METHODS 36
3.1 Introduction 36
3.2 Characterization of constituent materials 38
3.2.1 Cement 38
3.2.2 Limestone Powder 39
3.2.3 Fine Aggregate 40
3.2.4 Recycled Glass 42
3.2.5 Plastic Optical Fiber 43
3.2.6 Water 44
3.2.7 Superplasticizer 44
3.3 Equipment 45
3.4 Experimental Program 46
3.5 Mix Designs 48
3.5.1 Mix Formulation 48
3.5.2 Mix Proportioning 50
3.6 Mixing Procedure 51
3.7 Experimental Methods for SCM-RGA 52

3.7.1 Tests on Fresh SCM-RGA mixes 52
3.7.1.1 Slump Flow Test 53
3.7.1.2 V-funnel Flow Time Test 53
3.7.2 Tests on Hardened SCM-RGA mixes 54
3.7.2.1 Flexural Strength 54
3.7.2.2 Compressive Strength 55
3.7.2.3 Water Absorption by Immersion 56
3.7.3 Tests on Durability of SCM-RGA mixes 57
3.7.3.1 Sorptivity 57
3.7.3.2 Expansion due to Alkali-Silica-Reaction (ASR) 58
3.8 Experimental Methods for Translucent Concrete 59
3.8.1 Fabrication Process and Preparation of Translucent Concrete 59
3.8.2 Tests to Investigate Mechanical Properties of Translucent Concrete 62
3.8.2.1 Compressive Strength 62
3.8.2.2 Flexural Strength 63
3.8.3 Light Transmittance Test on Translucent Concrete 64
3.8.4 Tests on Structural Performance of Translucent Concrete Façade Panels 67
3.8.4.1 Fabrication Process of Translucent Concrete Façade Panels 67
3.8.4.2 Test Setup and Instrumentation of Translucent Concrete Façade Panels 69
3.8.4.3 Flexural Toughness of the Translucent Concrete Façade Panels 72
3.8.4.4 Load Analysis of the Translucent Concrete Façade Panels 73
CHAPTER FOUR 76
RESULTS AND DISCUSSION 76
4.1 Fresh, Hardened and Durability Properties of SCM-RGA Mixes 76
4.1.1 Fresh Properties of SCM-RGA Mixes 76
4.1.1.1 Slump Flow 76
4.1.1.2 V-Funnel Flow Time 79
4.1.2 Hardened Properties of SCM-RGA Mixes 82
4.1.2.1 Bulk Density 82
4.1.2.2 Compressive Strength 83
4.1.2.3 Flexural Strength 85
4.1.2.4 Water Absorption 87
4.1.3 Durability Properties of SCM-RGA Mixes 88
4.1.3.1 Sorptivity 88
4.1.3.2 Expansion due to Alkali-Silica Reaction (ASR) 91
4.2 Mechanical Properties of Translucent Concrete 94

4.2.1 Bulk Density 94
4.2.2 Compressive Strength 96
4.2.3 Flexural Strength 98
4.3 Light Transmittance Performance of Translucent Concrete 100
4.3.1 Light Transmittance Analysis of Translucent Concrete 100
4.3.2 Light Transmittance Analysis at varying distances of Light Source 106
4.3.3 Light Transmittance Analysis at varying distances of LDR 108
4.4 Structural Performance of the Translucent Concrete Façade Panels 112
4.4.1 Flexural Toughness of the Translucent Concrete Façade Panels 112
4.4.2 Experimental Load Analysis of the Translucent Concrete Façade Panels 115
CHAPTER FIVE 119
CONCLUSION AND RECOMMENDATION 119
5.1 Conclusion 119
5.1.1 Fresh, Hardened and Durability Properties of SCM-RGA Mixes 119
5.1.2 Mechanical Properties of Translucent Concrete 120
5.1.3 Light Transmittance Performance of Translucent Concrete 121
5.1.4 Structural Performance of Translucent Concrete Panels 122
5.2 Recommendation 123
5.2.1 Recommendation for Application Area 123
5.2.2 Recommendation for Future Work 124
REFERENCES 125
APPENDICES 132

LIST OF TABLES

Table 3.1 Chemical composition of the ordinary Portland cement Type-I 42.5 N 38
Table 3.2 Physical properties of the ordinary Portland cement Type-I 42.5 N 39
Table 3.3 Chemical composition of the limestone powder 40
Table 3.4 Physical properties of the limestone powder 40
Table 3.5 Chemical composition of the fine aggregate 41
Table 3.6 Physical properties of the fine aggregate 41
Table 3.7 Chemical composition of the recycled glass aggregate 42
Table 3.8 Physical properties of the recycled glass aggregate 42
Table 3.9 Specification of the plastic optical fiber (POF) 44
Table 3.10 Properties of Sika ViscoCrete-3088 superplasticizer 45
Table 3.11 Mix design proportioning of SCM-RGA mixes 50
Table 3.12 Mix design proportioning of SCM-RGA20% mixture for production of translucent concrete (TC-RGA20%) 51
Table 3.13 Code and sample number of the mix design 51
Table 3.14 Details of POF integrated on translucent concrete specimens for the compressive strength test. 63
Table 3.15 Details of POF integrated on translucent concrete specimens for the flexural strength test. 64
Table 3.16 Number of POF integrated into to the cubic specimens for light transmittance test (50x50x50 mm^3 specimen dimension). 66
Table 3.17 Details of POF integrated on translucent concrete panels 68
Table 4.1 Fresh properties of SCM-RGA mixes 76
Table 4.2 Compressive strength of SCM-RGA mixes 84
Table 4.3 Flexural strength of SCM-RGA mixes 85
Table 4.4 Sorptivity and ASR expansion of SCM-RGA mixes 88
Table 4.5 Mechanical properties of translucent concrete 94
Table 4.6 Flexural toughness parameters of translucent and reference concrete panels 114
Table 4.7 Details of experimental load analysis results of the translucent and reference concrete panels 116

LIST OF FIGURES

Figure 2.1 Conceptual framework..... 35
Figure 3.1 Particle size distribution of limestone powder (LP) 39
Figure 3.2 Particle size distribution of fine aggregate 41
Figure 3.3 Particle size distribution of recycled glass aggregate 43
Figure 3.4 Recycled Glass 43
Figure 3.5 Experimental program 47
Figure 3.6 Mixing procedure..... 52
Figure 3.7 Standard mortar mixer 52
Figure 3.8 Mini-slump cone..... 53
Figure 3.9 Mini V-funnel 54
Figure 3.10 Flexural strength test apparatus 55
Figure 3.11 Compressive strength test machine..... 56
Figure 3.12 Sorptivity test..... 58
Figure 3.13 Plastic optical fibers..... 59
Figure 3.14 Fixing and inserting of plastic optical fibers through low-density polyethylene (LDPE) sheets 60
Figure 3.15 Cubic molds for compressive strength and light transmittance tests 60
Figure 3.16 Prism molds for the flexural strength test..... 61
Figure 3.17 Concrete casting of translucent concrete specimens..... 61
Figure 3.18 Compressive strength test on translucent concrete 62
Figure 3.19 Translucent concrete specimens for flexural strength test..... 63
Figure 3.20 Schematic diagram of circuit setup for light transmittance test..... 65
Figure 3.21 Experimental setup and arrangement of light transmittance test 65
Figure 3.22 Illumination of the translucent concrete 66
Figure 3.23 The overall arrangement of light transmittance test 67
Figure 3.24 Pre-cast translucent concrete panel specimens 68
Figure 3.25 Pre-cast translucent concrete panel dimensions..... 69
Figure 3.26 Setup detail for structural performance of translucent concrete panel 69
Figure 3.27 Experimental test setup arrangement of structural performance of translucent concrete panel 70
Figure 3.28 Structural performance of translucent concrete panel 71
Figure 3.29 JSCE-SF4 flexural toughness and toughness factor definition..... 72
Figure 3.30 Normal stress profile of the structural panel/façade 74
Figure 3.31 Shear stress profile of the structural panel/façade 75

Figure 4.1 Relative slump flow of SCM-RGA mixes 77
Figure 4.2 Relationship between RGA content and superplasticizer dosage 78
Figure 4.3 Typical slump flow of SCM-RGA mixes 79
Figure 4.4 Relative flow velocity of SCM-RGA mixes 81
Figure 4.5 Relationship between RGA content and the flow time of SCM-RGA mixes 81
Figure 4.6 Paste design (Determination of retained water ratio, β_p) 81
Figure 4.7 Bulk density of hardened SCM-RGA mixes 82
Figure 4.8 Compressive strength development of SCM-RGA mixes 84
Figure 4.9 Relationship between RGA content and corresponding 28 days of compressive strength 84
Figure 4.10 Flexural strength development of SCM-RGA mixes 86
Figure 4.11 Relationship between RGA and corresponding 28 days flexural strength 86
Figure 4.13 Water absorption of SCM-RGA mixes 87
Figure 4.15 Evolution of cumulative capillary surface water absorption of SCM-RGA mixes 90
Figure 4.16 Relationship between the sorptivity value, and the 28 days compressive and flexural strength 91
Figure 4.17 ASR expansion of SCM-RGA mixes 92
Figure 4.18 ASR expansion as a function of RGA content 92
Figure 4.19 Weight change of SCM-RGA mixes after 14 days of curing in 1N NaOH solution at 80 ºC temperature 93
Figure 4.20 Bulk density of the translucent concrete at 7 days and 28 days of age 95
Figure 4.21 Relationship between POF volume ratio and 28 days bulk density of the translucent concrete 95
Figure 4.22 Compressive strength of the translucent concrete at 7 days and 28 days 97
Figure 4.23 Relationship between POF volume and 28 days compressive strength 97
Figure 4.24 Flexural strength of the translucent concrete at 7 days and 28 days 99
Figure 4.25 Relationship between POF volume ratio and 28 days flexural strength of translucent concrete 99
Figure 4.26 Light transmittance of translucent concrete 102
Figure 4.27 Light transmittance of translucent concrete 104
Figure 4.28 Effect of POF spacing on light transmittance of translucent concrete 105
Figure 4.29 Effect of number of POF on light transmittance of translucent concrete 106
Figure 4.30 Relationship between light transmittance and light source distance 107
Figure 4.31 Relationship between light transmittance and light source distance 108
Figure 4.32 Relationship between light transmittance and LDR distance 110

Figure 4.33 Relationship between light transmittance and LDR distance 111
Figure 4.34 Load-deflection (P-δ) graph of the translucent concrete panels and the reference concrete panel 113
Figure 4.35 Flexural toughness of the reference and the translucent concrete panels 115
Figure 4.36 Flexural toughness factor of the reference and translucent concrete panels/façades 115
Figure 4.37 Bending stress-strain curve 116
Figure 4.38 Normal stress-strain curve 117
Figure 4.39 Shear stress-strain curve 117

LIST OF ABBREVIATIONS AND ACRONYMS

AS/ NZS	Australian/ New Zealand Standard
ASR	Alkali-Silica Reaction
^oC	Celsius
$CaCO_3$	Calcium Carbonate
CO_2	Carbon Dioxide
dB/km	Decibel per kilometer
d_m	Average slump flow diameter
E_c	Elasticity Modulus
EFNARC	European Federation of National Associations Representing for Concrete
I	Moment of Inertia
LCPC	Laboratoire Central des Ponts et Chaussèes
LDPE	Low-density Polyethylene
LDR	Light Dependent Resistor
LP	Limestone Powder
LTC	Light Transmitting Concrete
LUX	Luminance
LVDT	Linear Variable Differential Transformer
m/sec^2	meter per second (Acceleration)
NaOH	Sodium Hydroxide
N/mm^2	Newton per millimeter square
N/sec	Newton per second
P-δ	Load- Deflection
PMMA	Poly Methyl MethAcrylate
POF	Plastic Optical Fiber
R^2	Reliability
RGA	Recycled Glass Aggregate

SCC	Self-Compacting Concrete
SCM	Self-Compacting Mortar
SCTC-RGA	Self-Compacting Translucent Concrete incorporating Recycled Glass Aggregate
T_b	Absolute Flexural Toughness
TC	Translucent Concrete
V	Voltage
VMA	Viscosity Modifying Agent
VSI	Visual Stability Index
W	Watt
XRD	X-ray Diffraction
τ_{stress}	Shear Stress
$\sigma_{bending}$	Bending Stress
σ_b	Flexural Toughness Factor
Γ_m	Relative slump flow
R_m	Relative flow velocity
β_p	Retained water ratio
Ø	Diameter
Ω	Ohm

CHAPTER ONE

INTRODUCTION

1.1 Background to the study

Sustainable construction is becoming a major concern and emerging issue in the construction industry, worldwide. Developing sustainable construction minimizes the depletion of raw materials and energy, and plays a significant role in protecting the environment. It also promotes the practice and design of structures in an eco-friendly manner (Nunes et al., 2013). Concrete is the most crucial and extensively used construction material in the construction industry. The density and opaque nature of concrete ingredients hinders the transmission of light and consequently results in opaqueness of the material. However, concrete could be transformed from opaque to translucent by integrating optical fibers with a concrete matrix. Translucent concrete is a new energy-saving building material that permits transmission of light into the indoor environment through the embedded optical fibers. Besides light transmittance, translucent concrete is able to show the silhouettes of any proximal objects situated on the brighter side of the wall, thereby, it can also be used for application in the architecture of prison, bank and museum to ensure safety, supervision, and security (Azambuja & Castro, 2015).

Natural light is a form of energy reflected as an electromagnetic wave that contains the full spectrum of the sunlight, which is healthy for human beings and a preference than artificial light (Philips Lighting Academy, 2008). Indoor environments with adequate natural light illumination have been proven to decrease the stress of occupant, improve visual comfort and render better employee retention (Long, 2015). It is then essential to develop a new type of construction material, which can allow transmittance of the

appropriate luminance level of natural light into buildings and integrate the concept of green energy saving (Al-Kurdi, Abdel-Aziz, & Alshboul, 2014).

Hungarian architect Áron Losonczi introduced the first concept of translucent concrete (light transmitting concrete) in 2001, and the first prototype of the translucent concrete panel was successfully developed in 2003 (Monica, 2013). Translucent concrete can be produced in an even distribution and parallel spatial pattern arrangement of plastic optical fibers embedded with a concrete matrix. The light transmittance properties rely on the volume ratio and numerical aperture of optical fibers incorporated. Plastic optical fiber (POF) is an optical fiber made of polymethyl methacrylate (PMMA) core and fluororesin cladding materials with more than 96% of the cross-section able to transmit light effectively. The structural components of optical fiber consist of three layers: core, cladding and buffer coating. However, fibers used in translucent concrete should not have buffer coating to reinforce the interfacial bondage between the concrete matrix and fiber surface. The refractive index profile of POF core can be step-index or graded-index depending on the mode of total internal reflection, while the cladding index is uniform to keep the propagation of the discrete path of light rays within the core (Fischer, Haupt & Joncic, 2011; Koike & Asai, 2009; Thorat, Warulkar, & Thombre, 2014). The mechanism of light transmittance through optical fibers is free of light-heat, photochemical and photoelastic effects.

Cement based translucent concrete is a combination of conventional concrete components such as cement, fine aggregate and water, and around 2% - 6% of optical fiber by percentage of the total specimen volume. Load bearing and non-load bearing translucent concrete panels or façades should fulfill the strength, serviceability and durability requirements to withstand expected ultimate loads with permissible

deflection (Tutikian & Marquetto, 2015). Furthermore, the light transmittance performance should be enough to meet the minimum illuminance level for the optical activity of people in indoor environments and comply with standards such as the Australian/New Zealand Standard (Australian/ New Zealand Standard, 2008). The intensity of light is usually measured using instruments such as light meter, optical power meter, lux meter and luminous photometer. The light can also be measured using electrical circuit set-up with a light dependent resistor in a laboratory.

Solid waste management is one of the major challenges of our present society to protect the environment. Solid wastes such as glass, plastic and rubber tire which are non-degradable contribute to environmental pollution and result in the unhealthy living area. The growing environmental concern focuses on the environmental protection, solid waste disposal, safeguarding of natural resources and recycling of waste materials. The increasing scarcity of landfills, rapidly depleting sources of virgin aggregate, growing landfill costs are also the driving forces promoting the recycling of waste materials as components in new concrete (Koh, 2014).

Consumption of natural aggregate as the largest constituent of concrete is constantly and rapidly increasing with the increase in utilization of concrete in the construction industry. Waste materials are a valuable resource as a replacement for virgin aggregate in concrete. Utilization of solid wastes in concrete is one way to solve solid waste disposal, safeguarding of the ecology and also an approach to optimize the cost of concrete production.

Production of concrete in conventional vibration method poses several environmental, health and technical problems. Vibration noise generally has an intensity greater than 93dB which can cause a potential deafness, fatigue, and stress, and compaction with

more than 0.25 m/sec^2 acceleration causes stiffness in limbs, pain in back and neck. Poke vibrator which is a commonly used equipment in construction to compact concrete have an acceleration greater than 0.75 m/sec^2 that can cause a serious problem called ‘‘white finger’’ (blood circulation problem) to the vibrator operator (Walraven, 2003). The noise pollution due to vibration adversely affects the working environment, and the life quality and health of nearby residents. Furthermore, placement and casting operations of concrete in a congested area and complex architectural forms in a conventional way is difficult. It is then imperative to address such problems by modifying or enhancing the production and operation techniques of concreting.

Self-compacting mortar (SCM) is an integral part of self-compacting concrete (SCC) and is principally used in structural retrofitting, rehabilitation and repair of structures, grouting, and production of light transmitting concrete. According to EFNARC (2002) self-compacting concrete (SCC) is “concrete that is able to flow under its own weight and completely fill the formwork, even in the presence of dense reinforcement, without the need of any vibration, whilst maintaining homogeneity”. SCC is an emerging advanced concrete technology that offers overall technical, health and environmental advantages over conventional concrete. SCC was first developed at the University of Tokyo by Prof. Okamura in 1988 to enhance concrete durability and avoid workmanship defects during concreting operation (Okamura & Ozawa, 1996). Moreover, the first SCC mix design method was advocated by Japanese Okamura & Ozawa (1995) and it is also known as Japanese mix design method. The mix design of SCC is highly dependent on the applied material properties, and extensive researches have been carried out in different countries considering various circumstances (Midorikawa, Pelova, & Walraven, 2009). In Africa, particularly East Africa the

practice of SCC is in infant stage at this time, and this might be due to the absence of guidelines or standards that support the design, production, and application of SCC in the region. The present study aims to develop SCM mixes based on locally available materials to boost and support the design and manufacturing of SCC in East Africa.

The workability of fresh SCC basically depends on the fundamental engineering properties of fresh SCM (Karataş, Benli, & Ergin, 2017). In fact, the design of SCC is trial and error that requires plenty of time and effort. However, the design of SCM requires relatively less time and cost and helps to achieve a target SCC easily. It is then prominent to study and proportion SCM to minimize SCC phase trials (Mohseni et al., 2015). Generally, SCC or SCM requires higher cement content than conventional concrete to achieve self-consolidation. Mineral admixtures such as limestone powder (LP) are introduced as fillers to reduce the amount of cement and heat of hydration, enhance flowability and durability, and retard or accelerate the time of setting. In addition, superplasticizer (S_P) is used to lower yield stress and increase segregation resistance of SCM or SCC (Okamura & Ouchi, 2003; Rizwan & Bier, 2012).

Mechanical vibration of translucent concrete is very difficult due to the presence of embedded optical fibers that can be severely damaged, the tilt of orientation and losses of patterns. As a conventional practice, the vibration of translucent concrete is usually executed by shaking machine to achieve a certain degree of compaction. In this study, the self-compacting mortar was developed using locally available materials as a mitigation measure towards the production of translucent concrete without the need for external mechanical vibration. Self-compacting mortar has the ability to pass through congested optical fibers and filling ability under its own weight guaranteeing coverage of fibers.

Self-compacting translucent concrete incorporating recycled glass aggregate (SCTC-RGA) is a new composite construction material that contains cement, limestone powder, fine aggregate, recycled glass aggregate, plastic optical fiber, water and superplasticizer as ingredients, which possesses the fresh properties of the self-compacting mortar (SCM) and the hardened properties of the translucent concrete (TC) with an ability to transmit light. SCTC-RGA is categorized under fiber reinforced concrete since it is reinforced with optical fibers principally as a medium of light transmittance.

1.2 Statement of the Problem

Energy conservation is a key and emerging global issue for sustainable infrastructure development. The building sector energy demand accounts approximately 34% of the world's energy demand (Johansson et al., 2012). Artificial lighting consumes around 19% of the total delivered electricity worldwide (Phillips, 2015). The electric lighting demand has constantly been increasing with the increase in the population, urbanization, and construction of high-rise buildings. The production of electricity contributes to the increase in the greenhouse gas emissions. According to Energy Information Administration (2007) report, the total CO_2 emission related to lighting was approximately 7% of the total global CO_2 emission in 2005. A lot of efforts have been made to reduce the energy consumption of lighting by fabrication of energy efficient lighting equipment, improving lighting design and using lighting control systems. Translucent concrete is an innovative solution towards significantly reducing the need for artificial lighting. This, in turn, reduces carbon footprint by allowing transmission of natural light into building interior when the translucent concrete is

used as structural façades and architectural walls, thus fostering the development of green buildings and sustainable construction.

Sustainable waste management, especially for non-degradable solid wastes such as glass, is one of the major challenges that face developing countries. Due to rapid population growth, urbanization and paramount economic growth, the rate of waste generation in aforementioned countries is increasing rapidly and consequently poses serious health and environmental problems. Fortunately, there are mitigation measures commonly employed in solid waste disposal; recycling, landfilling and incinerating. However, recycling of solid wastes for new material manufacturing in developing countries is not a viable solution because it is capital intensive. Landfilling and incinerating are not eco-friendly solutions. Therefore, there is a need for a reliable and cost-effective method to curb this menace. Concrete is worthy considered as a host of solid wastes and industrial by-products, thus, recycling of solid wastes in concrete production is then a prevailing and feasible option towards sustainable solid waste management and infrastructure development (Topçu & Canbaz, 2004).

The construction industry is growing rapidly, leading to high consumption of concrete. Concrete is a primary consumer of natural resources as more than 70% of the volume consists of aggregates. In developing countries, particularly Africa, the aggregates are acquired by extensive extraction of natural rocks and rivers which adversely affects the ecology of riparian habitats, forested areas, riverbeds and land use (Langer, Drew, & Sachs, 2004). Hence, utilization of wastes and industrial by-products as substitution of aggregates in concrete or mortar is a fascinating and viable option to secure natural resources and environmental conservation (Sharifi, Afshoon, & Firoozjaie, 2015).

Worldwide, discarded and post-consumer waste glass is becoming a substantial burden in stockpiles and landfills (Corinaldesi, Nardinocchi, & Donnini, 2016). According to Chandak (2010) report, globally 2% of the solid waste composition is waste glass in low-income and middle-income countries, and 7% in high-income countries. In Nairobi city, it has been estimated that about 22,630 tons of waste glass are generated each year (Kasozi & Harro, 2010). Even though glass is recyclable, that can be reused for new glass production, the high cost of recycling and a limited number of glass industries in Africa impede the recycling of waste glass. These are also the driving forces promoting the recycling of waste glass as components in the production of mortar or concrete (Nunes et al., 2013).

There is no scientific work on the design, construction, and application of translucent concrete in East Africa as well as Africa. This research intends also to gain insight into the development of translucent concrete using locally available materials which have gained a lot of momentum in recent years in the sustainable construction and building efficiency issues, worldwide.

1.3 Objectives

1.3.1 Main Objective

The main objective of this study is to develop self-compacting translucent concrete incorporating recycled glass aggregate for sustainable construction.

1.3.2 Specific Objectives

1. To explore the viability and investigate the effect of incorporating recycled glass aggregate as replacement of natural fine aggregate on self-compacting mortar (SCM) fresh, hardened and durability properties.

2. To assess the effect of plastic optical fibers (POF) on the mechanical properties of self-compacting translucent concrete incorporating recycled glass aggregate (SCTC-RGA).
3. To evaluate the light transmittance performance of self-compacting translucent concrete incorporating recycled glass aggregate (SCTC-RGA).
4. To examine the structural performance of translucent concrete façade panels for application as structural façade and architectural wall in green buildings and other civil infrastructures.

1.4 Justification of the study

Residential and commercial buildings are one of the most electric lighting energy consuming sectors. When high-rise buildings are built close to each other, natural sunlight is hindered to pass through due to the obstruction from nearby structures. During daytime, the brightness of the indoor environment in buildings is entirely maintained by artificial light, which consumes a large amount of electric energy. Using natural sunlight in indoor environment reduces the need for artificial lighting and cost of energy, and promotes better comfort environments for occupants. Developing a new kind of building material that can reduce the demand for artificial lighting energy is vital. This research attempts to address such issues through the development of translucent concrete using locally available materials that can be used as energy-saving building material in a variety of architectural wall of buildings, without compromising the fundamental engineering properties of the material. Translucent concrete is aesthetically pleasant concrete that offers daylight scheme in buildings and overall fosters development of green buildings and sustainable construction.

The growth of population, industrialization, urbanization, and increase in the manufacturing of products led to an increase in solid wastes generation. Solid wastes such as glass, plastic and so more pose an environmental and health problems. One of the challenges in solid waste management is waste disposal. Waste glass which is nonmetallic and inorganic is considered one of the important parts of waste materials. It can neither be incinerated nor decomposed. Recycling of solid wastes as ingredients of concrete to substitute aggregate in the production of concrete is one way to resolve solid waste disposal problem while maintaining acceptable strength and durability of the structural concrete. In this study, waste glass was collected from local landfills, crushed manually to obtain recycled glass aggregate to substitute natural river sand in a self-compacting mortar. The use of recycled glass aggregate in self-compacting mortar also contributes to the safeguarding of natural resources and protection of the environment by partial substitution of aggregates. Moreover, recycled glass aggregate has the potential to improve the durability of concrete and eventually reduce the cost of materials involved in making a concrete composite.

1.5 Scope and Limitations of the study

1.5.1 Scope of the study

In this research, soda-lime silicate glass was collected from local landfills and crushed manually to produce graded recycled glass aggregate. To explore the possibility and viability of utilizing recycled glass aggregate as a substitution of natural fine aggregate in self-compacting mortar, the fresh (flowability and passing ability), hardened (bulk density, compressive strength, flexural strength and water absorption) and durability (sorptivity and expansion due to alkali-silica-reaction) properties were experimentally assessed with an approach to be used in the production of translucent concrete. Self-

compacting mortar containing 20% of RGA was used for prototyping of translucent concrete. The mechanical properties (mass density, compressive strength, and flexural strength) of translucent concrete were also investigated. The light transmittance performance of translucent concrete was also evaluated using an electrical circuit set-up with a light dependent resistor. Furthermore, translucent concrete panels/ façades containing 6% of plastic optical fibers volume ratio were produced and their structural performance was examined with a consideration to be used in architectural walls of green buildings and other civil infrastructures. This study focuses generally on embracing the application of self-compacting mortar containing recycled glass aggregate in the production of translucent concrete and to add cognizance of translucent concrete in the construction industry of Africa.

1.5.2 Limitations of the study

Clear glass sheet which is of interest in this study was processed into recycled aggregate. However, other forms of waste glass such as discarded cathode ray tubes, mirrors, and colored bottles were not a concern of the study. Plastic optical fibers of 2 mm and 3 mm diameters were used to reinforce concrete, while other types of optical fibers such as glass fibers and optical fibers less than 2 mm diameters were not within the concern of the research.

1.6 Thesis Layout

The thesis comprises of preliminary pages and five chapters. The preliminary pages entail declaration, dedication, acknowledgments, table of contents, list of tables, list of figures, list of abbreviations and acronyms, and abstract. A brief description of the thesis content is presented below;

Chapter One (Introduction): This chapter introduces general background to the study, statement of the problem, general and specific objectives, justification, scope and limitation of the study as well as the thesis layout.

Chapter Two (Literature review): This chapter reviews the literature survey of past studies related to the mix design method of self-compacting mortar/concrete, the use of recycled glass aggregate in concrete and translucent concrete.

Chapter Three (Materials and methods): This chapter illustrates material characterizations, instruments and equipment's, experimental program, mix design (mix formulation and mix proportioning), mixing procedures, test procedures and methodology for self-compacting mortar, and translucent concrete, the fabrication process of translucent concrete.

Chapter Four (Results and discussion): This chapter comprises detailed data analysis, results and in-depth discussion on each specific objectives.

Chapter Five (Conclusions and recommendations): This chapter highlights the relevant conclusions drawn from the findings of the research and outlines recommendations for future investigations. Moreover, references and appendices are also included.

CHAPTER TWO

LITERATURE REVIEW

2.1 Self-Compacting Mortar/Concrete

Self-compacting concrete (SCC) is an advanced concrete with a higher flowing and passing fresh properties, and self-consolidating property under its own weight to achieve full compaction without the need for mechanical vibration.

2.1.1 Mix Design Methods of Self-compacting Mortar/Concrete

Mix design methods are essential to obtain the optimum proportion of constituent materials that guarantee the required degree of workability and rheology of SCC. For SCC mix design, there are no specific standard methods. However, several methods have been developed based on empirical and scientific evidence such as the general mix design method (Japan), CBI (Sweden), LCPC (France) and so on.

2.1.1.1 Japanese Mix Design Method (General purpose mix design method)

The general purpose mix design method has been developed in University of Tokyo, Japan by Okamura and Ozawa who are considered a pioneer in SCC area (Okamura & Ozawa, 1995). This mix design is a step-by-step process starts from paste design, optimizing mortar phase and finally the concrete phase. The initial water to powder ratio required to develop SCM is based on the paste design examined from paste slump flow test. The mini-slump flow test conducted with different water to powder ratio (V_W/V_P) to determine the water required to initiate the mix flow. During the test the resulting slump flow diameter (d_m) for each water to powder ratio trials recorded and the respective relative slump (Γ_m) computed. There is a linear relationship when relative slump (Γ_m) set out against water to powder ratio (V_W/V_P). The point of intersection of the straight line with y-axis ($\Gamma_m=0$) designated as β_p (retained water

ratio) value indicates the water content where no slump takes place, in another word the water retained by the powder completely. β_P reflects the initial water to commence flow, which includes the water absorbed on the surface of the powder and fills the voids between the powder and it depends on the composition and fineness of the powder. Once retained water ratio estimated (β_P), then the fine aggregate content must set in the range of 40% – 50% of the mortar volume. Slump flow and V-funnel flow conducted in the mortar phase of the mix with a target workability values to achieve self-compactibility requirements. This method emphasizes the essence of highly viscous paste matrix to control segregation and avoid blockage of aggregates. Moreover, superplasticizer used to control the flowability of the mix.

2.1.1.2 CBI mix design method

The Swedish Cement and Concrete Research Institute proposed the CBI mix design method of SCC (Billberg, 1999). The principle of CBI method is to use minimum paste content to produce optimum aggregate skeleton that secures passing ability of SCC in obstacles. The general steps in this method are determining minimum volume of paste that prevents blockage, the composition of paste and SCC proportion evaluation. Although CBI method yields a mix of higher strength and durability because powder composition and water to powder ratio are derived based on strength requirements, determining blockage of aggregates is tedious (Liu, 2009).

2.1.1.3 LCPC mix design method

The Laboratoire Central des Ponts et Chaussèes (LCPC) developed a Solid Suspension Model (SSM) on the basis of Compressive Backing Model (CBM) to describe the rheological and workability of SCC (Sedran & De Larrard, 1999). This is a computer-based French approach SCC mix design method. The model requires gradation of

particles, packing density, unit weight, and superplasticizer dosage saturation point to predict the paste content between aggregate skeleton simultaneously to reduce the water content of SCC (Utsi, 2008). Several preliminary tests are required to use LCPC method but SCC trials are reduced. This method is limited to SCC mixes without viscosity modifying agents (Liu, 2009).

2.1.2 Principles to achieve Self-compactibility

Fresh SCC must possess high rheological stability, flowability, and deformability without bleeding or segregation so that it's able to flow under gravitational force and passes a congested obstacle such as reinforcements and optical fibers in case of translucent concrete. Any SCC mix design must satisfy three key requirements: flowability, filling ability and passing ability. According to Okamura & Ouchi (2003), there are three basic principles to achieve self-compactibility of fresh SCC: using superplasticizer, reducing water to powder ratio and limiting aggregate content.

2.1.2.1 Using superplasticizer

The optimum dosage of superplasticizer in SCC mix yields maximum flowability and passing ability while guaranteeing the homogeneity of the mix at an acceptable level. The optimum dose of superplasticizer has a tendency of dispersion effects on flocculated cement molecules by increasing the repulsive force and decreasing attractive forces among the particles (Hameed, 2012).

2.1.2.2 High paste volume

High paste content guarantees the separation of aggregates to ensure flowability and passing ability of particles in SCC. Okamura & Ouchi (2003), research proves that when concrete deforms the internal stress increases especially near to obstacles. This phenomenon results in blockage because of the energy required for flowing dissipated

by the internal stress. Higher content of powder in SCC increases cohesiveness and workability simultaneously reduce the blockage behavior by decreasing the inter-molecular interaction between aggregate particles (Khayat, 2000). Partial substitution of cement by using limestone powder or other admixtures is essential to minimize excessive heat generated and cost of powder materials.

2.1.2.3 Limiting aggregate content

The workability of fresh SCC is highly influenced by the texture, size, and type of aggregate (Khaleel, Al-Mishhadani, & Razak, 2011). Moreover, the friction between aggregate particles restricts the filling ability, deformability and passing ability of SCC mix. The packing density of aggregate skeleton can be improved by limiting the maximum aggregate size and reducing the volume fraction to enhance the spreading and filling ability of SCC.

2.1.2.4 Using viscosity modifying agents (VMA)

VMA's are a water-soluble polymers or colloidal suspensions that increase the viscosity of mixing water and improves the adhesive property of cement paste in SCC. VMA stabilizes the rheology of SCC, minimizes bleeding and segregation of mixes. In addition, SCC becomes less sensitive to water variations in the presence of VMA in the mix (Boukendakdji et al., 2016).

2.1.3 Guidelines for Self-compacting Mortar/Concrete

Despite the many methods, there is no common globally accepted specification and guideline for the mix design, testing and production of SCC. Attempts have been made to create standardized methods of testing, specifications and guidelines in institution, company, country and continent level. The Japanese and European guidelines are widely accepted guidelines in the production of SCC (Liu, 2009).

2.1.3.1 Japanese SCC Guideline

Self-compacting concrete originates from Japan in 1986. Different organizations extensively studied SCC since 1990 in Japan and based on the experimental research results several recommendations were made to widen the paramount application of SCC to the construction practices. The Architectural Institute of Japan (1997), the Japan Society of Civil Engineers (1998) and the National Ready-mixed Concrete Industry Association of Japan (1998) have been successfully provides recommendations for mix design, construction practice and manufacturing of SCC for producers, contractors, users and researchers. The recommendations compiles constitute materials, fresh and hardened properties, on-site quality control and mix design of SCC (Liu, 2009).

2.1.3.2 European SCC Guideline

SCC has been widely accepted in the construction practice across Europe since early 1990's and the first SCC European guideline was published in February 2002 by EFNARC (European Federation of National Associations Representing for Concrete). The guideline clearly defines SCC/SCM test methods, key properties i.e. flowability, filling ability and passing ability and constitute materials requirements based on latest several research results. In addition, it also deals with possibility of using mineral admixtures such as silica fume, fly ash, finely crushed stones and so more, as alternative elements in SCC/SCM. The slump flow requirement for self-compactibility of SCM ranges 240 to 260 mm and V-funnel time 7 to 11 sec. Generally, EFNARC guideline provide acceptable criteria for the design, production and manufacturing of SCC, and has been gradually accepted beyond Europe in many other countries (Liu,

2009). For this particular research, (EFNARC, 2002) guideline adopted for testing the self-compactibility requirements of SCM.

2.1.4 Properties of Self-compacting Mortar/Concrete

2.1.4.1 Fresh Properties of Self-compacting Mortar/Concrete

Deformability, passing ability, stability and robustness are the key characteristics of fresh SCC to flow under gravity force even in congested obstacles and to maintain its self-compactibility without any vibration (Liu, 2009).

Deformability: The flowability and filling ability known as deformability are the fundamental properties of SCC to deform both horizontally and vertically to fill formwork under self-weight. Deformability expressed in two concurrent mechanisms: the deformation capacity (the maximum distance to deform) and velocity (time taken to flow). Slump flow and V-funnel are the most common tests to investigate deformability of SCC/SCM.

Passing ability: is the ability of SCC to pass through closely spaced obstacles or reinforcement whilst secure its homogeneity during flow. It is mainly assessed using J-ring and L-box tests.

Stability: is the ability of SCC to resist segregation between paste and aggregate or between cement and water during placement and transportation. In the mix, design stage its essential to consider the specific gravity and size of constitute materials to come up with the homogenous concrete mix (Liu, 2009). Visual stability index (VSI) test is such test to visually evaluate the stability of SCCSCM mix.

Robustness: is the resistance of SCC to changes in its fresh properties due to various factors such as superplasticizer dosage, fineness, the moisture content of aggregates

etc. Incorporating viscosity modifying agent (VMA) generally improves the robustness of SCC.

2.1.4.2 Hardened properties of self-compacting concrete

The fundamental hardened strength properties of SCC are a compressive, tensile and flexural strength. However, hardened SCC can be also assessed for ultrasonic pulse velocity, absorption, permeability, absorption and electrical resistivity.

Compressive strength: is the key mechanical property of hardened concrete. The compressive strength of SCC basically depends on water to powder ratio, the degree of compactibility, paste to aggregate ratio and composition of the mixture.

Flexural strength: it is also called modulus of rupture, is the property of SCC to carry tension or flexure under static or dynamic loading.

2.1.4.3 Durability of self-compacting concrete

The durability of SCC is related to its performance and service life under various environmental conditions.

Sorptivity: is an engineering property of hardened SCC to absorb water due to capillary action and higher affinity of the concrete surface towards the water. It is directly proportional to the porosity of the concrete microstructure skeleton.

Alkali-Silica-Reaction (ASR): The mechanism of ASR is the chemical process between siliceous aggregate particles and hydroxyl ion in hardened concrete that leads to the evolution of viscous alkali-silicate gel (Rajabipour, Maraghechi, & Fischer, 2010). The formation of alkali-silicate gel followed by inward diffusion of hydroxyl ion and alkali metals due to intake of water in the pores skeleton through osmotic pressure that alters and softens aggregate particles and consequently generates

swelling pressure, tensile failure and potential cracks in the structural concrete (Corinaldesi et al., 2016; Du & Tan, 2013; Maraghechi & Al., 2012).

2.1.5 Effect of Recycled Glass Aggregate on Self-Compacting Concrete/Mortar

Utilization of waste products such as waste glass, waste plastic and so on in concrete as a replacement of aggregate is one way to reduce the environmental impact of the construction industry and a triggered solution towards sustainable solid waste disposal. However, the successful usage of waste products in the production of concrete lies and limited to its consequent effects on the workability, strength and serviceability requirements of concrete on the provision that the mix designed properly.

The potential effects of utilizing glass aggregate in concrete reported by previous research (Corinaldesi et al., 2016; Maraghechi & Al., 2012; Sharifi et al., 2016; Siad et al., 2017) were an alkali-silica reaction (ASR) between the amorphous silicate glass grains and alkali of cement in the presence of water that might results in volumetric expansion and spalling. However, experimental evidence proved that the potential problem of ASR decreased with reduced glass aggregate particle size. Du & Tan (2013), revealed that glass aggregate less than 2.36mm would effectively mitigate ASR expansion and assured pozzolanic activity.

Several previous studies revealed that incorporating of recycled glass as fine aggregate in concrete decreases slump flow due to the harsh texture and geometry of glass grains. Ismail & AL-Hashmi (2009) reported that the slump of concrete containing waste glass showed lower slump compared to control concrete. Afshinnia & Rangaraju (2016), was also found that the use of crushed glass in concrete as fine aggregate significantly decreases the workability. Similarly, Tan & Du (2013) observed a reduction in flowability of mortar as the ratio of waste glass increases in cement-based mortar

mixes. The higher aspect ratio, as well as the sharp edge and angular shape of glass particles, hinders the movement of cement matrix and other particles during the flow of mortar mix. Limbachiya (2009) investigated the use of washed glass sand as a direct replacement of natural sand in concrete. The experimental results showed that the workability of concrete decreases as the percentage replacement of natural sand by washed glass sand increases.

In contrary, other authors reported that the use of recycled glass in concrete improves the workability of concrete mixes. The improvement in workability of the concrete mixes attributed to the smooth surface of glass grains. Ling, Poon, & Kou (2012) deduced that inclusion of recycled glass in self-compacting concrete increases the flowability of fresh mixes. Glasscrete mixes require less superplasticizer dosage to achieve a similar target slump compared to reference concrete mixes without glass (Wright et al., 2014). On average, Glasscrete requires 30% – 40% less superplasticizer dosage to obtain the same slump flow as the reference concrete mixes. The impermeable nature of glass particles plays a significant role in reducing the superplasticizer dosage. The investigation of the effect of recycled glass on fresh properties of self-compacting concrete conducted by Sharifi, Houshiar, & Aghebati (2013) shows that the V-funnel time of SCC mixes decreases with increase in recycled glass content. The slump flow test results indicate the flowability of the SCC was increased as the content of glass aggregate increases. Ali & Al-Tersawy (2012) investigates the use of glass as aggregate in self-compacting concrete. The inclusion of glass aggregate in SCC showed a tendency of increasing the slump flow, flow ratio and V-funnel of the mixes relative to conventional SCC mixes.

Extensive experimental research conducted on concrete containing recycled glass aggregate (RGA) has consistently reported that its compressive and flexural strength is lower, compared to concrete containing a natural aggregate. Limbachiya (2009), reported that the strength performance of concrete with up to 20% of glass sand had similar performance compared to conventional concrete but thereafter gradual reduction in strength was observed as glass sand content increases. In addition, the density and water absorption of concrete containing glass sand were lower than that of the reference concrete with natural sand.

A research conducted by Ali & Al-Tersawy (2012) shows as the content of glass aggregate increases the compressive strength, tensile splitting strength, and static modulus of elasticity of self-compacting concrete decreases. Another work conducted by Kou & Poon (2009), indicates a similar trend of the waste glass on strength characteristics of concrete. The compressive strength of SCC mixes contains 15%, 30% and 45% of waste glass was reduced by 1.5%, 4.2% and 8.5%, respectively compared to the reference concrete. Almesfer & Ingham (2014) examined the influence of crushed waste glass bottles as a replacement of coarse and fine aggregates on mechanical properties of Portland cement concrete. It was evident that with the addition of waste glass the compressive and flexural strength of mixes were decreasing, although the effect of waste glass on flexural strength was not as detrimental as on the compressive strength of concrete.

De Castro & De Brito (2013) investigated the durability of concrete made with crushed glass aggregate at 5%, 10% and 20% replacement of natural aggregate. Durability performances such as sorptivity, water absorption by immersion, carbonation resistance, chloride penetration, and shrinkage were examined. The test results

demonstrated that the sorptivity of concrete with crushed glass reduced 9% – 19% compared to reference concrete, consistent with findings of Sikora et al. (2017). In the other hand, the water absorption, shrinkage, carbonation resistance and chloride penetration of concrete integrating waste glass were marginally higher than those control concrete.

The major technical obstacle of utilizing waste glass in concrete is the formation of alkali-silica reaction (ASR). Alkaline content of cement, size, and color of glass particles are the main factors affects the ASR. Corinaldesi et al. (2016) evaluate the effect of both size and color of crushed glass on the durability of cement mortar. Quartz sand was replaced partially (50%) and fully (100%) by glass cullet of three different colors (clear, green and amber). Three mortar bars of 70x70x280 mm^3 dimensions were prepared for each mixture according to ASTM C1260 (2007). The ASR expansion subsequently measured after 2, 4, 7, 14, 21, 28, 35 and 42 days of curing in 1 N NaOH. It was evidently observed that clear glass at 100% replacing sand, showed higher ASR expansion. The use of clear glass of less 8 mm grain size should not exceed 50% replacement of sand due to detrimental ASR expansion when the replacement goes beyond.

Tan & Du (2013) conducted an experimental investigation on the effect of the color of waste glass o ASR expansion of mortar. The ASR result clearly showed that green and brown waste glass aggregates are unreactive whereas clear glass is potentially deleterious. The ASR expansion was significantly increased as the content of clear waste glass increases. Incorporating of lithium compounds, fibers, fly ash and powder glass remarkably mitigates the risk of ASR expansion of glass in concrete.

2.1.6 The Influence of Chemical and Mineral Admixtures on Concrete

The use of mineral admixture such as limestone powder in self-compacting concrete/mortar reduces the amount of cement, increases the packing density of particles, lowers void ratio and accelerates pozzolanic activity (Tironi, Scian, & Irassar, 2017). Limestone powder also amplifies the rate of cement hydration, lowers time of setting and improves fluidity of SCM (Bentz et al., 2017). In addition, the use of chemical admixture (superplasticizer) ensures deflocculating and reduces water demand of SCM mixtures and intensify intermolecular interaction of particles (Georgiadis, Sideris, & Anagnostopoulos, 2009). The flowability of SCM mixtures mainly depends on the dosage of superplasticizer, whereas, the passing ability (V-funnel) depends on the ratio of powder in the paste matrix.

Christianto (2004), studied the influence of chemical and mineral admixtures in the fresh properties of self-compacting mortar. Polycarboxylate and melamine formaldehyde based superplasticisers were used as chemical admixtures. Moreover, limestone powder, brick powder, fly ash, and kaolinite were used as a mineral admixture in the SCM mixtures. The experimental results show that the use of fly ash and limestone powder enhances the workability of SCM. It was observed that polycarboxylate based mineral admixtures are much more effective than melamine formaldehyde based superplasticisers.

The relationship between fluidity and stability of self-consolidating mortar containing chemical and mineral admixtures was studied (Libre, Khoshnazar, & Shekarchi, 2010). Limestone powder and fly ash, as well as superplasticiser and viscosity modifying agents, were used to prepare SCM mixes. The test results show that water to cement ratio and superplasticiser dosage is the two main parameters that significantly

influences the fluidity and rheology of SCM mixes. However, as the fluidity increases, the stability of the mixes remarkably decrease. It is, therefore, recommended that instead of increasing water to cement ratio, it is prominent to introduce superplasticizer to stabilize the mixes flow. The use of fly ash and limestone powder were only effective in controlling bleeding and aggregate blockage.

Topçu & Uyğunolu (2010), reports that the introduction of mineral admixtures such as limestone powder, marble powder, brick powder and fly ash reduces the yield stress and increases the flowability of self-consolidating mortar. The effectiveness of mineral admixture in enhancing SCM properties is similar to chemical admixture and water to powder. It was also observed that as the water to powder and superplasticizer dosage increases, the yield stress of SCM mixes decreases.

A study on the replacement of cement with limestone powder conducted by Beeralingegowda & Gundakalle (2013), showed that up to 20% replacement of cement by limestone powder improves workability and increases the strength of SCC. It was found that 20% of limestone powder replaces cement, the compressive, flexural and split tensile strength increases by 17.74%, 8.43%, and 18.91%, respectively. The chloride ion penetration depth remarkably decreased with increasing percentage ratio of limestone powder. However, SCC mixes contain limestone powder shows higher weight loss due to acid attack relative to reference mix. Generally, SCC mixes with up to 30% of limestone powder showed higher strength and improved workability compared to reference mix.

2.1.7 Advantages and Disadvantages of Self-compacting Mortar/Concrete

Properly designed and proportioned self-compacting concrete offers the following economic, health, environmental and technical advantages (Deeb, 2013; EFNARC, 2002).

i. Eliminates vibration and reduces noise extent. This improves the construction environment and also prevents ‘‘white finger Syndrome’’ in laborers which is mainly caused due to the use of vibrating equipment.
ii. The impressive futures of SCC i.e. flowability, passing and filling ability leads to ease of concrete placement operations.
iii. Ensures uniform surface finish and void-free architectural surface.
iv. Saves construction time and reduces the cost of manpower.
v. Confers better structural durability and improves the bondage with reinforcement bars.
vi. Reduces load exerted into formworks due to vibration force and hence contribute to the safety of formworks.
vii. Imparts fast-track construction in high-rise buildings.
viii. Enhances water-tightness and early stage strength of concrete.
ix. Easy to handle casting of complex architectural structures such as in iconic architectural forms and congested reinforcement.

The disadvantages of SCC relative to conventional concrete include the higher cost of materials, requires a higher degree of controlled mix accuracy and high cement content. In addition, up to date, there is no globally agreed standard and guideline for mixing and testing of SCC.

2.1.8 Application of Self-compacting Mortar/Concrete

Self-compacting concrete has similar application as conventional concrete. It has been applied in the construction of buildings, towers, bridges, culverts, tanks, airport control towers, dams, rigid pavements, retaining walls, precast structures and so on. It has been also applied in repair and maintenance of existing structures. The following are some particular examples which have been constructed using SCC (Okrajnov-Bajić & Vasović, 2009):

i. Burj Dubai, United Arab Emirates
ii. Dragon Bridge, Alcalá De Guadaira, Seville, Spain
iii. Arlanda Airport Control Tower, Stockholm, Sweden
iv. Wall of a large LNG tank belonging to Osaka Gas Company, Japan
v. St George Wharf, London Docklands
vi. Anchorages of Akashi-Kaikyo suspension bridge, Japan
vii. Sodra Lanken, Stockholm, Sweden
viii. National Museum of 21st Century Arts (MAXXI) in Rome, Italy
ix. Ušće Shopping Center, Belgrade, Serbia
x. Robert Moses Dam, New York Power Authority, United States of America

In this research, a new area of application of self-compacting concrete/mortar incorporating recycled glass aggregate studied to be used and applied in the production of pre-cast translucent concrete for construction of light transmitting architectural walls, panels, and structural façades. To date, the method of production of translucent concrete is dependent on a conventional approach that requires vibration to achieve a high degree of compaction.

2.2 Translucent Concrete

2.2.1 Mechanical Properties of Translucent Concrete

Hungarian architect Áron Losonczi introduced the first concept of light transmitting concrete in 2001, and the first prototype of the translucent concrete panel was successfully developed in 2003. TC is a new eco-friendly construction material and there exist few previous experimental studies. Altlomate et al. (2016) studied the strength and light transmittance of TC containing POF of diameter 0.3 mm, 0.5 mm, 0.75 mm and 1.5 mm. The results showed that incorporation of POF has a variable effect on compressive strength. The direct ultrasonic pulse velocity (UPV) showed that the quality of TC was excellent despite inclusive of POF. Moreover, the physical and mechanical properties of POF was also investigated. The tensile strength of 0.3 mm, 0.5 mm, 0.75 mm and 1.5 mm POF obtained was 20 MPa, 23 MPa, 25 MPa and 30 MPa respectively. Generally, the inclusion of POF improves strength and aesthetics of concrete as well as enables concrete to transmit light through. Thus, TC contributes to sustainable construction in a way by reducing the power consumption of buildings.

Li et al. (2015), examined the compressive and flexural strength of cement based TC containing polymethyl methacrylate (PMMA) fibers. Both compressive and flexural strength of TC decreased when the volume of fibers increased. In addition, the strength of all TC specimens was lower than the reference concrete and thus, incorporating of PMMA fibers led to a reduction of compressive and flexural strength despite the volume fraction of fibers. Li, Li, & Guo (2015), reported that the compressive strength of sulfoaluminate cement based TC linearly decreased as the volume of optical fibers increased at various curing conditions. According to the microstructural analysis of

pore structures in TC, the author deduced pores formed around the interface of paste matrix and optical fibers.

Salih, Joni, & Mohamed (2014a), studied TC prepared using self-compacting mortar (SCM) and POF as reinforcement. The inclusion of POF generally decreased the compressive and flexural strength of TC. However, the variation on diameter and volume of POF showed the fluctuating effect on strength properties of TC. It was found that 2 mm diameter PMMA fibers produced TC with higher flexural and compressive strength compared to 1mm and 2 mm diameter fibers. Furthermore, the authors deduced that SCM is very suitable for the production of TC due to higher flowability on congested optical fibers and ease of concreting.

Another research conducted by Tutikian & Marquetto (2015), was on the investigation of translucent concrete walls produced with a random arrangement of optical fibers for use in the pre-cast construction of Brazil. The experimental results revealed that the value of capillary water absorption of TC slightly decreased due to the inclusion of optical fibers. The compressive and tensile strength in bending of TC decreased as the percentage volume of optical fibers increased.

It is observed that high-performance concrete using optical fibers can also be utilized as a decorative and structural material to improve elegance of structure by making it transparent. Kankriya (2016), evaluates the effectiveness of smart transparent concrete by combining optical fibers and glass rods at different percentages ratio. Samples were prepared by compaction in a table vibrator. The cubes were tested for compression and light transmittance test, and cost comparison was also performed. Translucent concrete is applicable in partitions rather than structural elements such as a beam, column, and slab. The initial cost of translucent concrete is higher than conventional concrete due

to the high cost of optical fibers. However, in regard to benefits of reducing energy consumption, the cost of translucent concrete is justified. Based on the cost analysis, payback period of translucent concrete is 1 year for a domestic consumption, and 0.72 years for commercial and industrial consumption in regard to the electric light tariff.

A work conducted by Halbiniak & Sroka (2015), was on the evaluation of the compressive strength of translucent concrete containing cement, water, die, superplasticizer, 1.5 mm diameter POF and fine aggregate. The samples were designed in a form of prism 40x40x160 mm^3 size and 3.2% of POF was embedded at a spacing of 5 mm. The compressive test was performed after 28 days of age in two ways: one way was when the compressive load applied parallel to the POF direction of embedment and the other was in a perpendicular direction to assess the effect of POF embedment. The experimental results showed that the compressive strength of translucent concrete decreased by 38.3% and 18.9%, where the direction of compressive force applied parallel and perpendicular to the direction of plastic optical fibers embedment, respectively. It is evidently observed that the direction of POF embedment is critical in strength characteristics of translucent concrete.

Tiwari & Saharan (2016), studied the behavior of translucent concrete using rice husk and steel fiber. The translucent concrete specimens were prepared using cement, fine aggregate, coarse aggregate, POF of 0.5mm diameter, rice husk, and steel fiber. The percentage of POF integrated in the translucent concrete was 0%, 0.5%, 1%, 2%, 3% and 4%. The samples were compacted properly on the vibrating table. The compressive strength of translucent concrete decreases as the percentage of POF increases but adding rice husk and steel fiber improves its strength.

2.2.2 Light Transmittance Performance of Translucent Concrete

A few previous studies have been reported on the light transmittance properties of optical fiber based translucent concrete. Li et al. (2015) reported that the optical power of the transmitted light gradually decreased as the distance between the specimen and light source increased. Test results show that regardless of red or white light, the optical power increases with the increase in a number of fibers integrated. Uneven and irregular section of fibers on the concrete surface affects the propagation of light waves which consequently decreases the wavelength of lights transmitted through the specimen.

Momin et al. (2014) investigated the comparative light transmission properties of concrete embedded with glass rods and optical fibers. It is observed that, for the same spacing, the light guiding efficiency of the optical fiber is much higher than glass rod. The ratio of light transmitted obtained was ranging 0.25% – 1.5% and 7.4% – 9.5 % using glass rod and optical fiber respectively. Li, Li, & Guo (2015) observed that the fiber diameters and volume fraction, as well as the thickness and the degree of surface roughness of sulfoaluminate cement-based specimens, affects the amount of light transmitted. Moreover, different curing conditions such as water bath at 80 ºC significantly reduced the light transmitted through the specimens.

Zhou et al. (2009) examined the transmitting performance of smart epoxy resin concrete blocks using Fiber Bragg Grating (FBG) and POF for application in civil infrastructure and structural health monitoring (SHM). The optical power meter test results show that at a range of 400 – 775 nm wavelength, transmittance ratio varies 1% – 2.5% corresponding to POF area ratio of 3.14% – 5.3%. Incorporation of POF could yield a steady transmittance ratio for both visible and infrared ray lights.

Altlomate et al. (2016) deduced that the transmission of light through light transmitting concrete completely depends on the surface area of POF used. The authors found a maximum luminance of 75.53 LUX transmitted through the cubic specimen containing 1.43% of 1.5 mm diameter fibers, which is above the minimum standard lux level for architecture applications on corridors, passageways, and indoor storage tanks according to Australian/New Zealand Standard (Australian/ New Zealand Standard, 2008).

2.2.3 Advantage and Disadvantages of Translucent Concrete

Translucent concrete is an environmental-friendly construction material that offers the following advantages to the construction industry (Gawatre, Giri, & Bande, 2016):

i. It gives aesthetically pleasant view to the structures and buildings
ii. It imbues indoor environments with natural sunlight
iii. Reduce artificial daylight energy i.e. conserve energy
iv. It is a heat insulator while natural sunlight pass through
v. It is ultra-violate resistant while light passing through the mass concrete
vi. Display shadow of objects on the back side of the concrete
vii. The light transmittance of translucent concrete is independent of its thickness
viii. Offers better security to prisons, banks, schools and so on.

The disadvantage of translucent concrete in comparison to the conventional concrete is (Gawatre et al., 2016):

i. It is very costly due to the cost of optical fibers
ii. The production of translucent concrete is difficult and hence requires a special trained workmanship

2.2.4 Application of Translucent Concrete

Translucent concrete can be applied in various areas of architecture, construction, decoration, and furniture fetch technical and ecological solutions to the conventional construction (Paul & Dutta, 2013).

i. As a construction material for internal and external walls to illuminate rooms
ii. In hotels, clubs, banks and company buildings entrances to create logo, pictures or inscriptions with an amazing view.
iii. As pavement in passable floors illuminated from below
iv. In lighting fixture decoration
v. In-ceiling of buildings to reduce daylight energy consumption
vi. Speed bumps of highways can be built using translucent concrete with under beneath light source or light up directly from another vehicle to make navigation easier.
vii. As lane marks of highways to clearly show up in the night to reduce traffic accidents and secure passage of passengers in the night.
viii. In sidewalks with light source beneath to create a beautiful scene, for safety as well as to encourage walking during the night on the foot.
ix. To add visibility in airports and subways
x. In prisons, museums, banks, schools where security and supervision is a must.

2.3 Summary of Literature Review

Although a number of researchers have studied the potential for using recycled glass aggregate as replacement of natural aggregate in structural concrete, an experimental study that investigated the viability and potential of using recycled glass aggregate in self-compacting mortar is scant. This research aims at exploring the possibility and

viability of using recycled glass aggregate as fine aggregate in self-compacting mortar for development of translucent concrete and application in the construction industry of Africa particularly East Africa.

According to this literature review, it is noted that few studies examined the effect of integrating plastic optical fiber on the mechanical (compressive and flexural strength) properties of translucent concrete. It is apparent that previous studies have not shown conclusively the influence of optical fibers on the compressive and flexural strength of concrete. Moreover, no researcher has examined the impact of optical fiber on the mass density of concrete and the use of SCM on the production of translucent concrete. This research address an in-depth knowledge on the use of SCM containing recycled glass aggregate in the production of translucent concrete as well as the mechanical effect of optical fiber on concrete.

There are very few previous studies demonstrate the light transmittance of translucent concrete using optical fiber of less than 1.5 mm diameters. In addition, extensive studies on light transmittance performance of translucent concrete are still very rare. This experimental research evaluates the light transmittance performance of translucent concrete containing optical fiber diameters of 2 mm and 3 mm using a light dependent resistor (LDR) for application in building construction and structural panels/façades.

The effect of plastic optical fiber on the structural performance of pre-cast translucent concrete panel has not been studied comprehensively. This research has also investigated the ductility/toughness impact of incorporating plastic optical fiber in concrete panels.

2.4 Conceptual Framework

A conceptual framework is an analytical tool that conceptualizes the relationship between variables in the research graphically or diagrammatically. The conceptual framework of this study is shown diagrammatically in Figure 2.1.

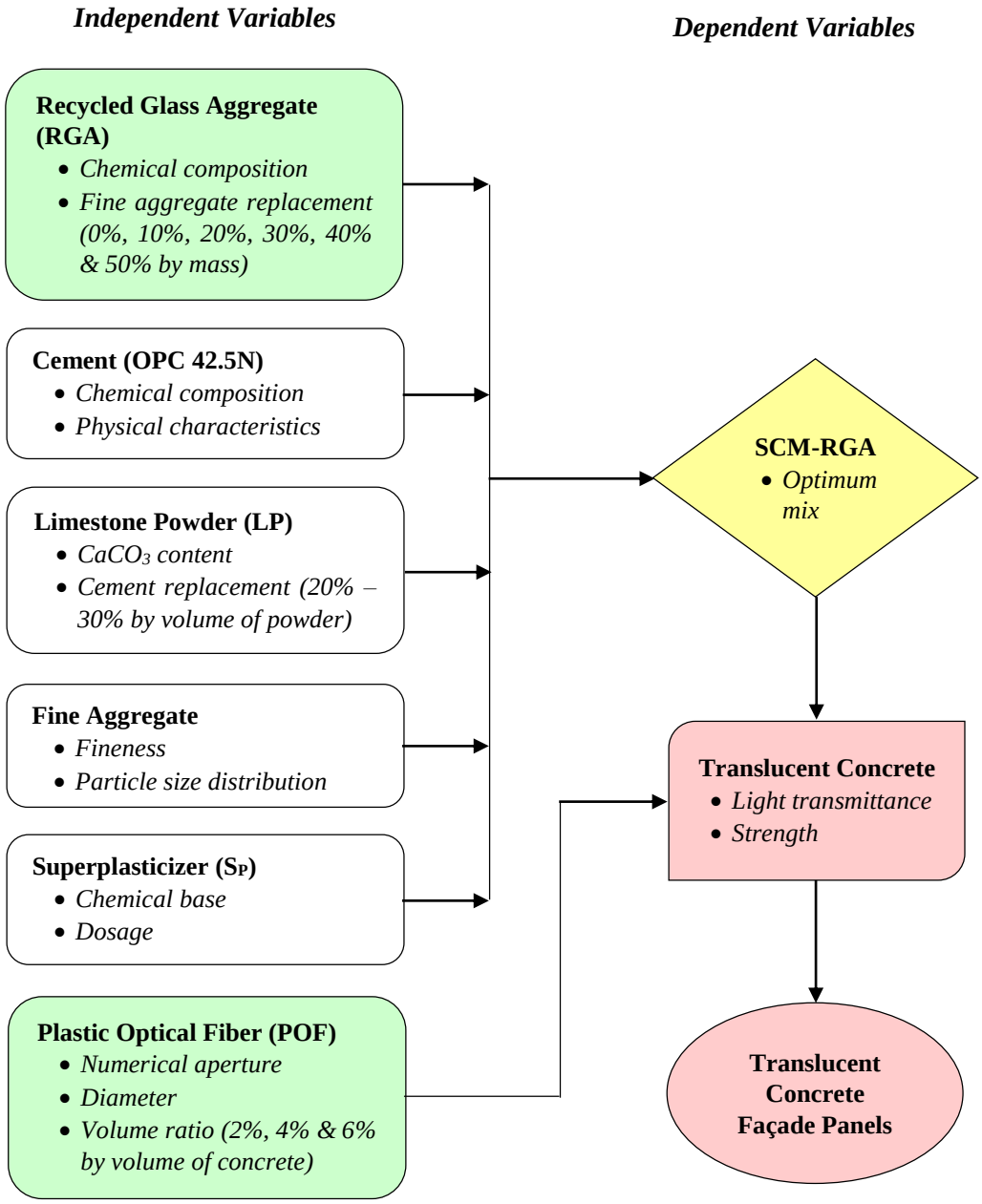

Figure 2.1 Conceptual framework

CHAPTER THREE

MATERIALS AND METHODS

3.1 Introduction

This chapter comprises a characterization of the constituent materials and experimental program used to develop translucent concrete for sustainable construction.

The experimental investigation of this research work comprises of two phases:

Phase-1: Development of self-compacting mortar (SCM) incorporating recycled glass aggregate

Phase-2: Prototyping and experimental analysis of translucent concrete

In phase-1, the experimental investigation focused on proportioning of self-compacting mortar containing recycled glass aggregate (SCM-RGA) based on Japanese Mix Design Method. The effect of incorporating RGA on fresh (workability), hardened (bulk density, compressive strength, flexural strength and water absorption) and durability (sorptivity and alkali-silica-reaction) properties of SCM was also studied. The fresh properties of the proportioned SCM-RGA mixes were evaluated based on EFNARC using slump flow and V-funnel flow time tests to ensure the self-compactibility requirements. The slump flow and V-funnel flow time tests were used to examine the filling ability (viscosity) and passing ability of SCM-RGA mixes. Moreover, the flow of the mixes was also visually observed for bleeding, segregation, and inconsistency. The SCM-RGA mixes that fulfil the self-compactibility requirements were further tested for compressive strength, flexural strength, bulk density, water absorption, sorptivity (capillary water absorption) and alkali-silica-reaction (ASR).

Phase-2 dealt with the experimental investigation of mechanical properties (compressive strength and flexural strength) and light transmittance performance of translucent concrete as well as the structural performance of translucent concrete panels. The translucent concrete specimens were prepared using optimum SCM-RGA mixture proportioned and evaluated in Phase-1 embedded with plastic optical fibers (POF). The light transmittance performance of translucent concrete specimens was analyzed using electrical circuit set-up with a light dependent resistor (LDR). The influence of POF on ductility properties of translucent concrete was assessed based on JSCE-SF4 (Method of testing for the flexural toughness of fiber reinforced concrete) using linear variable differential transducer (LVDT), strain gauges and load cell.

The properties of materials used in this research are also discussed such as specific gravity, particle size distribution, unit weight, soundness, specific surface, fineness modulus and chemical composition. Moreover, the apparatus and experimental methods are also illustrated in this chapter.

3.2 Characterization of constituent materials

The constituent materials used for the production of translucent concrete include ordinary Portland cement, limestone powder, natural fine aggregate, recycled glass aggregate, water, superplasticizer and plastic optical fibers.

3.2.1 Cement

An ordinary Portland cement Type I (CEM I 42.5N) conforming to the requirements of EN 197-1 (2000) was used as a binding agent. The ordinary Portland cement was primarily composed of calcium oxide (63.37%), silicon oxide (20.61%), aluminum oxide (5.05%) and iron oxide (3.24%). The chemical composition and physical properties of cement are presented in Table 3.1 and 3.2, respectively.

Table 3.1 Chemical composition of the ordinary Portland cement Type-I 42.5 N

Chemical Composition	**Cement (%)**	***EN 197-1 (2000)* Specification**
Calcium oxide, CaO	63.37	—
Silicon oxide, SiO_2	20.61	—
Aluminum oxide, Al_2O_3	5.05	≤ 8
Iron oxide, Fe_2O_3	3.24	—
Magnesium oxide, MgO	0.81	≤ 3
Sulphur trioxide, SO_3	2.75	≤ 3.5
Potassium oxide, K_2O	0.52	—
Sodium oxide, Na_2O	0.15	—
Chloride, Cl-	< 0.01	≤ 0.1
Tricalcium Aluminate, C_3A	7.91	—
Free CaO	0.63	—
Na. Eq	0.49	≤ 0.6
Insoluble Residue (I.R.)	1.00	≤ 5
Loss On Ignition (LOI)	2.90	≤ 5

Table 3.2 Physical properties of the ordinary Portland cement Type-I 42.5 N

Physical Test		Cement	*EN 197-1 (2000)* Specification
Specific Surface (cm^2/g)		3197	—
Bulk Density (kg/m^3)		1433	—
Specific Gravity		3.15	—
Soundness (mm)		0.30	≤ 10
Normal Consistency (%)		25.65	—
Setting Time (min)	Initial	160	≥ 60
	Final	252	—
Compressive Strength (N/mm^2)	At 2 days	19.30	≥ 10
	At 28 days	48.94	≥ 42.5

3.2.2 Limestone Powder

The mineral admixture used as filler was limestone powder (LP) with the $CaCO_3$ content of 85.5% by mass which met the standard requirement (≥ 75%) of EN 197-1 (2000). The fineness of the limestone powder passing 185 µm, 75 µm, 45 µm and 2 µm was 100%, 90.85%, 75.77% and 10.60% respectively. Details of the particle size distribution curve, chemical composition and physical properties of the limestone powder are given in Figure 3.1, Table 3.3 and Table 3.4, respectively.

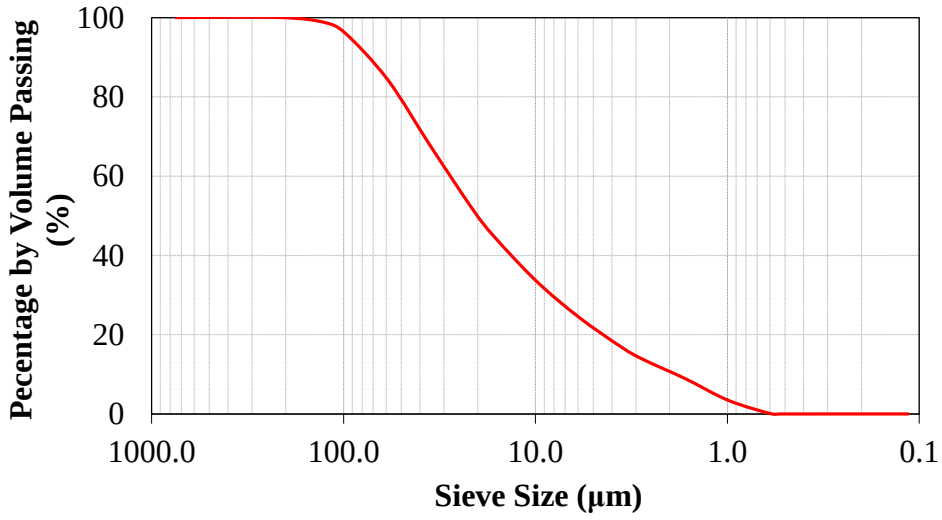

Figure 3.1 Particle size distribution of limestone powder (LP)

Table 3.3 Chemical composition of the limestone powder

Chemical Composition	Limestone Powder (%)
Calcium oxide, CaO	47.86
Silicon oxide, SiO_2	12.20
Aluminum oxide, Al_2O_3	0.60
Iron oxide, Fe_2O_3	0.30
Magnesium oxide, MgO	0.90
Phosphorus pentoxide, P_2O_5	0.15
Insoluble Residue (I.R.)	0.20
Loss on Ignition (LOI)	37.65

Table 3.4 Physical properties of the limestone powder

Physical Test	Limestone Powder
Specific Surface (cm^2/g)	1029
Bulk Density (kg/m^3)	1365
Specific Gravity	2.80
pH value	8.90
Moisture content (%)	0.20

3.2.3 Fine Aggregate

The fine aggregate used was natural river sand procured locally. The fine aggregate was first dried in an oven for 24 hours and sieved through #8 sieve (2.36 mm) to remove any particle greater than 2.36 mm including debris and roots. Particle size distribution of the fine aggregate was conforming to the requirements of ASTM C33 (2011). The chemical composition the fine aggregate analyzed using Bruker S1 TITAN Handheld X-ray fluorescent spectrometer is detailed in Table 3.5. A finely ground and homogenized sample was used to identifies the phases present in a sample during XRF test. The physical properties and particle size distribution curve of the fine aggregate are given in Table 3.6 and Figure 3.2, respectively.

Table 3.5 Chemical composition of the fine aggregate

Chemical Composition	Fine Aggregate (%)
Calcium oxide, CaO	4.17
Silicon oxide, SiO_2	79.96
Aluminum oxide, Al_2O_3	8.65
Iron, Fe	1.53
Sulfur trioxide, SO_3	1.27
Potassium oxide, K_2O	2.82
Sulfur, S	1.27
Barium, Ba	0.15
Titanium, Ti	0.49
Phosphorus pentoxide, P_2O_5	0.79

Table 3.6 Physical properties of the fine aggregate

Physical Test	Fine Aggregate
Fineness modulus	2.35
Bulk Density (kg/m^3)	1610
Specific Gravity	2.37

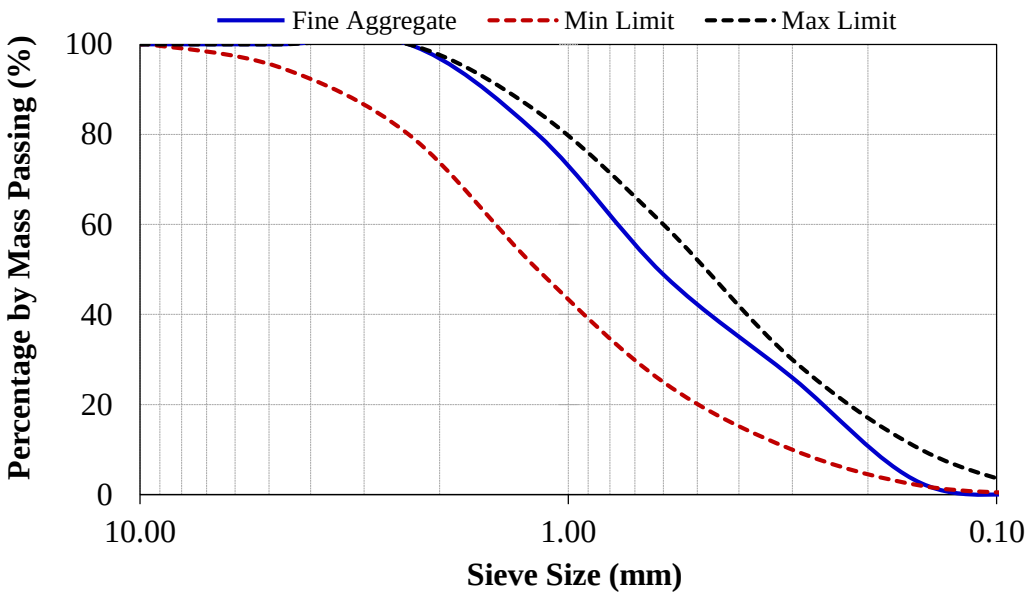

Figure 3.2 Particle size distribution of fine aggregate

3.2.4 Recycled Glass

Soda-lime silicate glass was collected from local landfills, then cleaned and crushed manually (see Figure 3.4) to produce graded finely crushed recycled glass aggregate (RGA) that met the requirements of ASTM C33 (2011). The unit weight, specific gravity and fineness modulus of the RGA was 1545 Kg/m^3, 2.32 and 2.70 respectively. The chemical composition of the recycled glass detected by X-ray fluorescent (XRF) is given in Table 3.7. The physical properties and particle size distribution curve of the recycled glass aggregate are presented in Table 3.8 and Figure 3.3, respectively.

Table 3.7 Chemical composition of the recycled glass aggregate

Chemical Composition	Recycled Glass Aggregate (%)
Calcium oxide, CaO	10.67
Silicon oxide, SiO_2	81.98
Aluminum oxide, Al_2O_3	0.86
Iron oxide, Fe_2O_3	0.23
Magnesium oxide, MgO	5.63
Sulfur trioxide, SO_3	0.19
Potassium oxide, K_2O	0.23
Sulfur, S	0.19
Strontium, Sr	0.01
Titanium, Ti	0.05
Phosphorus pentoxide, P_2O_5	0.12

Table 3.8 Physical properties of the recycled glass aggregate

Physical Test	Recycled Glass Aggregate
Fineness modulus	2.70
Bulk Density (kg/m^3)	1545
Specific Gravity	2.32

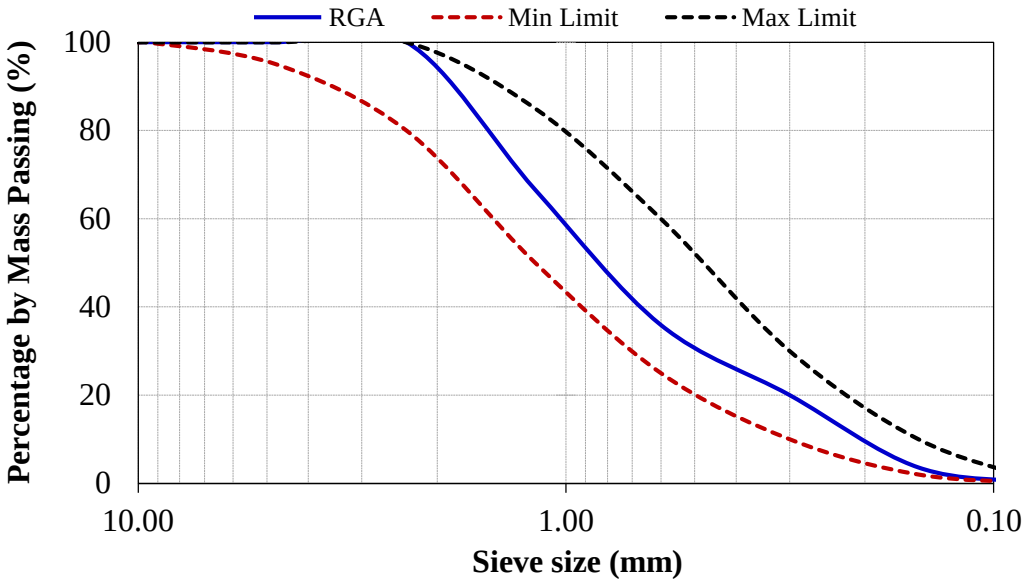

Figure 3.3 Particle size distribution of recycled glass aggregate

(a) The collected recycled glass before cleaning, crushing and sieving

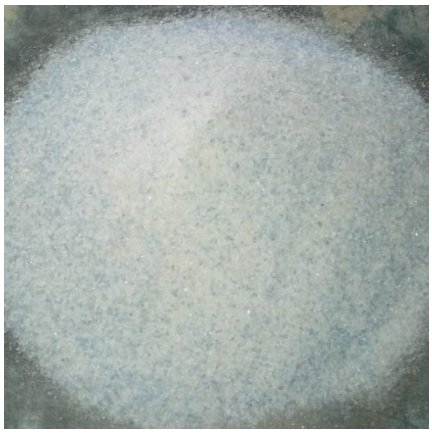

(b) Recycled glass aggregate after cleaning, crushing and sieving

Figure 3.4 Recycled Glass

3.2.5 Plastic Optical Fiber

The optical fibers used were made of polymethyl methacrylate (PMMA) with an outer diameter of 2 mm and 3 mm. The cladding material of the optical fiber was fluororesin. The core refractive index and the numerical aperture of the fiber were 1.49% and 0.5 respectively. The effective bending radius was ten times greater than the diameter of the fiber and its operating temperature ranges -40 ºC ~ +70 ºC. The fiber was non-conductive and, its refractive index profile was a step index. At 650 nm wavelength,

the white light transmittance loss rate of the fiber was less than 350 dB/km. The specification of POF is given in Table 3.9.

Table 3.9 Specification of the plastic optical fiber (POF)

Description	Property
Numerical Aperture	0.5
Core material	Polymethyl methacrylate (PMMA)
Cladding material	Fluororesin
Outer diameter (Ø)	2mm and 3mm
Appearance/ colour	Transparent, smooth
Refractive index profile	Step-index
Core refractive index (%)	1.49
Heat transfer	No
Conductivity	No
Outer jacket	No
Working temperature range	-40 ºC ~ +70 ºC
Allowable bending radius	≥10xØ
Elongation rate	≥4

3.2.6 Water

Ordinary potable tap water was used in making and curing of concrete. The water was clear and did not contain any measurable quantities of inorganic component and organic substances.

3.2.7 Superplasticizer

Sika ViscoCrete-3088, locally available polycarboxylate based superplasticizer that met the requirements for high range water reducing superplasticizer's according to EN 934 - 2 (2009) was used as a chemical admixture to improve workability and maintain rheology of fresh self-compacting mortar (SCM) mixes. The properties of the Sika ViscoCrete-3088 superplasticizer are presented in Table 3.10.

Table 3.10 Properties of Sika ViscoCrete-3088 superplasticizer

Description	Property
Appearance/color	Yellowish liquid
Density (kg/l)	1.06 (at +20 °C)
pH value	5.5 ± 0.5
Chemical base	An aqueous solution of modified polycarboxylate
Dosage	0.2 – 2% by weight of cement

Source: (Sika Kenya Ltd)

3.3 Equipment

The following equipment and tools were employed in this experimental study;

- Digital balance for measuring the weight of materials and specimens
- Sieves for sieving of fine aggregate and recycled glass
- Volumetric flask for measuring the volume of superplasticizer and water
- Pycnometer for determining the specific gravity of limestone powder, fine aggregate and recycled glass aggregate
- Le Chaterlier flask for determining the specific gravity of cement
- Heavy metallic tamper for crushing of recycled glass
- 2-liter metallic container for determining bulk density of materials
- A tamping rod for tamping of filled layers during bulk density test
- Oven for drying of materials and specimens
- Mortar mixer of capacity 3 liter
- Triple - gang moulds
- Cubic moulds
- A plastic container of capacity 2 liter for sorptivity test
- Curing tank
- Length comparator and Vernier calliper for measuring of ASR expansion

- Tape measure for measuring of slump flow
- Concrete cutter for polishing of translucent concrete specimens
- Hydraulic compressive strength machine
- Flexural strength testing machine
- Mini-slump cone for determining the flowability of fresh SCM mixes
- Mini V-funnel for determining the filling ability of fresh SCM mixes
- Low-density polyethylene (LDPE) sheets for insertion of POF strands
- Plywood for the casting of translucent panels and specimens
- The linear variable differential transducer (LVDT)
- Load cell
- Strain gauge
- Data Logger
- Loading frame
- Sensor box for light transmittance test
- 100 Ω resistor
- Dual power
- 11-watt incandescent bulbs used as a source of light during light transmittance test
- Ammeter for measuring current during light transmittance test
- Light Dependent Resistors (LDR)
- Simple tools (spatula, base plate, adjustable jaw, hammer, etc.)

3.4 Experimental Program

The experimental program deployed in order to achieve the objectives of this research is depicted in Figure 3.5.

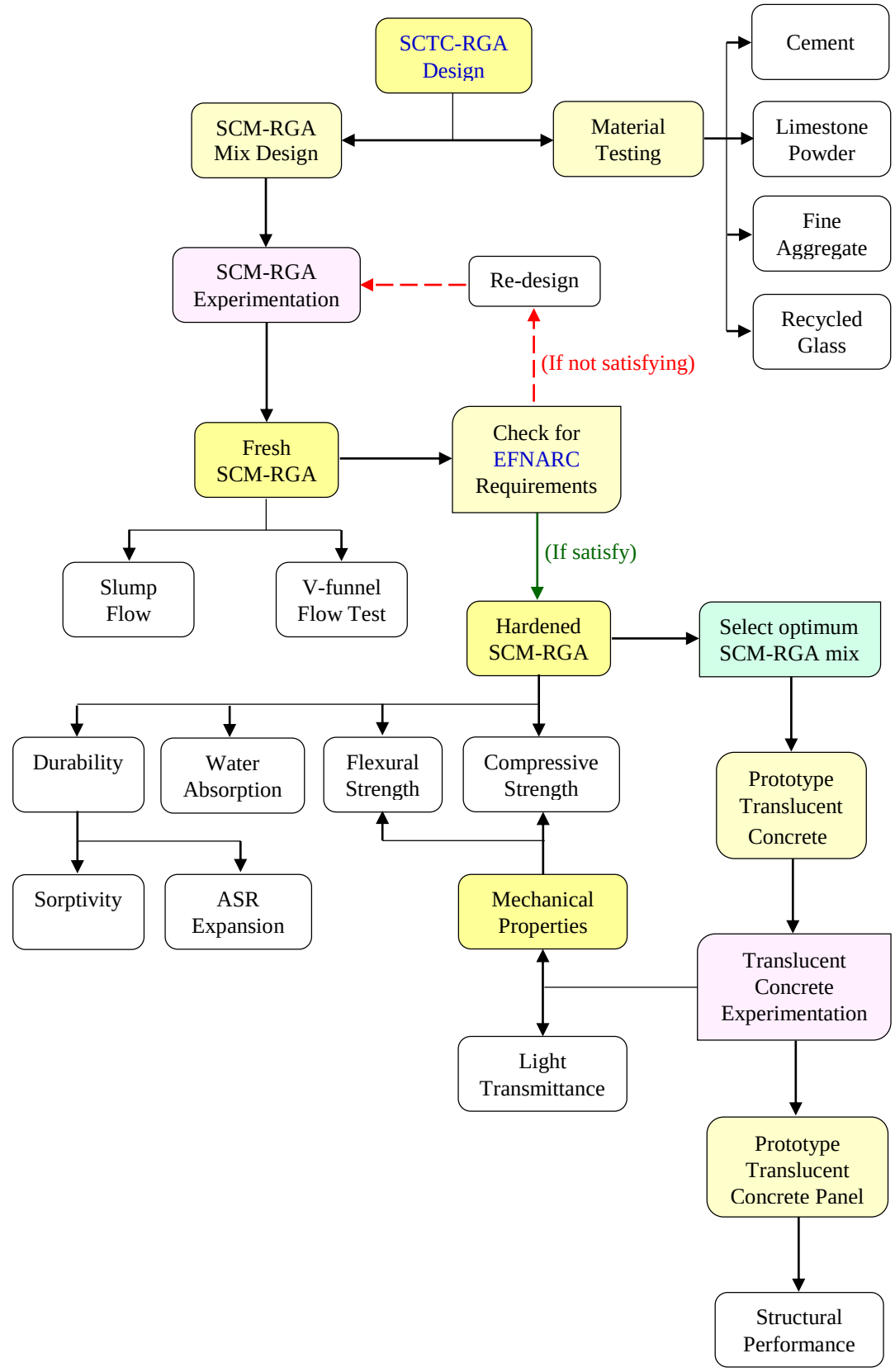

Figure 3.5 Experimental program

3.5 Mix Designs

3.5.1 Mix Formulation

The mix design of self-compacting mortar incorporating recycled glass aggregate (SCM-RGA) formulated based on Japanese Mix Design Method (Okamura & Ozawa, 1995). The parameters considered during mix design formulation includes;

- Sand to mortar volume ratio (V_S/V_M)
- Water to powder volume ratio (V_W/V_P)
- Water to cement weight ratio (W/C)
- Filler to powder weight ratio (F/P)
- Superplasticizer to powder weight ratio (S_P/P)

The SCM-RGA mix design was based on volumetric composition with subsequent conversion to proportions by weight. Mixture proportioning of SCM-RGA, per cubic meter, was obtained according to the following formulation;

For a volume of mortar, $V_M = 1\ m^3$ and a given value of (V_S/V_M), the sand volume (V_S) computed using equation (1);

$$V_S = \left(\frac{V_S}{V_M}\right) \times V_M \tag{1}$$

And for a given value of (V_W/V_P), the volume of powder and volume of water defined as given in equation (2) and (3), respectively.

$$V_P = \frac{1 - V_S}{1 + \left(\frac{V_W}{V_P}\right)} \tag{2}$$

$$V_W = \left(\frac{V_W}{V_P}\right) \times V_P \tag{3}$$

From the values of V_S, V_P and V_W, the weight values of sand (W_S), water (W_W), cement (W_C) and filler (W_F) can be computed using equation (4), (5), (6) and (7), respectively.

$$W_S = V_S \times \delta_S \tag{4}$$

$$W_W = V_W \times \delta_W \tag{5}$$

$$W_C = V_P \times \delta_C \times \left(1 - \left(\frac{F}{P}\right)\right) \tag{6}$$

$$W_F = V_P \times \delta_F \times \left(\frac{F}{P}\right) \tag{7}$$

Where; δ_S, δ_W, δ_C and δ_F are the relative density of sand, water, cement and filler, respectively.

From the given superplasticizer dosage (S_P/P), and the weight values of cement (W_C) and filler (W_F), the liquid weight of superplasticizer (W_{SP}) can be determined using equation (8).

$$W_{SP} = \left(\frac{S_P}{P}\right) \times \left(W_C + W_F\right) \tag{8}$$

The water added (W_{WA}) to the mixture should be corrected by subtracting the water content of superplasticizer and adding water to saturate the sand from a dry state, as given in equation (9):

$$W_{WA} = W_W - \left(W_{SP} \times \left(1 - \gamma_{SP}\right)\right) + \left(W_S \times A_S\right) \tag{9}$$

Where γ_{SP} and A_S are the solid content of superplasticizer and water absorption of sand, respectively.

3.5.2 Mix Proportioning

In all SCM-RGA mixes, the sand to mortar volume ratio (V_S/V_M) was kept 0.50 ($V_S/V_M = 0.50$). The filler (limestone powder) to cement weight ratio (F/C) was kept 0.20 (F/C = 0.20). Limestone powder was used as filler that constitutes 20% of the powder volume. Fine aggregate (sand) was replaced with RGA by weight at varying percentage of 0%, 10%, 20%, 30%, 40% and 50%. Water to powder volume ratio (V_W/V_P) and superplasticizer (S_P) dosage were varying until the desired mixture that fulfills the requirements of self-compactibility according to EFNARC (2002) was obtained. A total of 6 SCM-RGA mixes were proportioned and their details are given in Table 3.11.

Table 3.11 Mix design proportioning of SCM-RGA mixes

Mix Designation	W/C	Cement (kg/m^3)	Limestone Powder (kg/m^3)	Water (kg/m^3)	Fine Aggregate (kg/m^3)	RGA (kg/m^3)	SP (kg/m^3)
RGA0%	0.40	623.76	138.61	252.48	1185.00	—	5.95
RGA10%	0.40	623.76	138.61	252.48	1066.50	118.50	6.02
RGA20%	0.40	623.76	138.61	252.48	948.00	237.00	6.02
RGA30%	0.40	623.76	138.61	252.48	829.50	355.50	6.10
RGA40%	0.40	623.76	138.61	252.48	711.00	474.00	6.18
RGA50%	0.40	623.76	138.61	252.48	592.50	592.50	6.25

For the production of translucent concrete, the filler (limestone powder) to cement weight ratio (F/C) was increased from 0.20 to 0.30 to decrease the amount of cement so as to attain ordinary strength for general civil engineering infrastructure construction application. The mix design proportioning of SCM-RGA20% for production of translucent concrete detailed in Table 3.12.

Table 3.12 Mix design proportioning of SCM-RGA20% mixture for production of translucent concrete (TC-RGA20%)

Mix Designation	W/C	Cement (kg/m^3)	Limestone Powder (kg/m^3)	Water (kg/m^3)	Fine Aggregate (kg/m^3)	RGA (kg/m^3)	SP (kg/m^3)
TC-RGA20%	0.46	547.42	208.54	251.74	948.00	237.00	6.80

The code and sample number used in the mix designation of mixtures in this study are outlined in Table 3.13.

Table 3.13 Code and sample number of the mix design

Mix Designation	**Recycled Glass Aggregate (%)**	**Remark**
RGA0%	0	SCM mixture
RGA10%	10	SCM mixture
RGA20%	20	SCM mixture
RGA30%	30	SCM mixture
RGA40%	40	SCM mixture
RGA50%	50	SCM mixture
LT-RGA20%	20	TC mixture

(SCM: self-compacting mortar, TC: translucent concrete)

3.6 Mixing Procedure

The constituent materials were weighed properly, based on the mix design. The powder, fine aggregate or/and recycled glass aggregate were first placed in a standard mortar mixer and mixed thoroughly in the dry state. After mixing for 1 minute, 80% of the required water added to the mixer and continue mixing for 1 minute more under the normal speed of the mixer. Then the required superplasticizer and 20% of remaining water were introduced and the mixing continued further for 5 minutes. For dispersibility between superplasticizer and the matrix, the mix was kept resting for 2 minutes. Finally, the mixture mixed for 1 minute before being discharged. The

standard mixer used was complying with BS EN 196-1 (1995). The mixing procedure and standard mortar mixer used in this study are shown in Figure 3.6 and Figure 3.7.

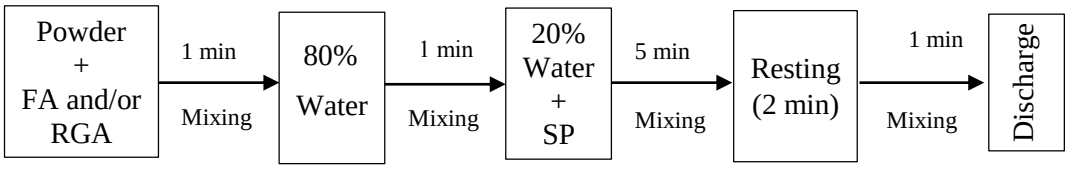

Figure 3.6 Mixing procedure

Figure 3.7 Standard mortar mixer

3.7 Experimental Methods for SCM-RGA

3.7.1 Tests on Fresh SCM-RGA mixes

The rheological properties of fresh SCM-RGA mixes influence the handling, placing, consolidation, furthermore the properties of hardened SCM. The rheological properties of fresh SCM-RGA mixes were assessed by conducting mini-slump flow and V-funnel flow time tests. All SCM-RGA mixes were designed to satisfy the flow properties (flowability and filling ability) requirements of self-compacting mortar set by EFNARC (2002).

3.7.1.1 Slump Flow Test

The deformability of SCM-RGA mixes was evaluated by slump flow test using mini-slump cone (refer to Figure 3.8). The slump flow test was performed according to EFNARC (2002) and the spread diameter (d_m) of all the mixtures kept within the range of 250 ± 10 mm. The flow of the mixtures was also visually observed for bleeding, segregation, and inconsistency. The deformability of SCM-RGA mixes was expressed in terms of relative flow area (Γ_m) using equation (10).

$$\Gamma_m = \left(\frac{d_m}{d_o}\right) - 1 \qquad (10)$$

Where; d_o is the diameter of the base of truncated mini-slump cone (d_o =100 mm), and d_m is the mean value of the two measured perpendiculars spread diameters of d_1 and d_2, $d_m = (d_1+d_2)/2$.

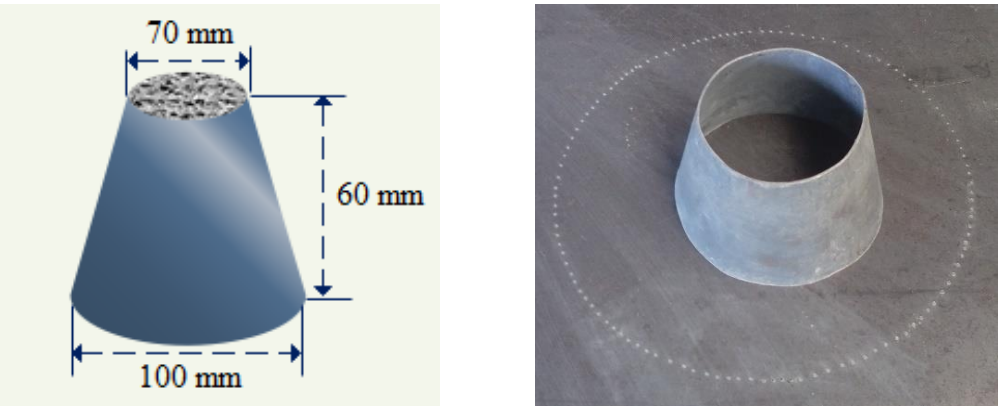

Figure 3.8 Mini-slump cone

3.7.1.2 V-funnel Flow Time Test

The viscosity and passing ability of SCM-RGA mixes were examined by conducting V-funnel flow time test according to the procedures outlined in EFNARC (2002). This test is a feasible and simple method to select suitable water to powder ratio of the mixtures using V-funnel (see Figure 3.9). The permissible value of the flow time (t) is

9 ± 2 seconds. The passing ability of SCM-RGA mixes can be expressed in terms of relative flow velocity (R_m) as given in equation (11).

$$R_m = \frac{t}{10} \tag{11}$$

Figure 3.9 Mini V-funnel

3.7.2 Tests on Hardened SCM-RGA mixes

3.7.2.1 Flexural Strength

The flexural strength of hardened SCM-RGA's was determined at 3, 7, 14 and 28 days according to ASTM C348 (2002). After the desired SCM-RGA mix was obtained, it was poured into 40x40x160 mm^3 triple – gang molds without applying any compaction. Then 24 hours after casting, the specimens were de-molded and cured in water at a temperature of 20 ± 1 ºC until the age of testing. The prism specimens were subjected to third point loading in rupture at a constant rate of 50 ± 10 N/sec. The flexural strength test setup apparatus is shown in Figure 3.10. The resulting flexural strength (modulus of rupture) of the specimens calculated using the relationship given in equation (12).

$$R_f = \frac{3FL}{2b^3} \quad (12)$$

Where; R_f is the flexural strength (N/mm^2), F is maximum applied load at fracture (N), L is the span length between the supports (mm), and b is the side of square section of the prism specimens (mm^3).

Figure 3.10 Flexural strength test apparatus

3.7.2.2 Compressive Strength

The compressive strength of hardened SCM-RGA's was determined using prism specimens broken in flexure at 3, 7, 14 and 28 days in accordance to ASTM C349 (2002). After the failure of prism specimens in bending, the two part of each broken prism were subjected to uniaxial compression stress at a constant loading of 0.25 MPa/sec. During the test, loading attachment with pedestal was used to hold the prisms properly in the machine. The compressive strength of each mix was the average of six measurements. The compression machine used in this study is shown in Figure 3.11.

Figure 3.11 Compressive strength test machine

3.7.2.3 Water Absorption by Immersion

Water absorption by immersion was determined according to ASTM C642 (2006) in three 40x40x160 mm^3 SCM-RGA specimens of each mixes after 28 days of curing. The specimens were dried in an oven for 24 hours with the temperature kept at 105 ± 5 ºC. The mass of oven-dried specimens was recorded after cooling to room temperature. Then the specimens were immersed in water at a temperature of 21 ºC for about 72 hours until a constant saturated surface-dried mass was achieved. The rate of water absorption was determined using a formula given in equation (13).

$$Water\ Absorption(\%) = \left(\frac{W_2 - W_1}{W_2}\right) \times 100 \qquad (13)$$

Where; W_1 is the weight of oven-dried test specimen, and W_2 is the wet weight of the test specimen.

3.7.3 Tests on Durability of SCM-RGA mixes

3.7.3.1 Sorptivity

The sorptivity coefficient of specimens was obtained by capillary water absorption test carried out according to ASTM C1585 (2004). For each SCM-RGA mixes three 50x50x50 mm^3 specimens were prepared and the test was carried out after 28 days of curing. The specimens were dried in an oven at 110 ± 5 ºC temperature for 24 hours. Then after the specimens cooled to room temperature, the four lateral faces of the specimens were sealed properly using box sealing tape to hinder the entrance of moisture while the opposite faces left open. The initial weight of the specimens was recorded after sealing and then submerged in water about 5 ± 1 mm above the bottom face. The weight gain due to sorption was determined by weighting the submerged specimen at a definite interval of time 5, 10, 30 minutes, 1, 2, 3, 4 and 5 hours. The sorptivity coefficient can be defined by the relationship given in equation (14).

$$k = \frac{\left(\frac{\Delta W}{A \times \delta_w}\right)}{\sqrt{t}} \tag{14}$$

Where; k is sorptivity coefficient ($mm/h^{1/2}$), ΔW is the amount of adsorbed water (g), A is the wetted area (mm^2), δ_w is the density of water (10^{-3} g/mm^3), and t is the time (h) at which the submerged weight was determined.

The value of k was obtained from the slope of the linear relationship between cumulative water absorption (ΔW/A) in (g/mm^2) and time $\sqrt{t}$ in ($h^{1/2}$) by using regression analysis in MS excel. The sorptivity (capillary water absorption) test set-up is illustrated in Figure 3.12.

Figure 3.12 Sorptivity test

3.7.3.2 Expansion due to Alkali-Silica-Reaction (ASR)

The alkali-silica reactivity and expansion development of SCM-RGA mixes were evaluated by using accelerated mortar bar method based on ASTM C1260 (2007). For each mixture, three 25x25x285 mm^3 specimens were prepared in accordance with ASTM C490 (2007). After 24 ± 2 hours, the specimens were de-molded and placed in a metal container with tap water in an oven maintained at a temperature of 80 ± 2 ºC for about 24 hours. The initial length of the specimens was recorded after curing in water and then transferred to a container with 1 N NaOH solution at 80 ± 2 ºC. The change in length of the mortar bars was subsequently measured after 3, 7, 10 and 14 days of curing in 1N NaOH solution. The ASR expansion rate of the specimens was calculated using the formula given in equation (15).

$$ASR\,Expansion(\%) = \left(\frac{L_X - L_O}{L_O}\right) \times 100 \qquad (15)$$

Where; L_O is the initial length of the test specimen (mm), and L_X is the length measured after immersion in 1N NaOH (mm).

3.8 Experimental Methods for Translucent Concrete

3.8.1 Fabrication Process and Preparation of Translucent Concrete

Plastic optical fibers were cut to the required length based on volume ratio and the size of molds using pliers as shown in Figure 3.13. Plywood and low-density polyethylene (LDPE) sheet were used to fabricate a formwork. The preparation of formwork for translucent concrete is illustrated in Figure 3.14 - Figure 3.17. The LDPE sheets were properly striped according to the required spacing and drilled using 2 mm and 3 mm metal needle to fit 2 mm and 3 mm optical fiber diameters, respectively. Then the fibers were woven into the drilled LDPE sheets in a parallel arrangement and uniform distribution. The LDPE sheets then carefully inserted into the prepared plywood formwork and the proportioned self-compacting mortar (SCM-RGA20%) was poured into the formwork without applying any external mechanical vibration. After 24 hours, the LDPE sheets and plywood were removed carefully, and the projected fibers were cut-off using pliers. Finally, the specimens were cured in water at room temperature until the age of testing.

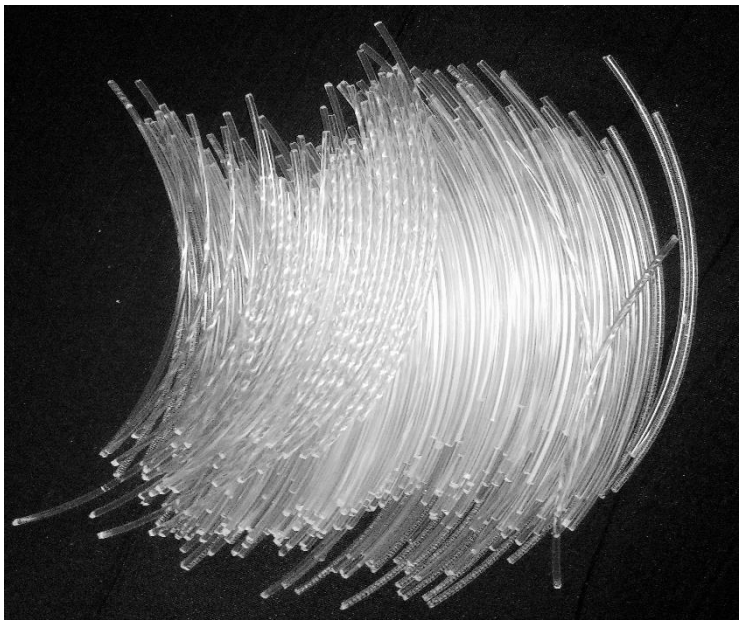

Figure 3.13 Plastic optical fibers

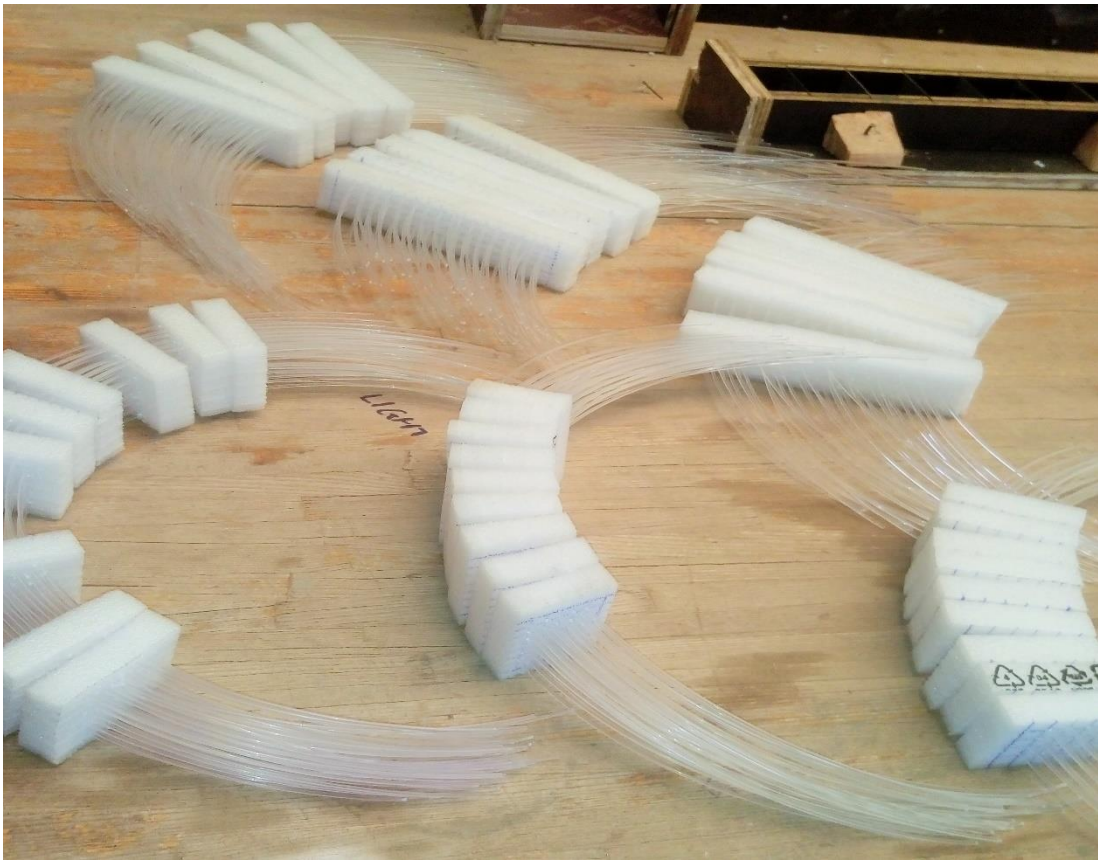

Figure 3.14 Fixing and inserting of plastic optical fibers through low-density polyethylene (LDPE) sheets

Figure 3.15 Cubic molds for compressive strength and light transmittance tests

Figure 3.16 Prism molds for the flexural strength test

Figure 3.17 Concrete casting of translucent concrete specimens

3.8.2 Tests to Investigate Mechanical Properties of Translucent Concrete

This is the second phase of the research design that deals with the mechanical properties, light transmittance and structural performance of translucent concrete. After the mix design of SCM-RGA, tests were conducted on fresh, hardened and durability properties of the mixes. An optimum SCM-RGA mix was selected based on the test results considering the strength performance and durability. Then, the next phase was the production of translucent concrete using the selected optimum mixture.

3.8.2.1 Compressive Strength

The compressive strength of translucent concrete was determined using specimens prepared on 50x50x50 mm^3 molds at 7 days and 28 days of curing according to ASTM C109 (2007). An average of three measurements was reported as the compressive strength of the translucent concrete specimens. The direction of loading was perpendicular to the arrangement patterns of optical fibers incorporated with a constant rate of loading of 0.25 MPa/sec. The typical compressive strength test and POF details are shown in Figure 3.18 and Table 3.14, respectively.

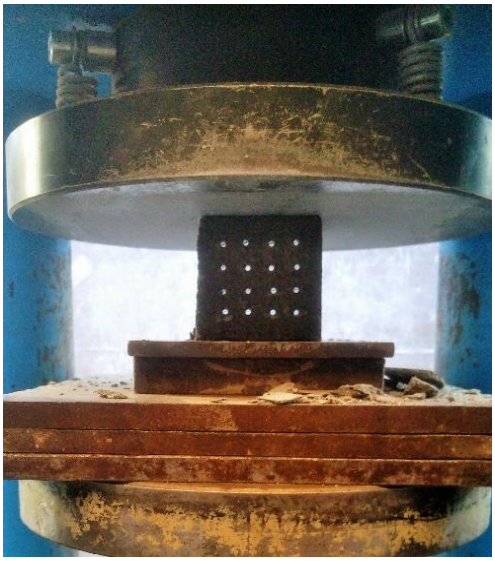

Figure 3.18 Compressive strength test on translucent concrete

Table 3.14 Details of POF integrated on translucent concrete specimens for the compressive strength test.

Sample Designation	Specimen Dimensions (mm)	POF Diameter (mm)	POF volume ratio (%)	No. of POF incorporated	POF spacing (mm)
RC-0%	50x50x50	—	—	—	—
Ø2-TC2%	50x50x50	2	2	16	10
Ø2-TC4%	50x50x50	2	4	32	7.1
Ø2-TC6%	50x50x50	2	6	48	6.2
Ø3-TC2%	50x50x50	3	2	7	12.5
Ø3-TC4%	50x50x50	3	4	14	10
Ø3-TC6%	50x50x50	3	6	21	8.3

3.8.2.2 Flexural Strength

The modulus of rupture of translucent concrete specimens was determined at 7 days and 28 days according to the procedures outlined in ASTM C348 (2002). Then overall procedures to determine the modulus of rupture of translucent concrete was similar to the flexural testing of SCM-RGA specimens. Typical specimens used for flexural testing and failure mechanism of translucent concrete are shown in Figure 3.19 (a) and (b). Moreover, the details of POF integrated on flexural specimens given in Table 3.15.

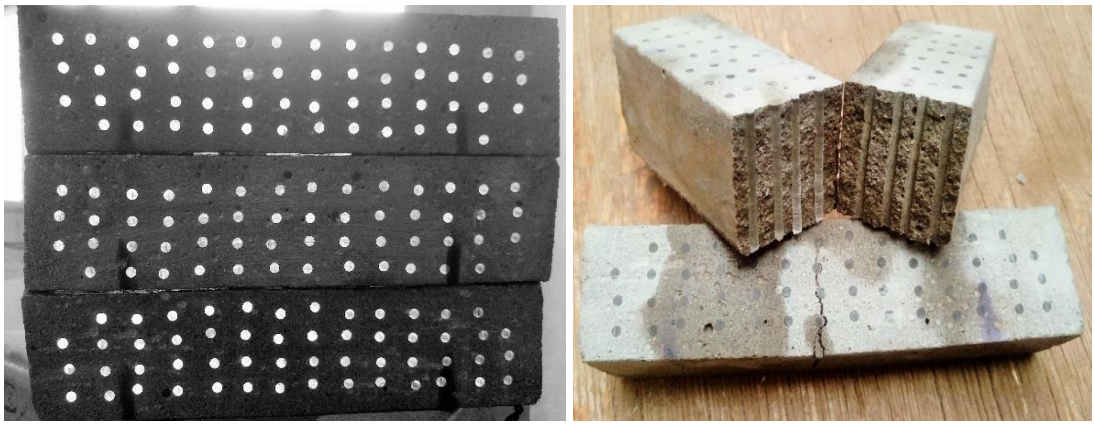

(a) Typical translucent concrete specimens for flexure testing

(b) Specimens after failure under flexural bending

Figure 3.19 Translucent concrete specimens for flexural strength test

Table 3.15 Details of POF integrated on translucent concrete specimens for the flexural strength test.

Sample Designation	Specimen Dimensions (mm)	POF Diameter (mm)	POF volume ratio (%)	No. of POF incorporated	POF spacing (mm)
RC-0%	160x40x40	—	—	—	—
Ø2-TC2%	160x40x40	2	2	41	11x10
Ø2-TC4%	160x40x40	2	4	82	9.2x6.7
Ø2-TC6%	160x40x40	2	6	122	7.5x5.7
Ø3-TC2%	160x40x40	3	2	18	16x13
Ø3-TC4%	160x40x40	3	4	36	12x10
Ø3-TC6%	160x40x40	3	6	54	11x8

3.8.3 Light Transmittance Test on Translucent Concrete

The light transmittance performance of the translucent concrete was investigated by measuring the current corresponding to the light intensity that transmitted through the prototype using electrical circuit set-up with a light dependent resistor (LDR). LDR (Photo-resistor) is a light-sensitive resistor whose resistance varies with the wavelength of the light. For this study, a sensor box with an inside dimension of 50x50x1300 mm^3 was prepared using plywood. The translucent concrete specimens were situated at the center of the sensor box and 11 W lamp was applied at varying distance of 100, 200, 300 and 400 mm. The lamp and LDR were situated in front and behind of the specimens inside the sensor box, respectively. A uniform DC voltage of 10 V was kept between the circuits and 100 Ω resistance was applied in the circuit setup. Figure 3.20 and Figure 3.21 show the schematic diagram of circuit set-up and the experimental arrangement of light transmittance test respectively.

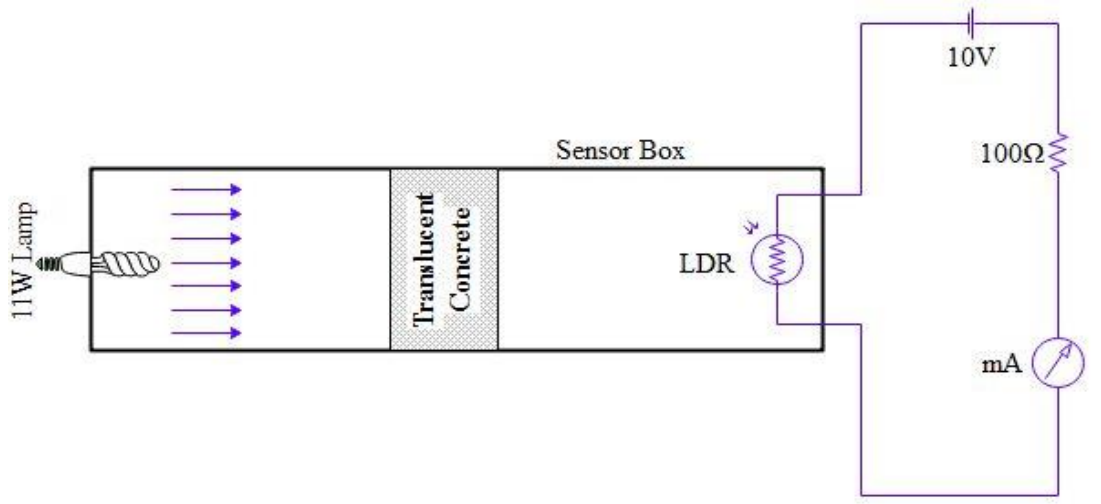

Figure 3.20 Schematic diagram of circuit setup for light transmittance test

Figure 3.21 Experimental setup and arrangement of light transmittance test

The light transmittance test of all cubic specimens was conducted after 28 days of curing. The light transmittance performance of translucent concrete was measured at distance of 100, 200, 300, 400 and 500 mm from the specimen location. Figure 3.22 demonstrates the illumination of typical translucent concrete prepared in this study. Moreover, the details of POF integrated on light transmittance cubic specimens and overall arrangement of the test setup are also presented in Table 3.15 and Figure 3.23,

respectively. The percentage of light transmitted through translucent concrete is calculated using a relationship given in equation (16).

$$LT\,(\%) = \left[1 - \left(\frac{A_1 - A_2}{A_1}\right)\right] \times 100 \qquad (16)$$

Where; A_1 is the reference current of the light intensity of the lighting source (mA) and A_2 is the current of the light intensity transmitted through the translucent concrete specimen (mA), LT is the light transmittance.

(a) Typical translucent concrete (Ø2mm, 6% POF)

(b) Translucent concrete and light transmitting testing equipment

Figure 3.22 Illumination of the translucent concrete

Table 3.16 Number of POF integrated into to the cubic specimens for light transmittance test (50x50x50 mm^3 specimen dimension).

Ø2 mm POF			**Ø3 mm POF**		
POF Volume (%)	No. of POF	Spacing (mm)	POF Volume (%)	No. of POF	Spacing (mm)
2	16	10	2	7	12.5
4	32	7.1	4	14	10
6	48	6.2	6	21	8.3

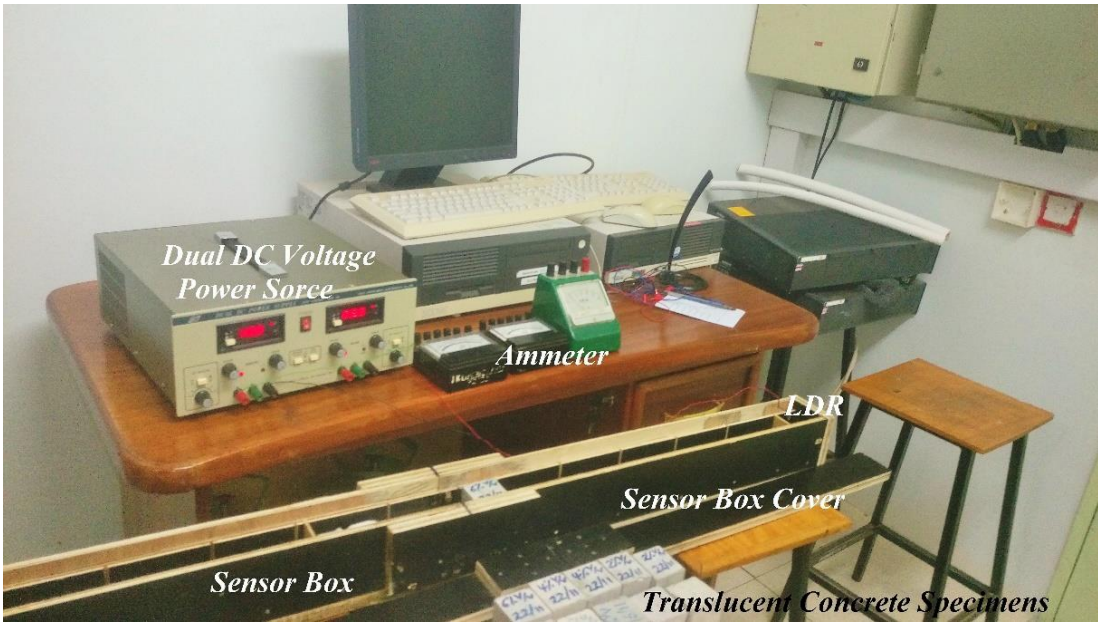

Figure 3.23 The overall arrangement of light transmittance test

3.8.4 Tests on Structural Performance of Translucent Concrete Façade Panels

From the light transmittance test results, translucent concrete reinforced with plastic optical fibers that perform better and provides sufficient light transmittance were selected for application as structural façades and architectural walls in green buildings. To investigate the structural performance of translucent concrete façades/walls, pre-cast translucent concrete panels were prepared.

3.8.4.1 Fabrication Process of Translucent Concrete Façade Panels

The structural façades/architectural wall panels were fabricated as pre-cast concrete reinforced with plastic optical fibers. The dimension of each panel was 300x100x150 mm^3. The total length of the panels was 400 mm with an effective span length of 300 mm. the width and depth of each panel were 100 mm and 150 mm, respectively. Orthogonal array holes were drilled in low-density polyethylene (LDPE) sheets according to the volume ratio of optical fibers incorporated, and the optical fibers were arranged in spatial distribution. Then the prepared low-density polyethylene (LDPE) sheets were fixed in plywood molds. SCM-RGA20% mix was poured into the molds

without applying any external vibration. After 24 ± 2 hours of casting, the specimens were de-molded and cured in water at a temperature of 20 ± 1 ºC until the age of testing. Generally, three samples were prepared for three different panels including reference concrete panel, translucent concrete panels containing 2mm and 3 mm POF diameter of 6% volume ratio and 3 mm POF diameter of 6% volume ratio. Details of the translucent concrete panels and the prepared panels are presented in Table 3.17 and Figure 3.24. The panel designation RCP is the reference concrete panel without optical fibers, whereas TCP-2 and TCP-3 refer to translucent concrete panels with 2 mm and 3mm optical fibers, respectively. Moreover, the pre-cast translucent concrete panel dimensions are illustrated in Figure 3.25.

Table 3.17 Details of POF integrated on translucent concrete panels

Panel Designation	Panel Dimensions (mm)	POF Diameter (mm)	POF volume ratio (%)	No. of POF incorporated	POF spacing (mm)
RCP	300x100x150	—	—	—	—
TCP-2	300x100x150	2	6	860	7.5x6.5
TCP-3	300x100x150	3	6	382	10.3x10.2

Figure 3.24 Pre-cast translucent concrete panel specimens

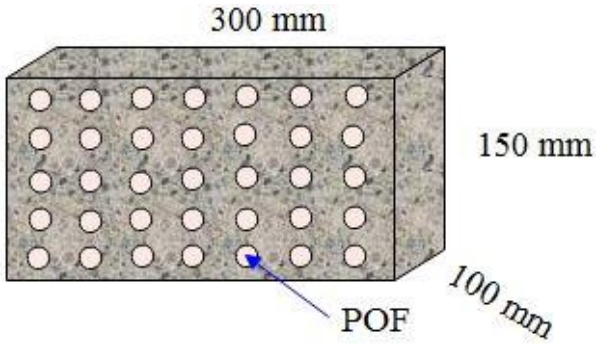

Figure 3.25 Pre-cast translucent concrete panel dimensions

3.8.4.2 Test Setup and Instrumentation of Translucent Concrete Façade Panels

Each panel was tested in three-point bending at age of 28 days according to JSCE-SF4 (1984). The test setup consisted of two steel column frames bolted to the reaction floor, and a horizontal steel beam acting as loading frame bolted to the two columns. A steel plate was placed on the concrete floor center to the loading frame. Two steel reaction rollers were attached to the steel plate where the panels were resting. Hydraulic jack and load cell were placed between the panel and loading frame. The details of the setup are shown in Figure 3.26.

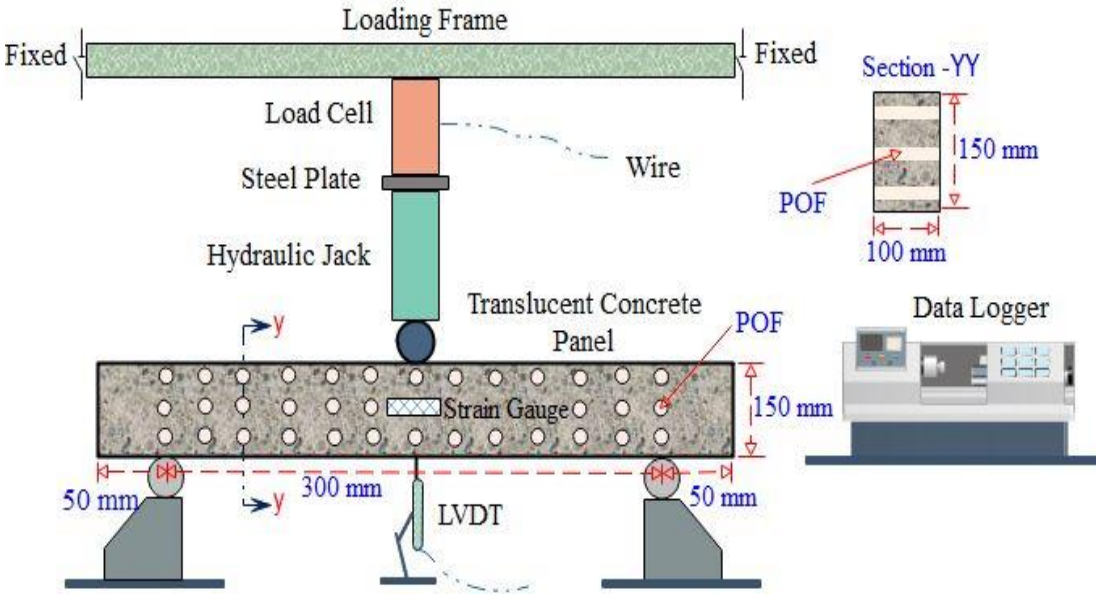

Figure 3.26 Setup detail for structural performance of translucent concrete panel

The applied load on the panels was measured using a load cell placed directly above the hydraulic jack. The midspan deflection of the panels was determined using a 100 mm linear variable differential transducer (LVDT) placed at the bottom face. Midspan strain was measured with electrical resistance strain gauge mounted at the mid-span of the panel. The experimental test setup is shown in Figure 3.27 and Figure 3.28.

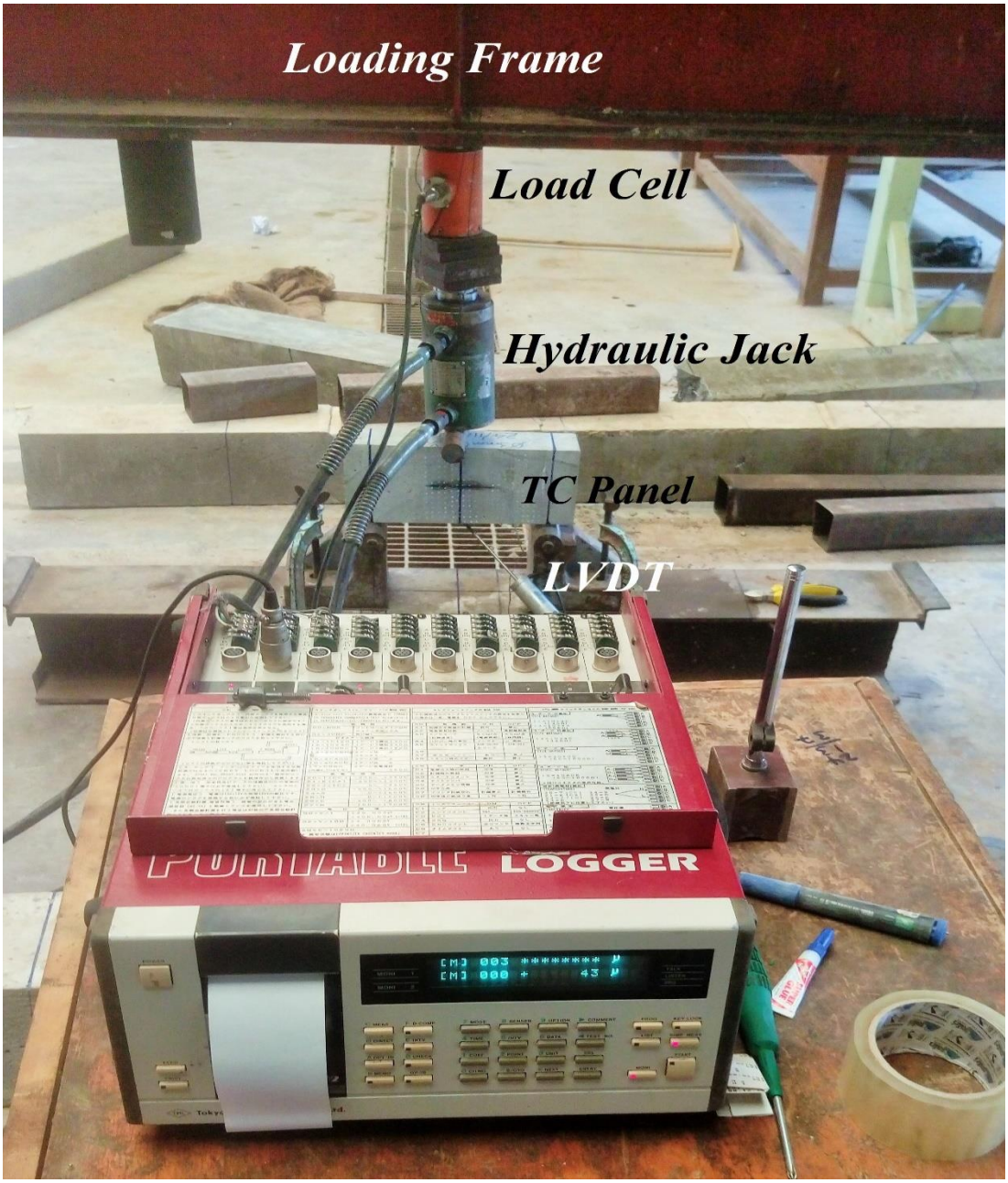

Figure 3.27 Experimental test setup arrangement of structural performance of translucent concrete panel

Figure 3.28 Structural performance test of translucent concrete panel

3.8.4.3 Flexural Toughness of the Translucent Concrete Façade Panels

The effect of adding POF in concrete's energy absorption capacity (flexural toughness) was analyzed using JSCE-SF4, which is a common Japanese absolute approach of flexural toughness test method. The two toughness parameters used in JSCE-SF4 are flexural toughness (T_{JSCE}) and flexural toughness factor (F_{JSCE}). Flexural toughness is the total energy required to deflect the POF reinforced translucent concrete up to (δ_{tb}= ℓ/150) deflection at the mid-span determined from the load-deflection (P-δ) curve in flexure, as shown in Figure 3.29. While the flexural toughness factor is the equivalent flexural strength or nominal tensile stress corresponding to the noted value of flexural toughness. The flexural toughness and toughness factor were calculated using relationships presented in equation (17 and 18).

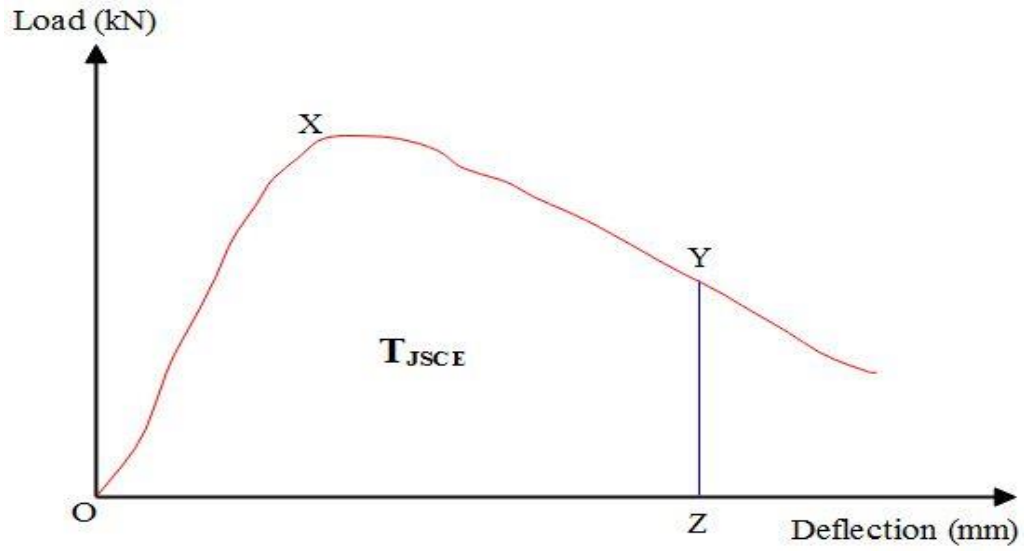

Figure 3.29 JSCE-SF4 flexural toughness and toughness factor definition

$$T_{JSCE} = T_b = AREA_{OXYZ} \tag{17}$$

$$F_{JSCE} = \sigma_b = \frac{T_b}{\delta_{tb}} \times \frac{\ell}{bh^2} \tag{18}$$

Where; T_{JSCE} (T_b) is absolute flexural toughness (kN.mm), F_{JSCE} (σ_b) flexural toughness factor (N/mm^2), ℓ is span length of the panel (mm), δ_{tb} is mid-span deflection (ℓ/150), b is the width of the panel (mm) and, h is the depth of the panel.

3.8.4.4 Load Analysis of the Translucent Concrete Façade Panels

The load and moment carrying capacity, bending stress, shear stress and normal stress of the translucent concrete façade panels were experimentally analyzed using the test results of the three-point flexural loading. The support condition of the panel was assumed as a simply supported system. Based on this assumption the resulting bending moment at the mid-span and the support reaction were calculated using equation (19) and equation (20), respectively.

$$M = \frac{P\ell}{4} \tag{19}$$

$$R = \frac{P}{2} \tag{20}$$

Where; M is the bending moment (kN.mm) corresponding to the applied load, P (kN).

As the bending moment tends to deflect the panel, an internal stress tends to resist the bending. The internal bending resistance of the panel is known as bending stress. Assuming the panel material is stressed to its elastic limits and the traverse section which are plane before bending and remains plane after bending also, the bending stress was determined by using equation (21).

$$\sigma_{bending} = \frac{My}{I} \tag{21}$$

Where; $\sigma_{bending}$ is the bending stress (N/mm^2), M is the bending moment at considered section (kN.mm), I is the moment of inertia of the panel (mm^4) and y is the extreme POF distance from neutral axis (mm). The section of the panel was rectangular and,

thus the moment of inertia was calculated as ($I = bh^3/12$) and the maximum stress occurred at y_{max} from neutral axis ($y_{max} = h/2$).

The normal stresses at the considered plane of the panel were determined from a relationship given in equation (22) derived from Figure 3.30.

$$\sigma_{normal} = \frac{P}{bh} \tag{22}$$

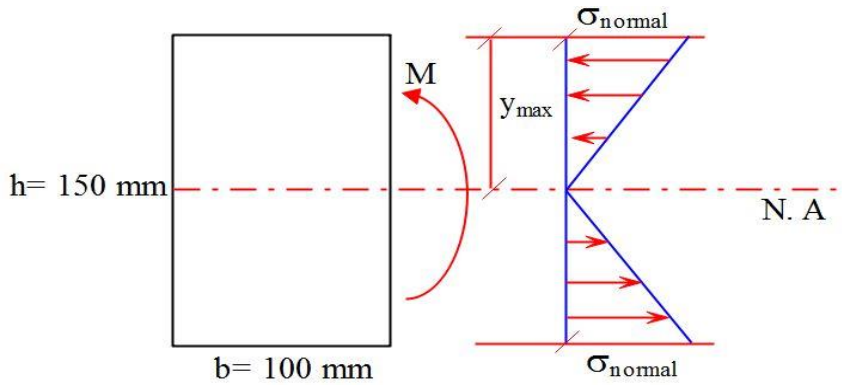

Figure 3.30 Normal stress profile of the structural panel/façade

Moreover, the shear stress of the panel was derived from Figure 3.31 assuming that the material of the panel is perfectly homogeneous and isotropic in all directions. The maximum shear stress occurred at the support where the bending moment is zero. From Figure 3.31, we can see that the shear force is distributed downward parabolically and the maximum shear stress is nearest to the neutral axis (N.A). The applied shear stress (τ_{stress}) can be defined by relationship given in equation (23).

$$\tau_{stress} = \frac{RQ}{It} \tag{23}$$

Where; τ_{stress} is the shear stress at a section (N/mm^2), R is the applied shear force at the support (kN), Q is the moment of the area of the section above neutral axis expressed in equation (24), and t is the thickness of the panel which is the same as the width, b (mm).

$$Q = \Sigma A' y' \tag{24}$$

Where; ΣA′= b*(h/2), and y′ is the centroid (y′= h/4), therefore equation (24) can be rewritten as presented in equation (25).

$$Q = \sum A' * y' = b * \left(\frac{h}{2}\right) * \left(\frac{h}{4}\right) = \frac{bh^2}{8} \tag{25}$$

Therefore, the shear stress is given in equation (23) can be rearranged as the following in equation (26).

$$\tau_{stress} = \frac{RQ}{It} = \frac{R * \left(\frac{bh^2}{8}\right)}{\left(\frac{bh^3}{12}\right) * b} = \frac{3}{2}\frac{R}{bh} \tag{26}$$

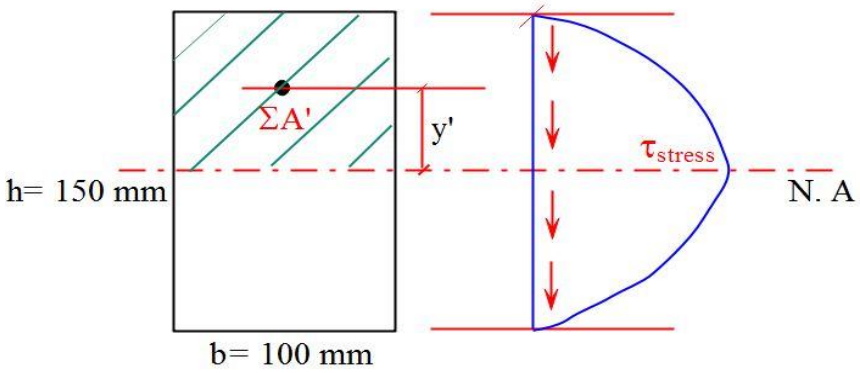

Figure 3.31 Shear stress profile of the structural panel/façade

Modulus of elasticity of the panels was also determined experimentally from the slope of the stress-strain curve and empirically using ACI 318 (2008) as given in the equation (27).

$$E_C = 0.043 W^{\frac{3}{2}} \sqrt{f_c'} \tag{27}$$

Where; E_c is the elasticity modulus (MPa), W is the density of concrete (valid for density range 1440 – 2560 kg/m^3), and f_c' is the28 days compressive strength (MPa).

CHAPTER FOUR

RESULTS AND DISCUSSION

4.1 Fresh, Hardened and Durability Properties of SCM-RGA Mixes

4.1.1 Fresh Properties of SCM-RGA Mixes

The fundamental fresh properties of SCM are flowability and filling ability. Test results of the fresh properties (slump flow and V-funnel flow time) of SCM mix incorporating RGA are presented in Table 4.1.

Table 4.1 Fresh properties of SCM-RGA mixes

Mix Designation	Slump Flow (mm)	V-funnel Flow Time (sec)
RGA0%	250	8.7
RGA10%	255	8.9
RGA20%	249	9.3
RGA30%	242	10.3
RGA40%	248	10.6
RGA50%	252	10.9
EFNARC (2002) Criteria	**250 ± 10**	**9 ± 2**

4.1.1.1 Slump Flow

The SCM mixtures were designed to deform 250 ± 10 mm conforming to EFNARC (2002) criteria, which was achieved by adjusting the dosage of superplasticizer (SP). The relative slump flow of SCM-RGA mixes is given in Figure 4.1, and as it can be seen, the values of a relative slump of all mixes are in the reference range. The experimental test results showed that as the content of RGA increased, the slump flow slightly decreased. This finding is consistent with the research outcomes, Limbachiya (2009) reported a reduction in slump flow as washed glass sand (WGS) percentage

exceeded 30%. A research conducted by Ismail & AL-Hashmi (2009) reported similar results that as the content of recycled glass increased, slump flow decreased. Similar observations were also reported by Afshinnia & Rangaraju (2016). The grain shape (sharp and angular edge) and higher aspect ratio of RGA attributed to the slight reduction of flowability of SCM mixtures (Tan & Du, 2013). Consequently, Figure 4.2 clearly indicates that to maintain the slump flow of mixtures containing glass aggregate within the range of 250 ± 10 mm, superplasticizer dosage was increased as the content of RGA increased (R^2=0.96). To understand the slump flow trendline, it is crucial to compare the slump flow of SCM-RGA10% and SCM-RGA20%. The dosage of superplasticizer of both SCM-RGA10% and SCM-RGA20% was the same (6.02 kg/m^3). However, the resulting slump flow of SCM-RGA10% and SCM-RGA20% was 255 mm and 249 mm, respectively. When the RGA content increased to 30% and the superplasticizer dosage kept constant (6.02 kg/m^3), the resulting slump flow was below the minimum limit (240 mm). Apparently, the superplasticizer dosage was increased to 6.10 kg/m^3 and the slump flow was 242 mm. This clearly indicates that incorporating of recycled glass aggregate decreased the slump flow of SCM mixes.

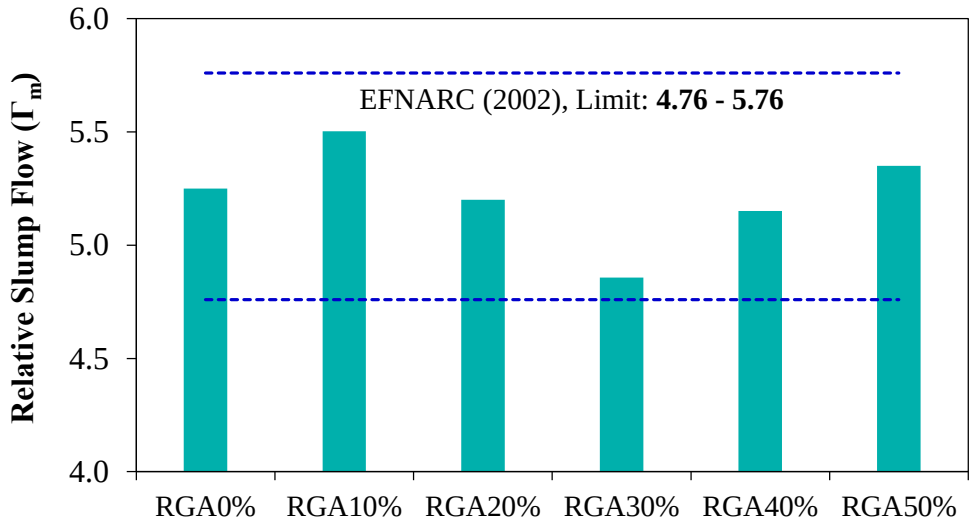

Figure 4.1 Relative slump flow of SCM-RGA mixes

The use of superplasticizer (SP) ensures deflocculating and reduces water demand of SCM mixtures and intensify intermolecular interaction of particles (Georgiadis et al., 2009). The dosage of superplasticizer for each mixture was determined based on the slump flow test to obtain the desired flowability that met self-compactibility requirements (Khaleel & Abdul Razak, 2012). The dosage of superplasticizer of all mixes was between 0.78% and 0.82% by weight of powder. Typical slump flow of SCM-RGA mixes developed in this study are shown in Figure 4.3 (a – f).

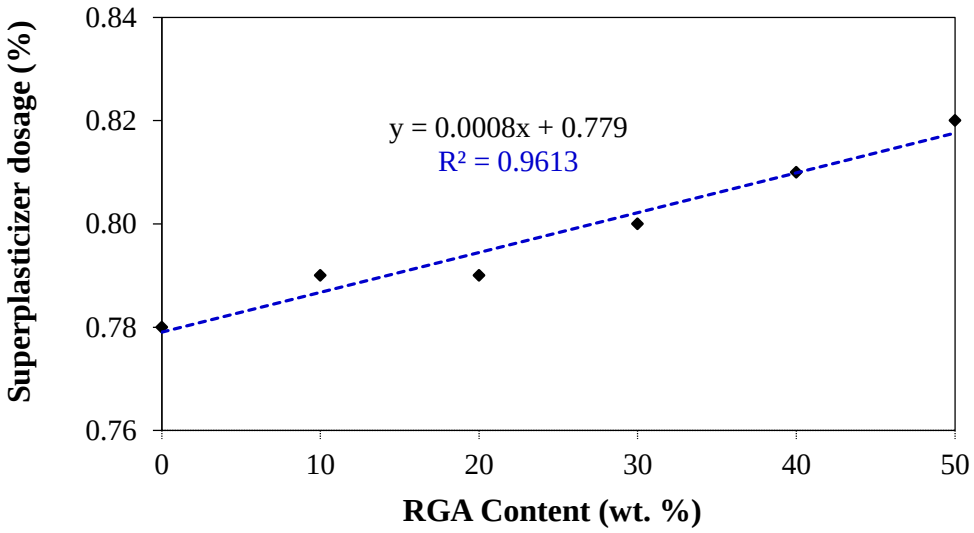

Figure 4.2 Relationship between RGA content and superplasticizer dosage

(a) SCM-RGA0% (b) SCM-RGA10%

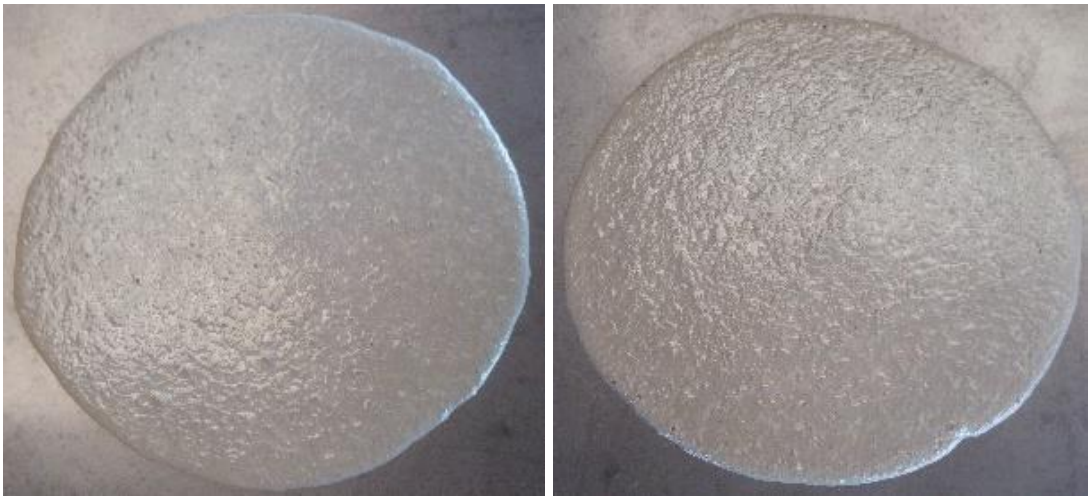

(c) SCM-RGA20% (d) SCM-RGA30%

(e) SCM-RGA40% (f) SCM-RGA50%

Figure 4.3 Typical slump flow of SCM-RGA mixes

4.1.1.2 V-Funnel Flow Time

Figure 4.4, presents the relative flow velocity of all mixes prepared in this study. The flow time of all SCM mixtures was in ranges of 8.7 – 10.9 sec. Incorporation of RGA slightly delay the flow time of SCM mixtures due to the geometrical shape of glass particles that hinders the movement of the paste matrix. It was observed that the flow time of SCM mixtures was affected by water to powder ratio (Midorikawa et al., 2009; Okamura, Ozawa, & Ouchi, 2000). To compensate and initiate better workability, limestone powder was introduced in all mixtures as filler that constitutes 20% of

powder volume. Limestone filler increases packing density of particles, lower void ratio and accelerates pozzolanic activity (Tironi et al., 2017). Furthermore, it amplifies the rate of cement hydration, lowers setting time and improves fluidity (Bentz et al., 2017). In this experimental study, the first charge of water to powder volume ratio (V_W/V_P) was considered the same value of β_p (retained water ratio) based on the recommendation of the Japanese mix design method. The value of retained water ratio (β_p=1.14) was obtained from the paste flow test given in Figure 4.6. However, after several trials mix the suitable water to powder volume ratio (V_W/V_P) was fixed at 1.02 (equivalent to water to powder weight ratio, W/P = 0.33) for all mixtures.

The flow time of the reference mixture and SCM containing 50% of waste glass content was 8.7 and 10.9 sec respectively. As illustrated in Figure 4.5, it was observed that utilization of recycled glass aggregates increased the flow time of fresh SCM-RGA mixtures. This was attributed to higher internal friction and high surface tension of glass particles (Rahma, El Naber, & Ismail, 2017). Keeping water to cement ratio constant, as the content of glass aggregates increased excess water in the mixes increased due to the fact that water absorption of glass is lower than that of fine aggregate and this phenomenon could result in bleeding and segregation of the matrix (Sharifi et al., 2015). In this study, it was visually observed during execution of slump flow test that the slump flow spread of all mixes was very consistent and stable (see Figure 4.3).

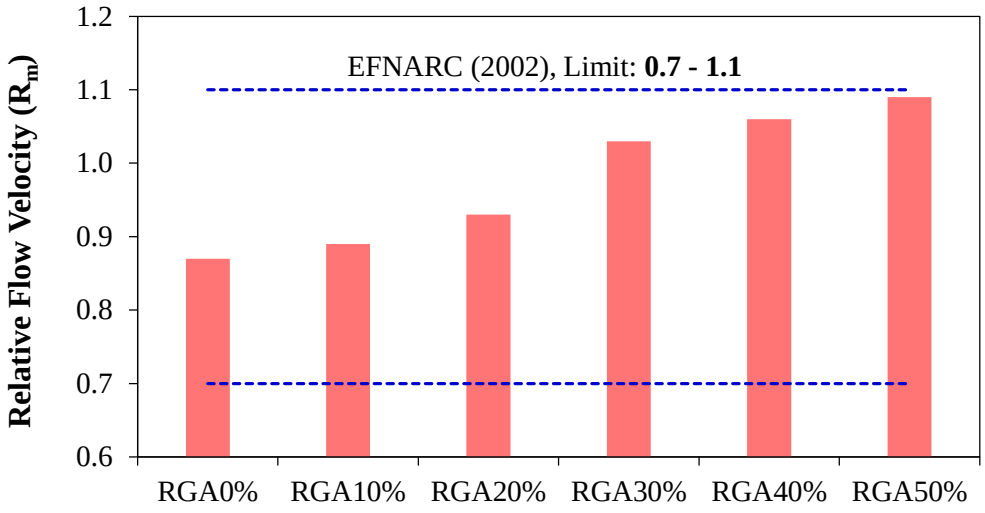

Figure 4.4 Relative flow velocity of SCM-RGA mixes

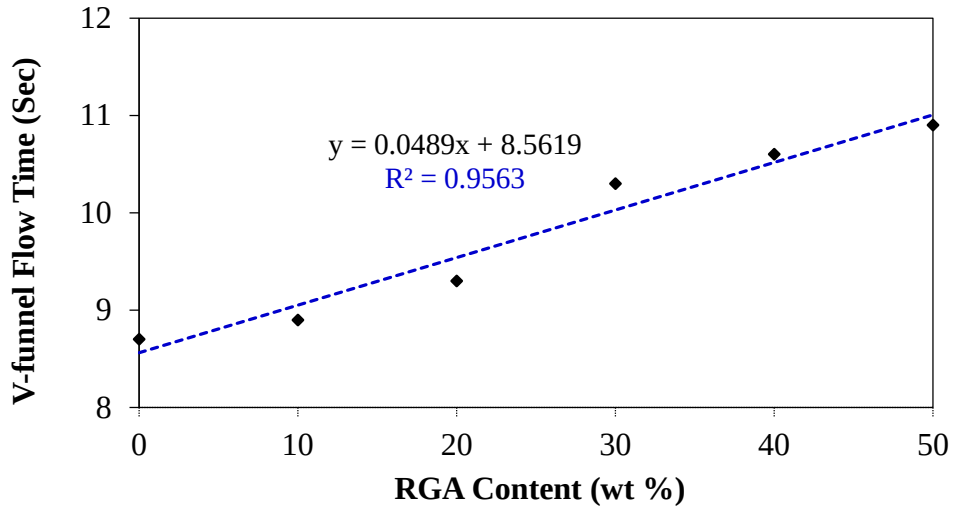

Figure 4.5 Relationship between RGA content and the flow time of SCM-RGA mixes

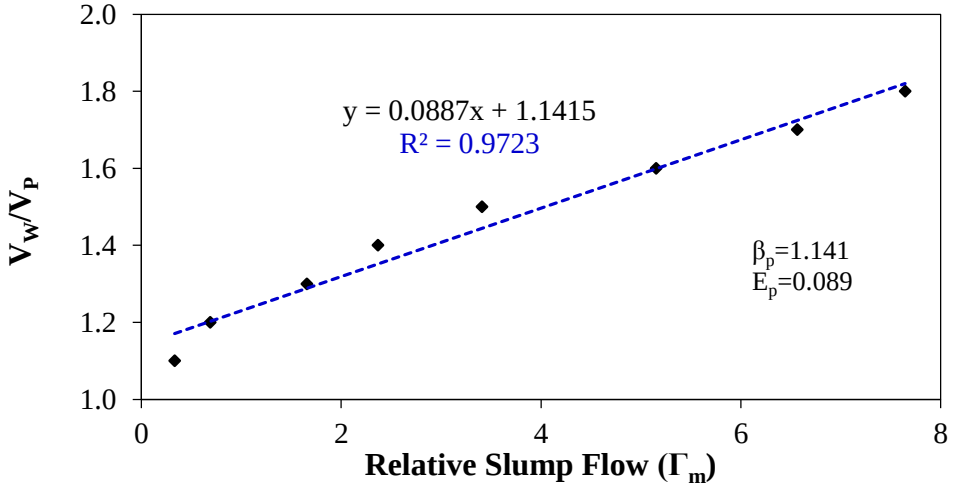

Figure 4.6 Paste design (Determination of retained water ratio, β_p)

4.1.2 Hardened Properties of SCM-RGA Mixes

4.1.2.1 Bulk Density

The hardened bulk density of all SCM-RGA specimens prepared in this study measured at 28 days are tabulated and graphically presented in Figure 4.7. Specimens containing RGA exhibits relatively lower hardened density when compared to specimens with natural fine aggregate. This reduction in density could be due to the fact that particle density of RGA used in this research were 1.3% lower than that of natural fine aggregate (Almesfer & Ingham, 2014; Ismail & AL-Hashmi, 2009; Kou & Poon, 2009; Penacho, De Brito, & Veiga, 2014; Tan & Du, 2013). The density of all specimens was in the range of 2347 kg/m^3 to 2386 kg/m^3. Moreover, the hardened specimens incorporating 50% RGA showed 1.6% reduction of bulk density relative to that of the reference specimens.

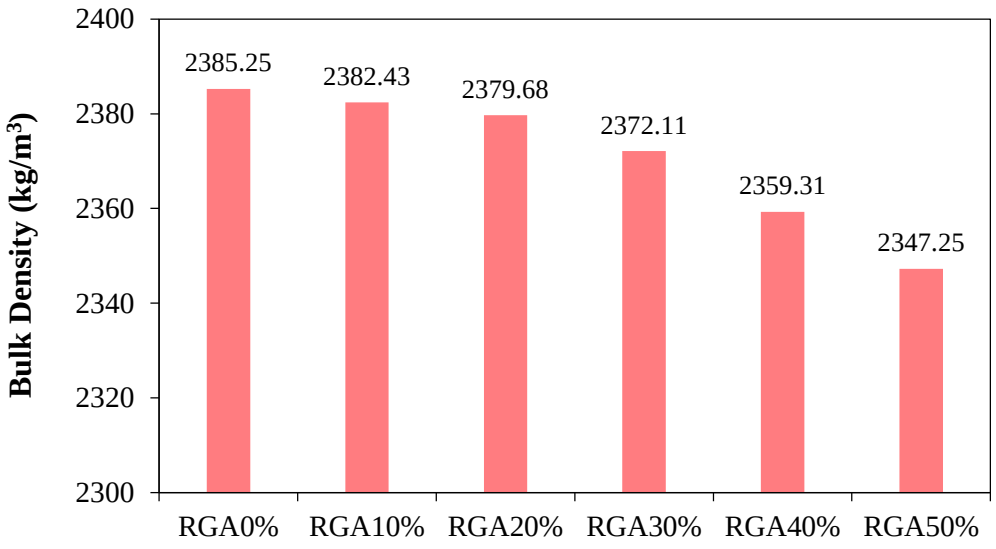

Figure 4.7 Bulk density of hardened SCM-RGA mixes

4.1.2.2 Compressive Strength

Experimental test results that show the development of compressive strength of SCM mixes at 3, 7, 14 and 28 days are presented in Figure 4.8. It is evident from the experimental results that incorporation of RGA as replacement of fine aggregate in SCM remarkably decreased compressive strength relative to control mix regardless of the percentage of replacement and age. This reduction could be attributed to lower toughness strength against fracture, smooth grain surface and weak interfacial adhesion between the cement paste matrix and glass particle (Choi, Choi, & Yang, 2016; Kou & Poon, 2009; Tan & Du, 2013; Wright et al., 2014). This finding is in concurrence with those of previous studies (Afshinnia & Rangaraju, 2016; Ali & Al-Tersawy, 2012; Almesfer & Ingham, 2014; Limbachiya, 2009; Ling et al., 2012). It was also observed that up to 30% of RGA content, the compressive strength was not significantly affected. At 28 days, the reduction in compressive strength in comparison to control mix was 1.78%, 2.52% and 6.57% for 10%, 20% and 30% replacement of RGA respectively. Similar results were also reported by (Sharifi et al., 2013; Tan & Du, 2013). On the other hand, reduction in compressive strength was apparent with the further increase in RGA content, especially beyond 30% replacement. The maximum reduction of compressive strength was 15.29% noted for 50% RGA content. The relationship between RGA content and the 28 days compressive strength given in Figure 4.9, showed a strong correlation (R^2=0.99). An average of six prism specimens represented in the data points was fitted with second order polynomial trend line regression function curve. The compressive strength test result of SCM-RGA mixes is presented in Table 4.2.

Table 4.2 Compressive strength of SCM-RGA mixes

Mix Designation	Compressive strength (MPa)			
	3 days	7 days	14 days	28 days
RGA0%	47.59	52.70	53.21	57.05
RGA10%	46.98	51.61	52.70	56.04
RGA20%	45.54	51.01	52.21	55.62
RGA30%	44.65	47.92	49.92	53.30
RGA40%	42.43	45.42	47.61	50.85
RGA50%	39.24	41.79	43.13	48.33

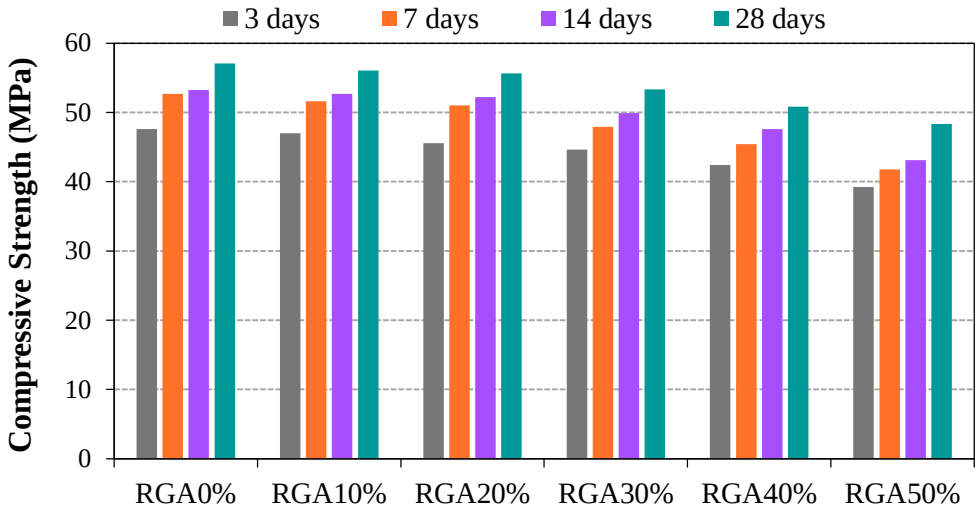

Figure 4.8 Compressive strength development of SCM-RGA mixes

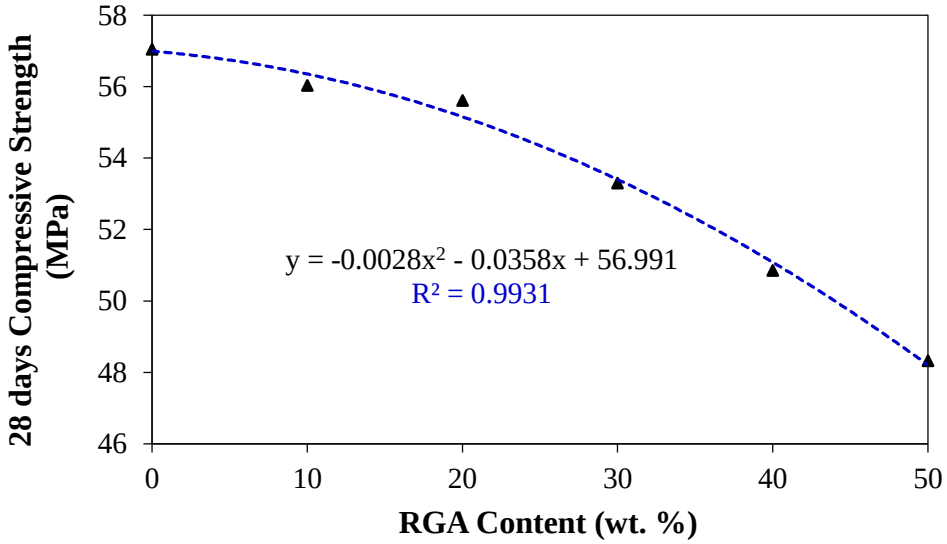

Figure 4.9 Relationship between RGA content and corresponding 28 days of compressive strength

4.1.2.3 Flexural Strength

Figure 4.10, presents the evolution of flexural strength at 3, 7, 14 and 28 days and experimental results show a trend that resembles the compressive strength results. However, the influence of RGA was not as pronounced on flexural strength as seen for compressive strength. According to experimental results, 28 days flexural strength tends to decrease by 1.38%, 2.52%, 5.97%, 9.40% and 11.70% for RGA content of 10%, 20%, 30%, 40% and 50% respectively. The results obtained in this research are consistent with other authors (Ali & Al-Tersawy, 2012; Almesfer & Ingham, 2014; Choi et al., 2016; Tan & Du, 2013) who reported that the flexural strength of mixes containing RGA decreased with respect to increases in replacement level. The average of three measurements plotted in Figure 4.11 indicates a correlation between RGA replacement level and 28 days of flexural strength with high reliability ($R^2 \approx 0.99$). Moreover, as shown graphically in Figure 4.12, the relationship between the 28 days compressive and flexural strength for SCM mixes incorporating RGA showed a strong correlation in a power regression function ($R^2=0.99$). It is evident that as compressive strength of SCM-RGA mixes increased, flexural strength also increased. Limbachiya (2009), reported a similar trend with a correlation factor of ($R^2=0.92$) for washed glass sand mixes. The flexural strength test result is shown in Table 4.3.

Table 4.3 Flexural strength of SCM-RGA mixes

Mix Designation	Flexural strength (MPa)			
	3 days	7 days	14 days	28 days
RGA0%	7.85	8.91	9.38	10.22
RGA10%	7.97	8.70	9.23	10.08
RGA20%	7.89	8.67	9.14	9.96
RGA30%	7.66	8.55	9.06	9.61
RGA40%	7.45	8.39	8.98	9.26
RGA50%	7.13	7.91	8.73	9.02

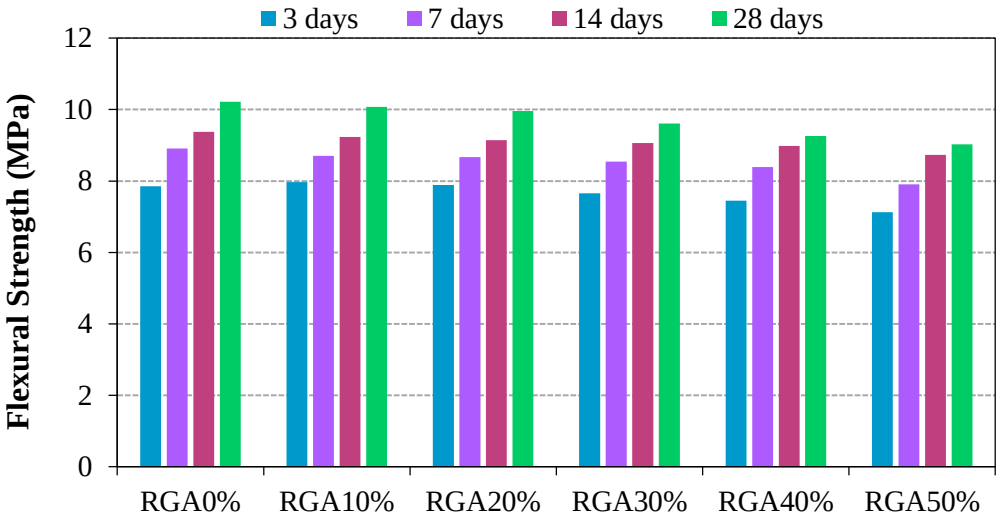

Figure 4.10 Flexural strength development of SCM-RGA mixes

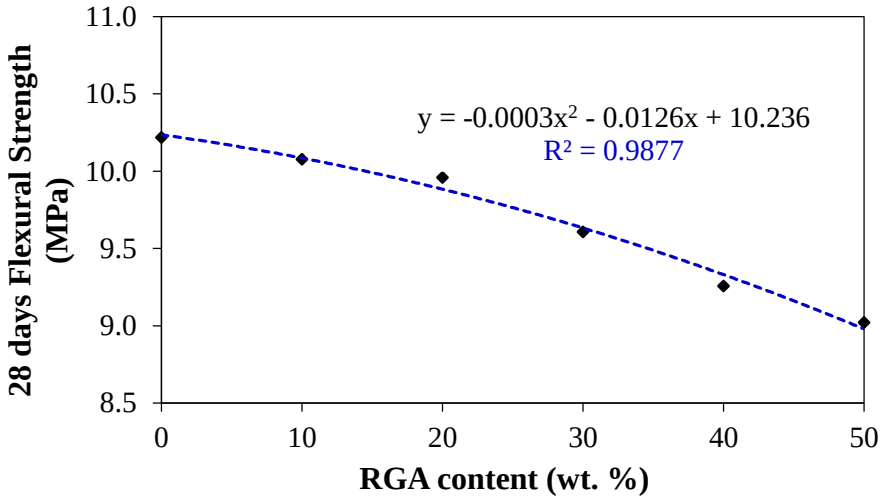

Figure 4.11 Relationship between RGA and corresponding 28 days flexural strength

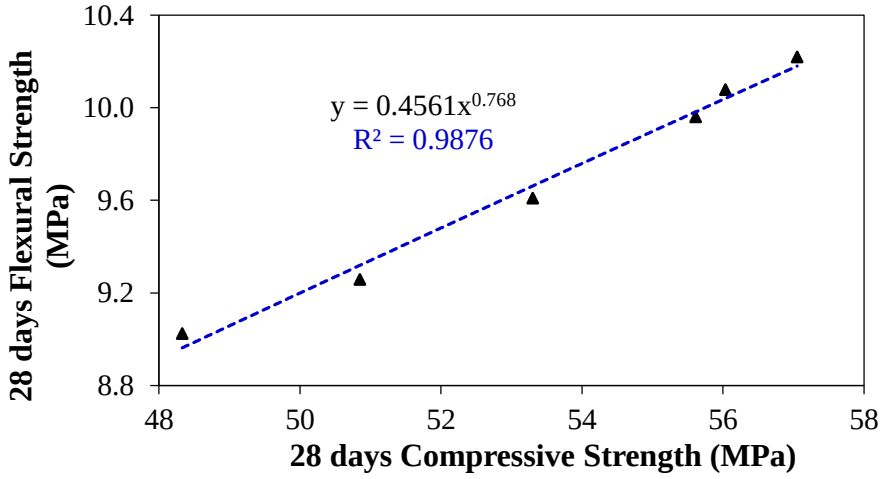

Figure 4.12 Relationship between 28 days compressive and flexural strength

4.1.2.4 Water Absorption

The water absorption by immersion test results of all SCM-RGA mixes is given graphically in Figure 4.13. It is found that inclusion of RGA slightly decreased water absorption. This reduction was due to the fact that glass does not absorb water. This result is in line with other authors (De Castro & De Brito, 2013; Ling & Poon, 2011, 2012). The maximum water absorption obtained after 72 ± 2 hours immersion was 7.11% for the control mix and the lowest was 6.29%, belonging to a mix of 50% RGA content. Based on the experimental results, the water absorption of SCM-RGA mixes tends to decrease about 0.58%, 3.30%, 7.06%, 8.32% and 11.64% corresponding to RGA content of 10%, 20%, 30%, 40% and 50% compared to the reference SCM-RGA0%, respectively. It is generally believed that good quality concrete has a water absorption of less than 10% (Medina et al., 2014). All the SCM mixes produced in this research met the requirements and can be regarded as a good quality concrete.

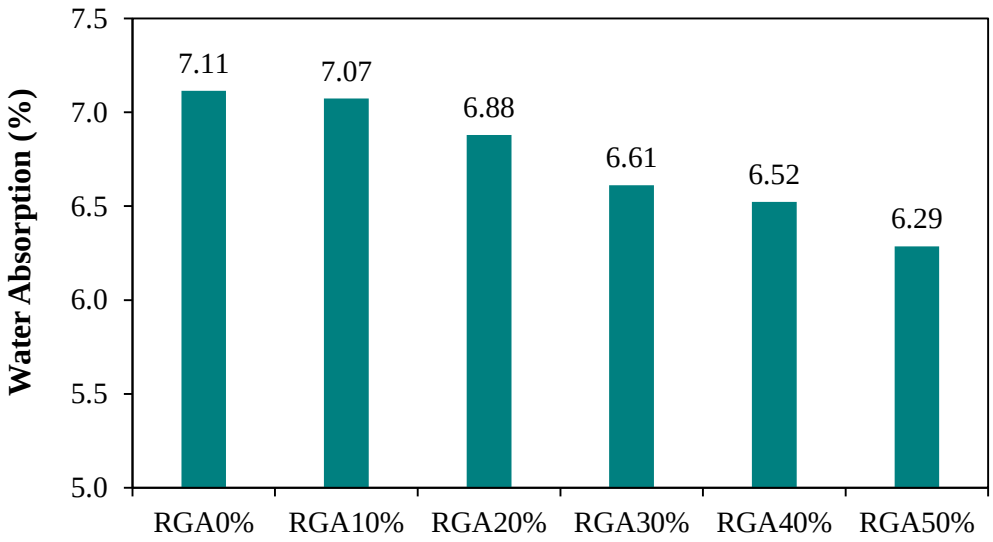

Figure 4.13 Water absorption of SCM-RGA mixes

4.1.3 Durability Properties of SCM-RGA Mixes

The durability (sorptivity and ASR expansion) test results of SCM-RGA mixes are detailed in Table 4.4.

Table 4.4 Sorptivity and ASR expansion of SCM-RGA mixes

Mix Designation	ASR Expansion (%)				Sorptivity ($mm/h^{1/2}$)
	3 days	7 days	10 days	14 days	
RGA0%	0.010	0.017	0.025	0.040	2.83
RGA10%	0.012	0.020	0.027	0.042	2.02
RGA20%	0.015	0.025	0.035	0.047	1.79
RGA30%	0.017	0.030	0.050	0.062	1.55
RGA40%	0.020	0.040	0.062	0.075	1.40
RGA50%	0.023	0.045	0.068	0.085	1.35
ASTM C1260 (2007) Criteria				**< 0.10**	
Menéndez (2007) Criteria					**≤ 3.00**

4.1.3.1 Sorptivity

When the surface of the hardened concrete is submerged in water or exposed to moisture, the concrete pores absorb water by the action of capillary suction and the rate at which water is absorbed is called sorptivity. Durability, deterioration under wet-dry cycle and service lifetime of concrete can be related to its rate of sorptivity. The results of capillary water absorption at 28 days of curing are presented graphically in Figure 4.14. The results showed that sorptivity values significantly decreased as the content of RGA increased due to lower moisture intake nature of glass particles compared to natural fine aggregates. Similar findings were reported by some other authors (De Castro & De Brito, 2013; Ling et al., 2012; Sikora et al., 2017; Wright et

al., 2014). The sorptivity value of the reference and 50% RGA specimens was 2.83 mm/$h^{1/2}$ and 1.35 mm/$h^{1/2}$ respectively. The sorptivity value of a mix containing 50% RGA decreased by 52.3%. Figure 4.15, shows cumulative water absorbed per unit area (g/mm^2) versus square root of time ($h^{1/2}$). The sorptivity value for each mix was determined from the gradient of linear trend line graph given in Figure 4.15 by using regression analysis. Furthermore, there exist a relationship between sorptivity coefficient and both 28 days of compressive and flexural strength plotted in Figure 4.16 and has shown good correlation. The experimental result clearly reveals for mixes containing RGA both strength and sorptivity values decreased as the content of RGA increased. This could be explained as the strength of SCM specimens decreased due to weak interfacial adhesion between glass particle and paste matrix, whereas sorptivity decreased due to impermeable nature of glass. Finally, according to Menéndez, Bonavetti & Irassar (2007), a concrete with less than 3 mm/$h^{1/2}$ of sorptivity value is regarded as durable concrete. The sorptivity value ensures the minimum concrete cover of 15 mm for reinforcement steel bars in reinforced concrete is sufficient to prevent corrosion. The value of sorptivity that is 3 mm/$h^{1/2}$, defined as water could penetrate to a depth of 15 mm in 24 hours rain that guarantees minimum concrete cover. On the ground of this suggestion, the SCM-RGA mixes prepared in this research could be considered as durable since they exhibited a sorptivity coefficient of lower than 3 mm/$h^{1/2}$.

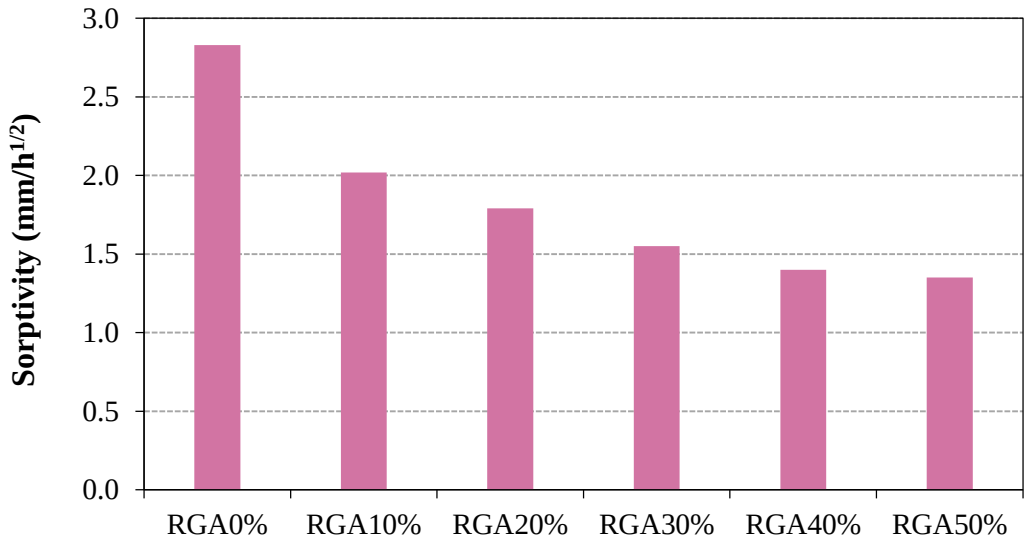

Figure 4.14 Sorptivity coefficient of SCM-RGA mixes

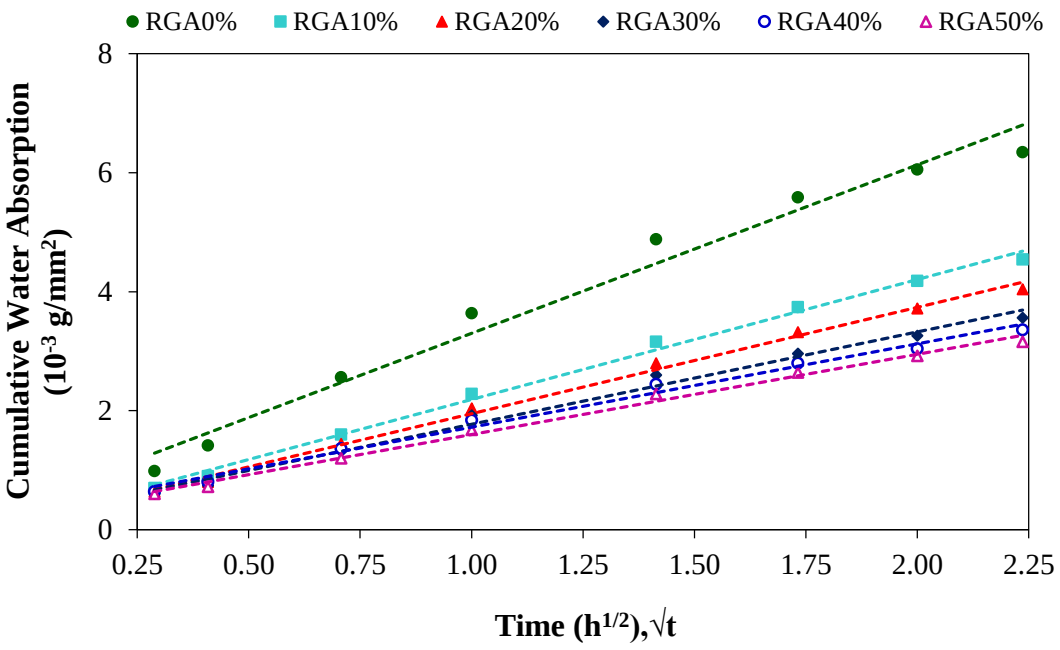

Figure 4.15 Evolution of cumulative capillary surface water absorption of SCM-RGA mixes

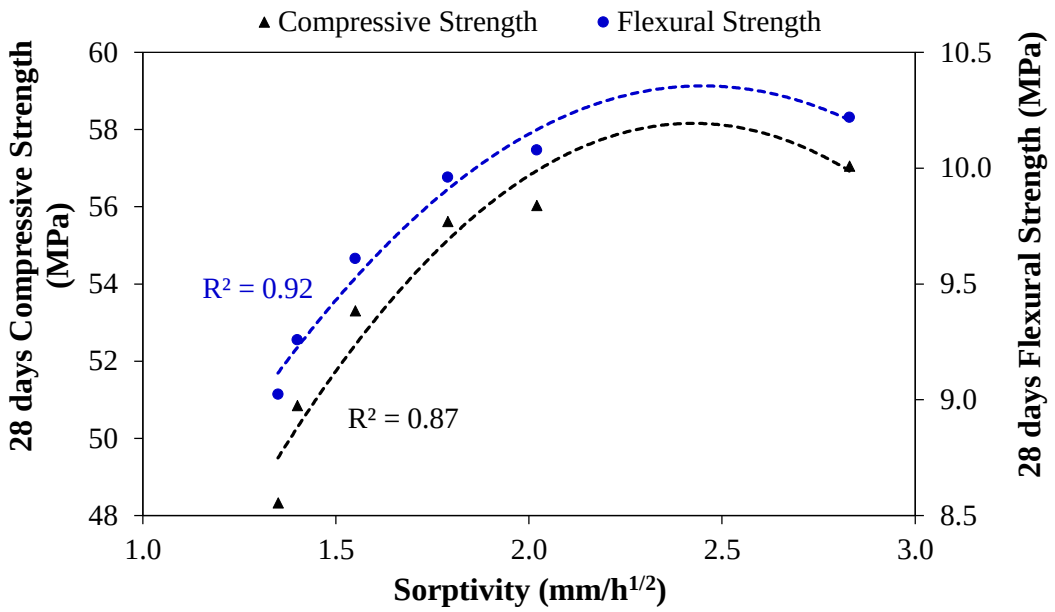

Figure 4.16 Relationship between the sorptivity value, and the 28 days compressive and flexural strength

4.1.3.2 Expansion due to Alkali-Silica Reaction (ASR)

The mechanism of ASR is the chemical process between siliceous aggregate and hydroxyl ion in hardened concrete that leads to the evolution of viscous alkali-silicate gel (Rajabipour et al., 2010). The formation of the alkali-silicate gel increases the volume of concrete i.e. exerts expansion pressure inside and causes potential cracks and disruption (Corinaldesi et al., 2016; Du & Tan, 2013; Maraghechi & Al., 2012). The accelerated mortar bar test results showed the expansion of specimens due to ASR measured at 3, 7, 10 and 14 days are graphically given in Figure 4.17 and Figure 4.18. It was clearly noted that as the content of RGA increased, ASR expansion also increased. This result is in concurrence with other studies (Kou & Poon, 2009; Limbachiya, 2009; Ling & Poon, 2012; Saccani & Bignozzi, 2010; Yuksel et al., 2013). Although the ASR expansion in mortar bars incorporating RGA increased substantially with age, expansion of all specimens at 14 days were below 0.1%, which could be considered as innocuous according to ASTM C1260 (2007). Based on visual

observations, specimens containing 40% and 50% RGA showed slight mapping micro-cracks on the surface after 14 days of curing in 1N NaOH solution, while all other specimens were sound.

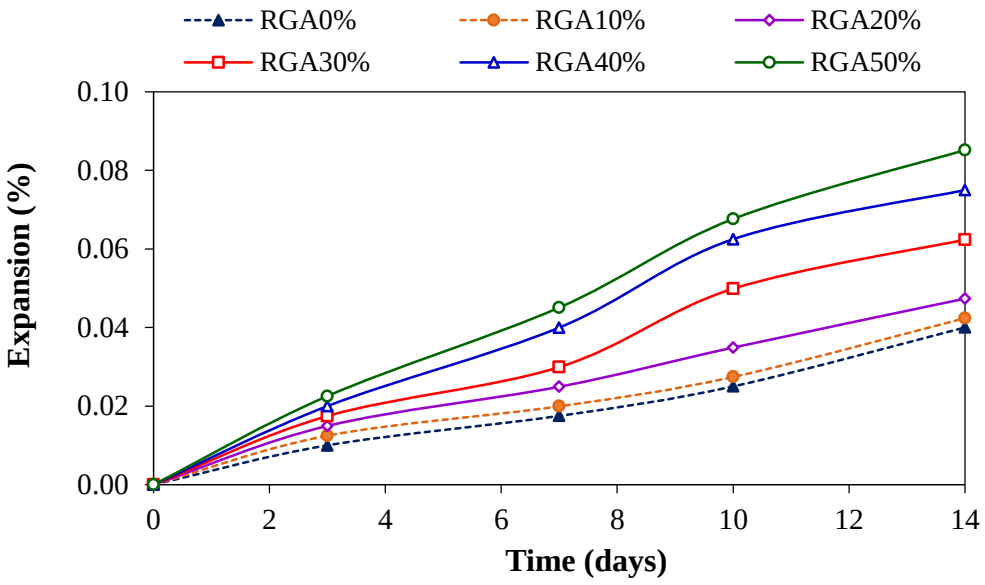

Figure 4.17 ASR expansion of SCM-RGA mixes

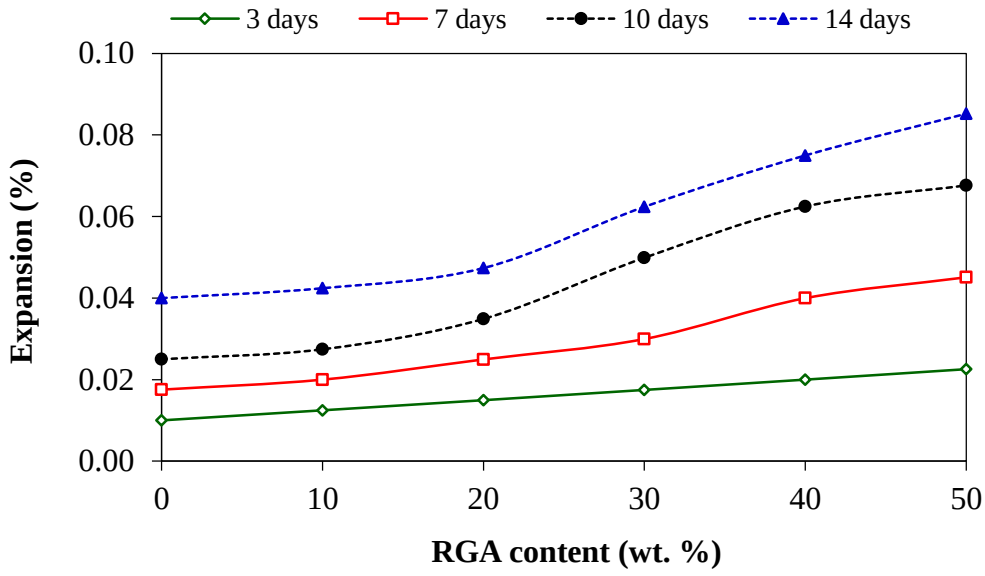

Figure 4.18 ASR expansion as a function of RGA content

Furthermore, the dissolution or solubility of RGA due to 1N NaOH solution was investigated. The rate of mass change of mortar bars due to the dissolution of RGA was obtained after 14 days of curing in 1N NaOH solution at 80 ºC. The mechanism of RGA dissolution is the result of the breakage of siloxane bonds in glass network structure due to alkali ion attack (Dhir, Dyer, & Tang, 2009; Maraghechi et al., 2016). The experimental result given in Figure 4.19 showed that the increase in RGA content increases the tendency for the rate of dissolution, that is, weight loss. The increase in weight change as RGA content increased attributed to the increase in affinity of glass siloxane bond dissolution rate and loss of gel. Saccani & Bignozzi (2010), reported that the content of RGA notably influences the solubility process and weight change increased with exposure days.

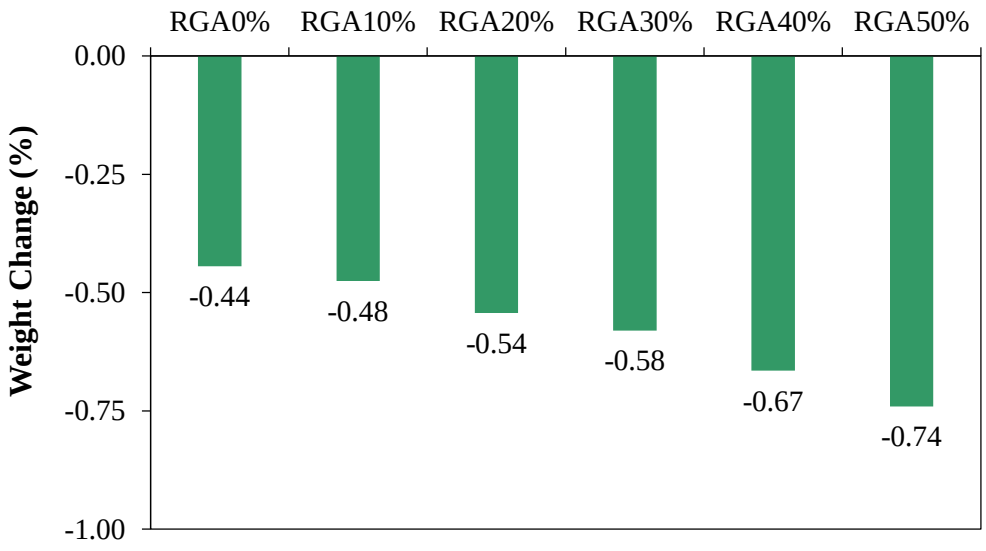

Figure 4.19 Weight change of SCM-RGA mixes after 14 days of curing in 1N NaOH solution at 80 ºC temperature

4.2 Mechanical Properties of Translucent Concrete

SCM-RGA20% was selected as optimum mix containing RGA to prototype and produce translucent concrete. The SCM-RGA20% mix was reinforced with different percentage volume of POF. The effect of plastic optical fiber (POF) on the mechanical properties of translucent concrete is summarized in Table 4.5.

Table 4.5 Mechanical properties of translucent concrete

Mix Designation	Bulk Density (kg/m^3)	Compressive strength (MPa)		Flexural Strength (MPa)	
		7 days	28 days	7 days	28 days
RC-0%	2401.33	36.78	40.66	6.66	7.97
Ø3-TC2%	2382.67	34.38	35.11	6.19	7.19
Ø3-TC4%	2349.33	32.62	35.66	5.65	6.80
Ø3-TC6%	2320.00	30.54	37.01	5.31	6.05
Ø2-TC2%	2396.00	29.15	31.16	5.94	7.03
Ø2-TC4%	2373.33	33.10	34.65	5.70	6.64
Ø2-TC6%	2345.33	35.37	36.14	5.23	6.17

4.2.1 Bulk Density

Figure 4.20, shows the bulk density value of hardened translucent concrete at 7 days and 28 days of age. Density was lower in translucent concrete (Ø2-TR and Ø3-TR) than in the reference concrete (RC-0%). The density of translucent concrete declined with rising volume ratio of plastic optical fiber (POF), regardless of the optical fibers diameter. This decline was the result of the lower density of optical fibers than the cement matrix (occupied by fibers). Density of the translucent concrete was decreased by about 0.22%, 1.17% and 2.33% for Ø2-TR (translucent concrete incorporating POF of 2 mm diameter), and 0.78%, 2.17% and 3.39% for Ø3-TR (translucent concrete incorporating POF of 3 mm diameter) compared to the reference concrete (RC-0%).

The density values obtained in this study concurred with the observations reported previously by Salih et al. (2014a). A quadratic relationship was observed between the volume ratio of POF and density values, illustrated in Figure 4.21. Generally, the density values of translucent concrete lay within the range of 2320 – 2400 kg/m^3.

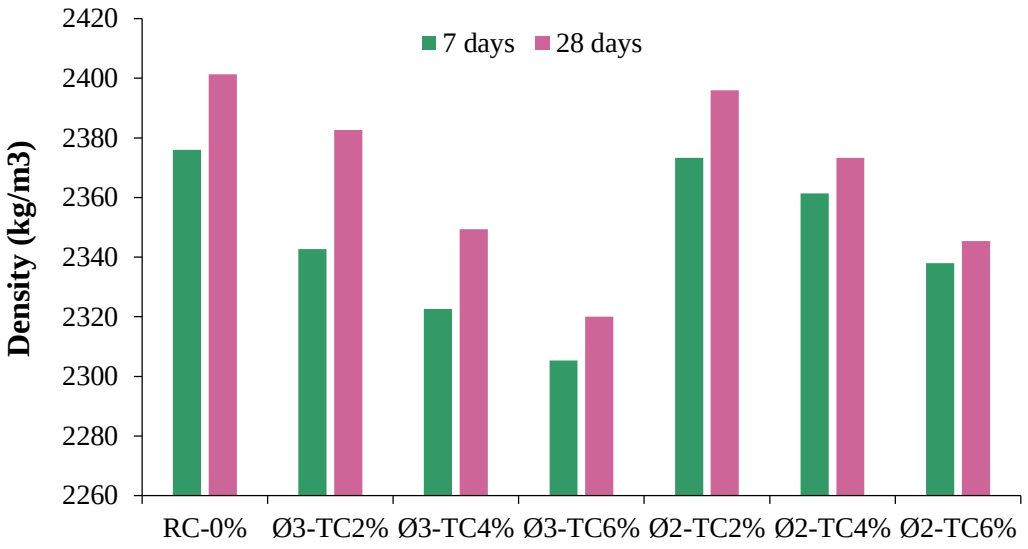

Figure 4.20 Bulk density of the translucent concrete at 7 days and 28 days of age

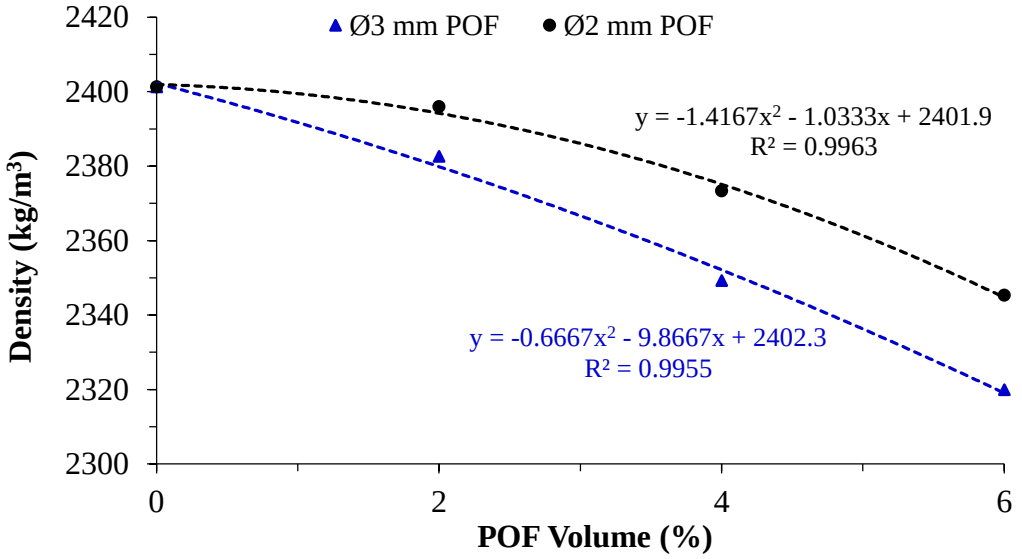

Figure 4.21 Relationship between POF volume ratio and 28 days bulk density of the translucent concrete

4.2.2 Compressive Strength

The relative compressive strength test results of the translucent concrete (Ø2-TR and Ø3-TR) with respect to the reference concrete (RC-0%), presented in Figure 4.22. It was clearly observed that all the translucent concrete specimens exhibited a compressive strength of lower than the reference concrete, regardless of the optical fibers diameter. On average, the 28 days compressive strength was 8% – 24% lower for the translucent concrete than for the reference concrete. These findings concurred with the observations reported by Salih et al. (2014a), who deduced that the 28 days compressive strength of translucent concrete containing 1.5 mm, 2 mm and 3 mm diameters of POF is 7.12% – 28.50% lower than the reference concrete. However, it was also evidently observed that the compressive strength of translucent concrete increased with increasing the volume ratio of optical fibers (POF). Compared to translucent concrete incorporating 2% POF volume (2 mm diameter), the compressive strength of translucent concrete containing 4% and 6% volume ratio of POF of 2 mm diameter increased by 11.21% and 15.99%, respectively. While, the compressive strength of translucent concrete specimens with 4% and 6% of POF volume (3 mm diameter) relative to specimens containing 2% of POF volume (3 mm diameter) increased by 1.56% and 5.41%, respectively. The findings on the effect of POF is consistent with the results of a study conducted by Altlomate et al. (2016), who reported that inclusion of POF improves the compressive strength of concrete. The compressive strength of all specimens increased with increasing curing age. Figure 4.22 also depicted that the compressive strength was slightly lower in translucent concrete containing POF of 2 mm diameter than in the corresponding translucent concrete containing 3 mm POF diameter. The effect seems to be significant at 2% of POF volume ratio. The relatively smaller spacing arrangement of 2 mm POF than 3

mm POF might result in a smaller distance of cement matrix interconnection surrounding the surface of POF that consequently accelerates the formation of macro-crack during compressive loading (Altlomate et al., 2016). The compressive strength values of the reference concrete and translucent concrete were within the range of 31 – 40 MPa. As shown in Figure 4.23, there is a good correlation between the compressive strength values and volume ratio of POF in a quadratic trendline form.

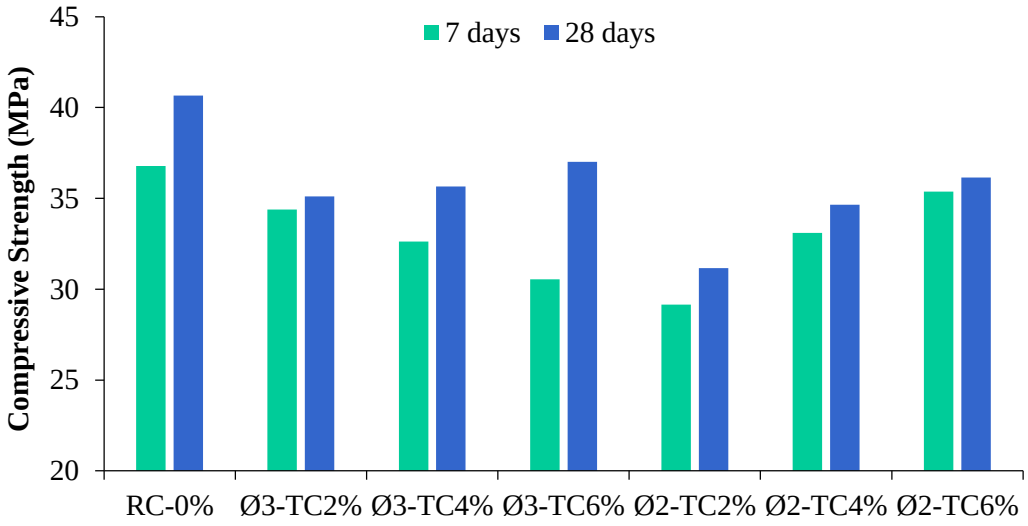

Figure 4.22 Compressive strength of the translucent concrete at 7 days and 28 days

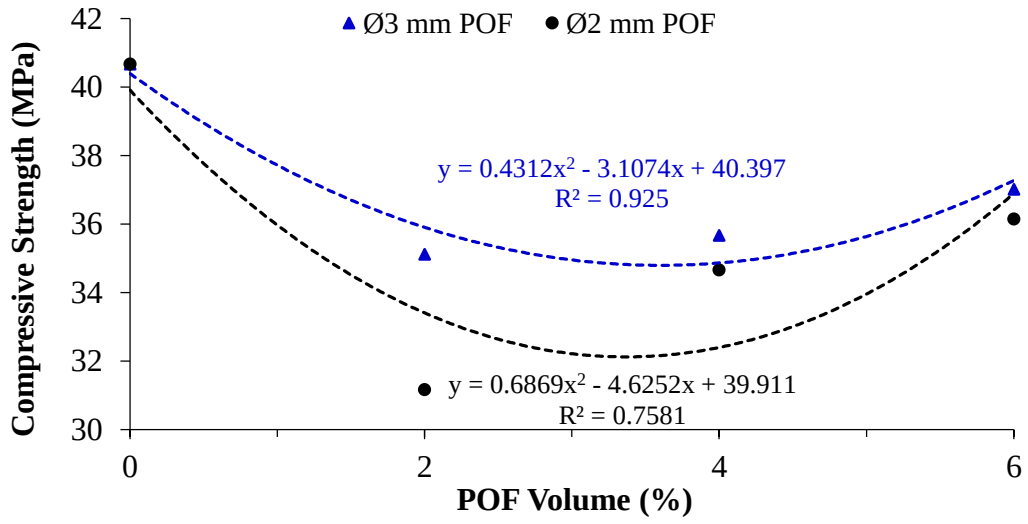

Figure 4.23 Relationship between POF volume and 28 days compressive strength

4.2.3 Flexural Strength

The flexural strength test results of reference concrete (RC-0%) and translucent concrete (Ø3-TR and Ø2-TR) graphically showed in Figure 4.24. The results appear to show that the flexural strength of all Ø3-TR and Ø2-TR specimens was lower than the strength of RC-0% specimens. In addition, it was clearly observed that the flexural strength of translucent concrete decreases with increasing POF volume ratio regardless of the difference in POF diameter. This may be attributed to the decrease in adhesion between cement matrix and POF during bending. It was observed that the fracture of flexure specimens occurred in the interfacial transition zone along the POF surface and surrounding cement paste. The phenomenon can be explained as when the specimens subjected to rapture, micro-cracks formed in the interfacial transition zone that leads to split of the bondage and failure. The results obtained in this study supports the findings reported by (Li et al., 2015; Salih et al., 2014a), who reported that incorporating of POF decreases the flexural strength. Based on the average of three measurements, the 28 days flexural strength was 9% – 24% lower for the translucent concrete than for the reference concrete. The relative percentage reduction in flexural strength for Ø3-TR specimens with 2%, 4% and 6% POF volume ratio was 9.80%, 14.71%, and 24.02%, while for Ø2-TR specimens was 11.76%, 16.67%, and 22.55%, respectively. Similar results were also reported by Salih et al. (2014a), who observed 17% – 40% reduction of the modulus of rupture for specimens containing 1.5 mm, 2 mm and 3 mm POF diameters of volume ratio 2%, 3% and 4%. Figure 4.25, shows a strong linear correlation between POF volume ratio and flexural strength values of Ø3-TR, Ø2-TR and RC-0%.

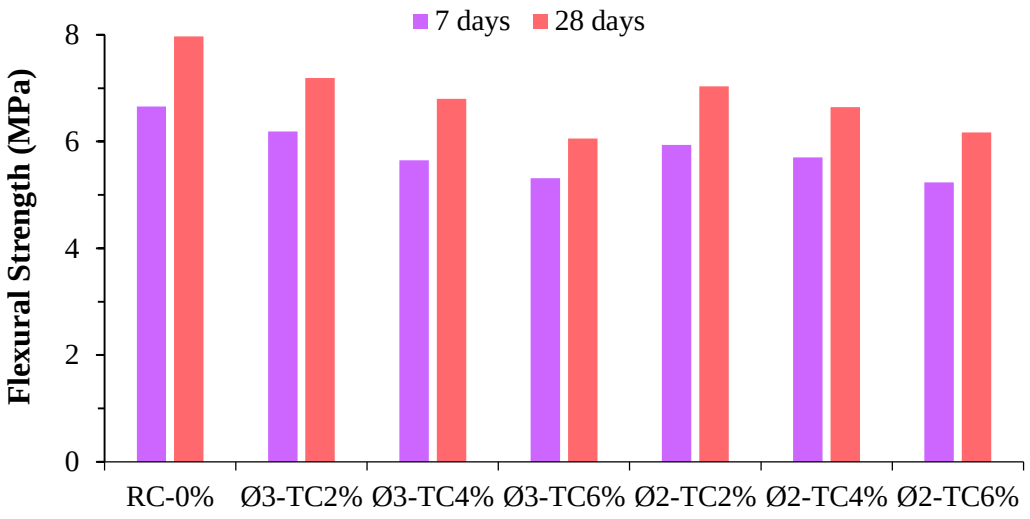

Figure 4.24 Flexural strength of the translucent concrete at 7 days and 28 days

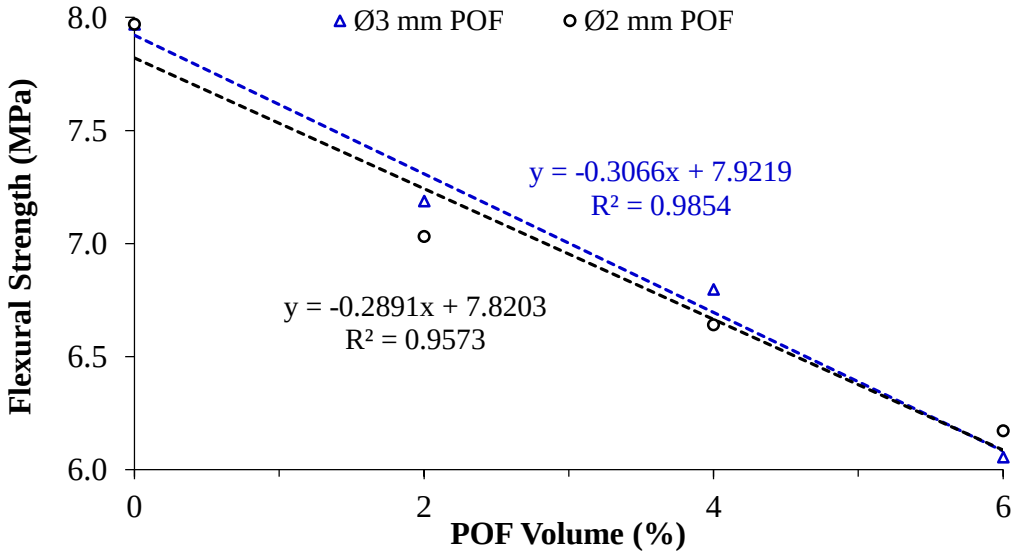

Figure 4.25 Relationship between POF volume ratio and 28 days flexural strength of translucent concrete

4.3 Light Transmittance Performance of Translucent Concrete

4.3.1 Light Transmittance Analysis of Translucent Concrete

The light transmission through translucent concrete is dependent on the percentage volume of optical fibers incorporated and the roughness degree of the surface area. Figure 4.26 (a), (b), (c) and (d) graphically presents the light transmittance efficiency of translucent concrete at 100 mm distance of the light source and different LDR distances. Furthermore, the measured transmittance of the specimens at 200 mm distance of light source are presented in Figure 4.27 (a), (b), (c) and (d). The amount of light transmitted was increased as the volume fraction of POF increased regardless of the diameter of fibers. This result concurs with the findings of (Altlomate et al., 2016; Zhou et al., 2009), who reported that the ratio of transmittance increased with an increased percentage volume fraction of optical fibers. This is due to the fact that as the volume fraction of POF increased, the number of POF also increased and consequently increased the amount of light transmitted through the prototype. The relationship between optical fibers volume ratio and transmittance showed a strong correlation ($R^2 \geq 0.95$) in quadratic trendline form. This result is in contrary to those of Paul & Dutta (2013), who reported that POF volume ratio and transmittance ratio have a linear relationship. The authors' used Optical Power Meter of wavelength 400 – 1100 nm to measure the light transmittance and the test was performed on the chosen middle part of the concrete surface considering a small number of POF. The contrary result may be attributed to the difference in experimental methodology and testing apparatus employed.The maximum transmittance obtained was 22.44% (average of three measurements) for specimens incorporating 6% volume of 2 mm diameter optical fibers that observed at 100 mm distance of both light source and LDR from the specimen location. Whereas, the lowest transmittance was 3.68% for specimens

containing 2% volume of 3 mm diameter of optical fibers measured at 400 mm and 500 mm distances of the light source and LDR respectively. Therefore, the percentage volume of POF incorporated in translucent concrete remarkably influences the transmittance property.

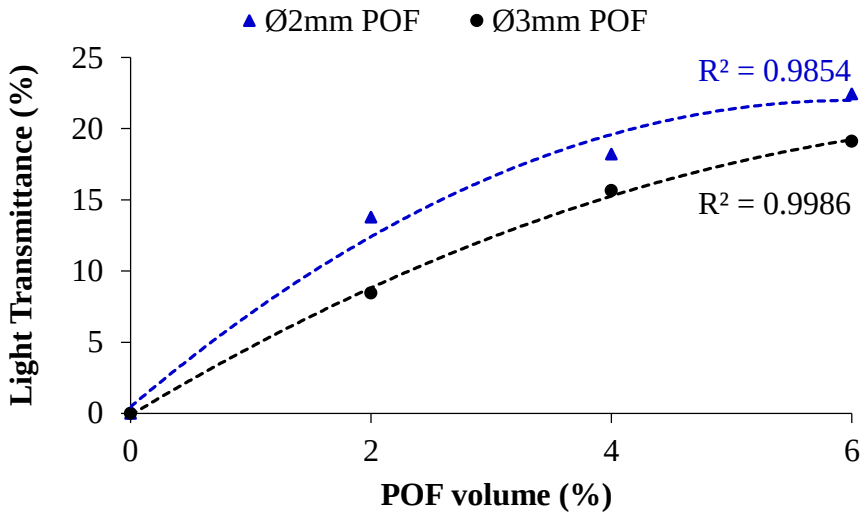

(a) At 100 mm LDR distance (100 mm distance of light source)

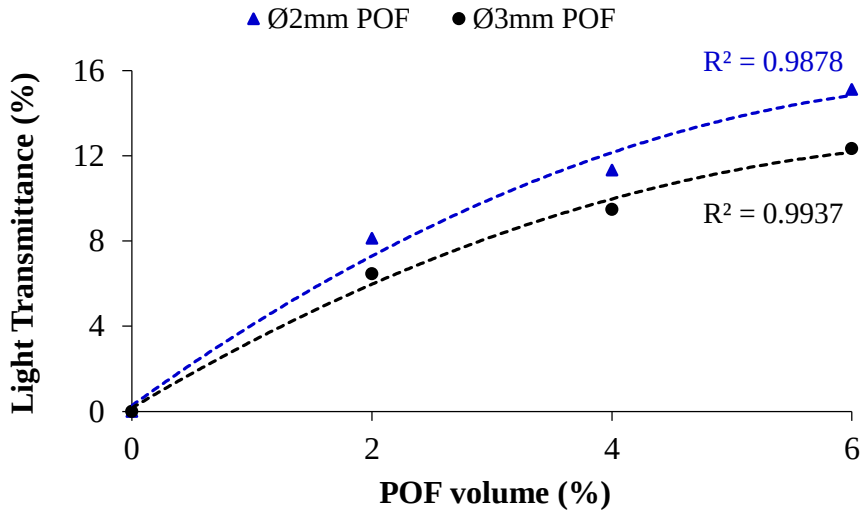

(b) At 200 mm LDR distance (100 mm distance of light source)

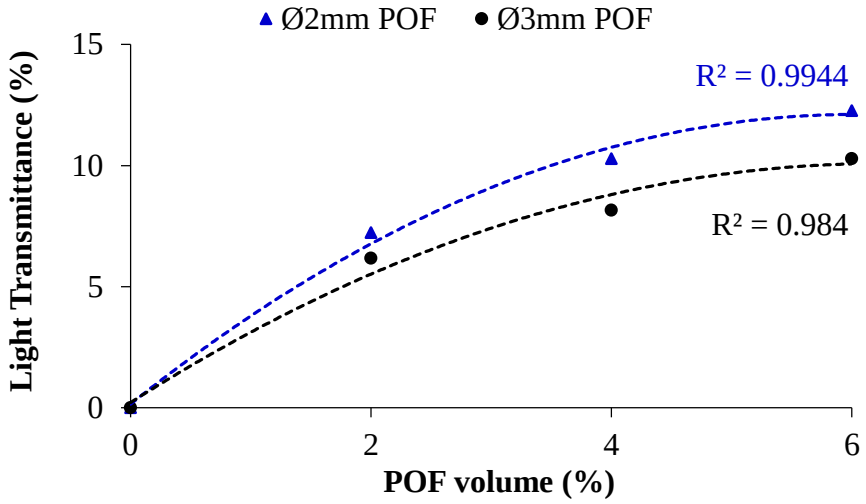

(c) At 300 mm LDR distance (100 mm distance of light source)

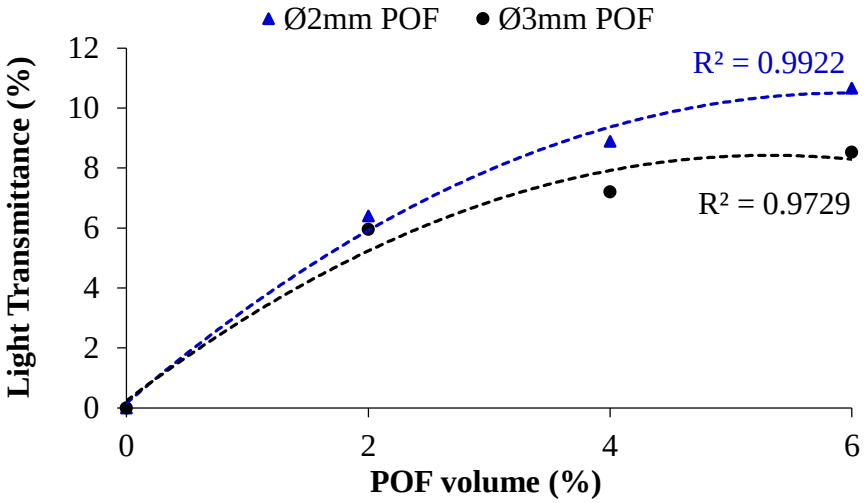

(d) At 400 mm LDR distance

Figure 4.26 Light transmittance of translucent concrete

(At 100 mm distance of light source)

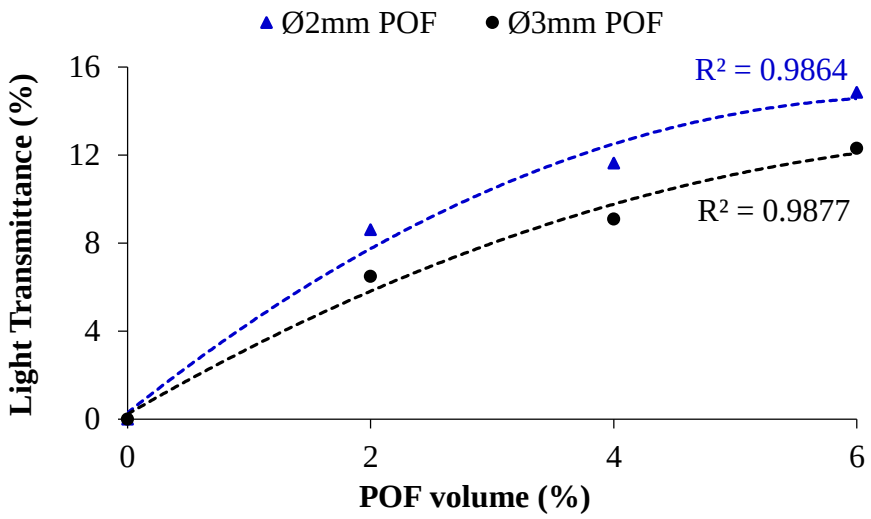

(a) At 100 mm LDR distance (200 mm distance of light source)

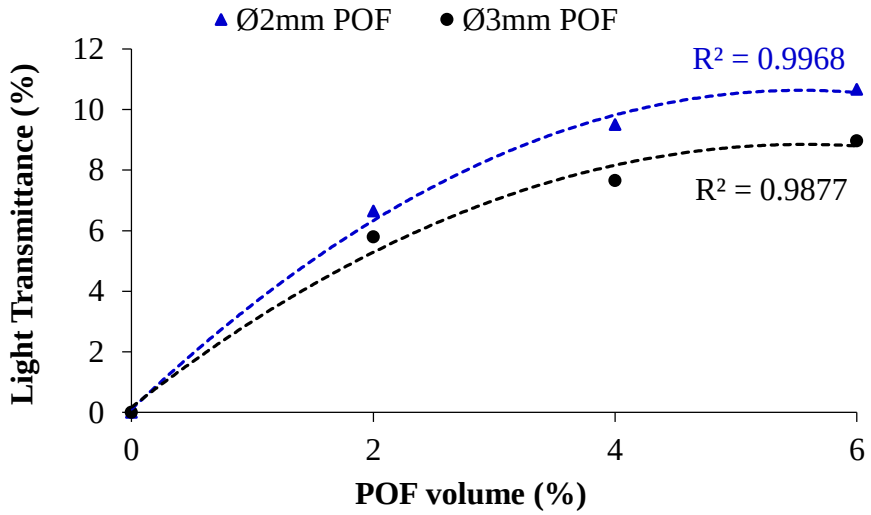

(b) At 200 mm LDR distance (200 mm distance of light source)

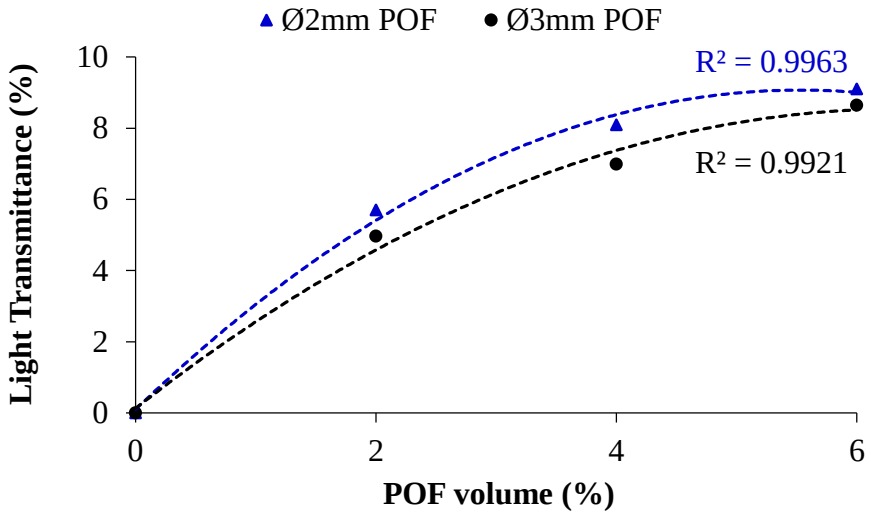

(c) At 300 mm LDR distance (200 mm distance of light source)

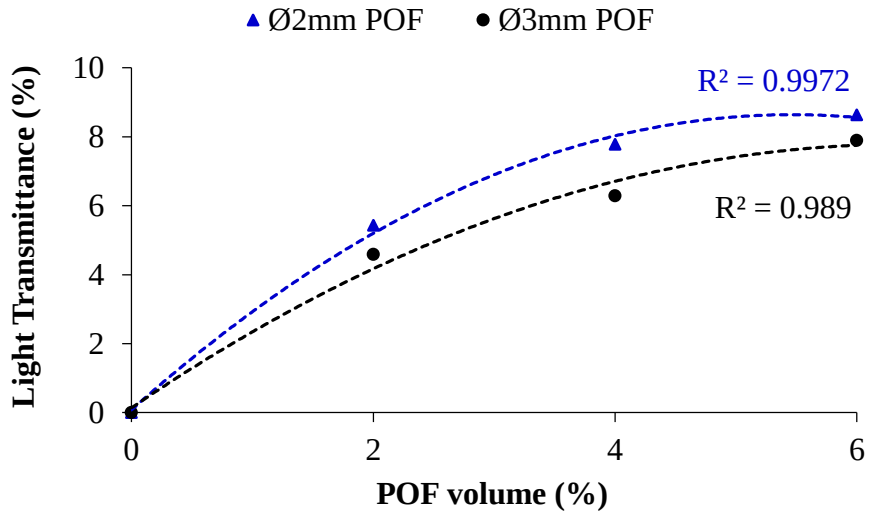

(d) At 400 mm LDR distance

Figure 4.27 Light transmittance of translucent concrete

(At 200 mm distance of light source)

It was evidently observed that the diameter of POF slightly affected the amount of light detected by the LDR. For the same POF volume fraction, fibers of 2 mm diameter yields relatively higher light transmittance than 3 mm fiber diameter. This attribute could be explained as the number of fibers for 2 mm diameter were higher than that of 3 mm fibers, and this affects the brightness region on the surface of translucent concrete and thereby, the amount of light detected. Furthermore, the spacing between

the fibers was smaller for 2mm POF compared to 3 mm POF, and this significantly contributed to the amount of light transmitted. Figure 4.28 and Figure 4.29 illustrates the effect of spacing and number of POF on the amount of light transmitted respectively. As it can be seen in Figure 4.28, the percentage of light transmitted through translucent concrete decreased when the spacing between POF increased. At 6% POF volume fraction, the spacing for 2 mm fibers is 6.2 mm and a light transmittance of 22.44%, while for 3 mm POF, the spacing is 8.3 mm with a light transmittance of 19.11% (the light transmittance measurement was taken at 100 mm distance of both light source and LDR). The experimental test results obtained in the present study support findings by other authors (Momin et al., 2014; Nikhil et al., 2016). As illustrated graphically in Figure 4.29, the transmittance of light significantly increased as the number of POF increased. Specimens containing 4% of POF volume, 32 and 14 optical fibers were incorporated with 2 mm and 3 mm fiber diameters, and the resulting light transmittance was 18.22% and 15.64% respectively. A high number of optical fibers on the surface of concrete increased the interference and superposition of lightwave as well as propagation of the transmitted light.

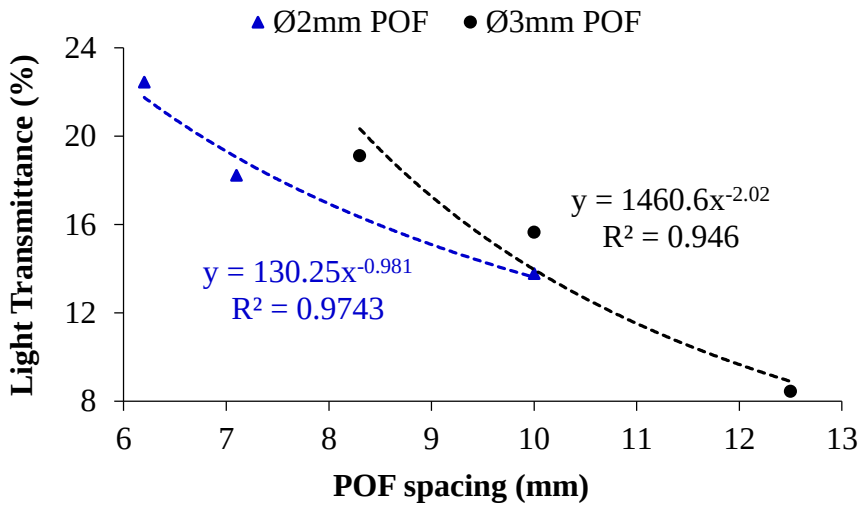

Figure 4.28 Effect of POF spacing on light transmittance of translucent concrete

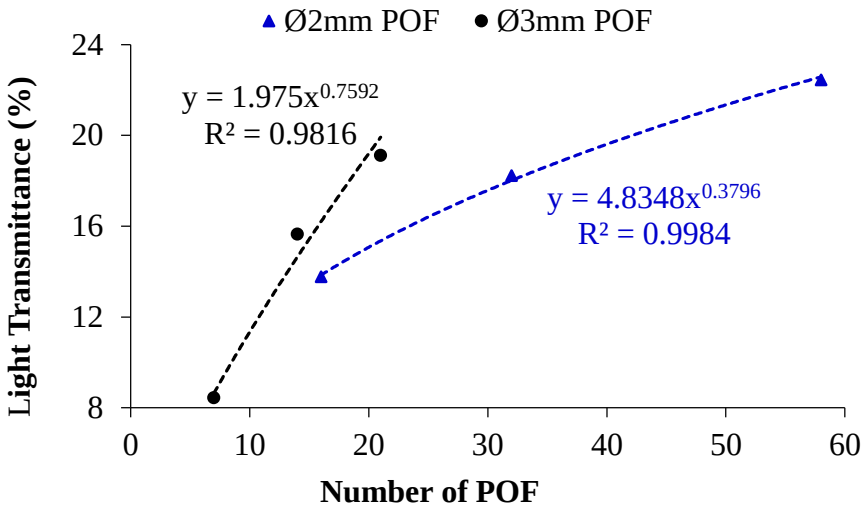

Figure 4.29 Effect of number of POF on light transmittance of translucent concrete

4.3.2 Light Transmittance Analysis at varying distances of Light Source

Figure 4.30 (a), (b) and Figure 4.31 (a), (b) shows the ratio of light transmitted values for specimens situated at 100, 200, 300 and 400 mm distances from the light source during experimentation. Figure 4.30 (a) and (b) illustrates the effect of light source distance on the transmittance of light through the prototypes observed at 100 mm of LDR distance. Similarly, Figure 4.31 (a) and (b) presents the effect of light source distance when the LDR distance was maintained at 200 mm. It was observed that the transmission of light was significantly decreased with an increasing distance between the translucent concrete specimen and source of light regardless of the volume ratio and diameters of optical fibers. These results concurred with the findings previously reported by Li et al. (2015). The decline rate of light transmittance was the result of the gradual decline of the light intensity that approaches the surface of the translucent concrete as the distance of light source increased. When the light source distance was increased from 100 mm to 200 mm, the amount of light transmitted decreased significantly, then as the distance increased beyond 200 mm, the decline rate of transmittance decreased gradually. For instance, when the distance from light source

to specimen was increased from 100 mm to 200 mm, the rate of light transmittance decreased by 33.84% and 35.62% for specimens containing 6% volume of 2 mm and 3 mm diameters fibers at 100 mm LDR distance respectively. However, when the light source distance increased from 300 mm to 400 mm, the rate of transmittance decreased by 10.35% and 7.33% for fibers diameter of 2 mm and 3 mm respectively. The decline rate of transmittance showed a strong correlation in power trendline with respect to the distances of the light source.

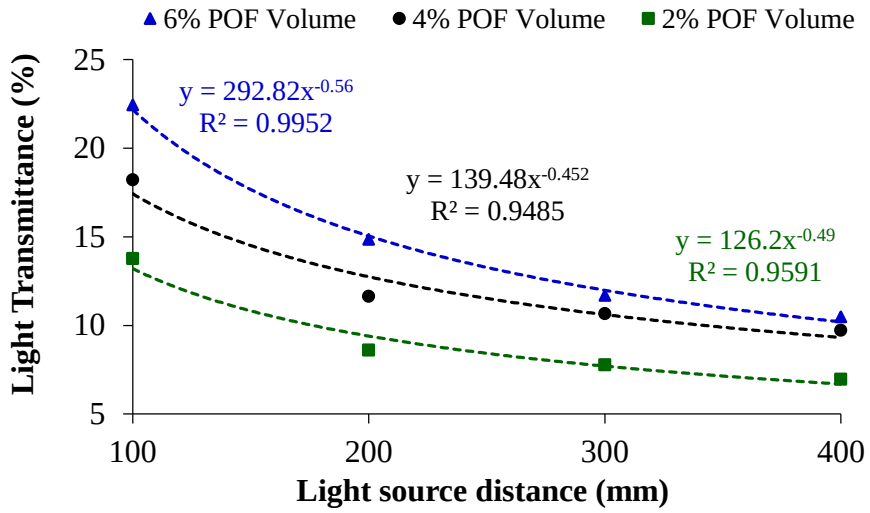

(a) Ø2 mm POF

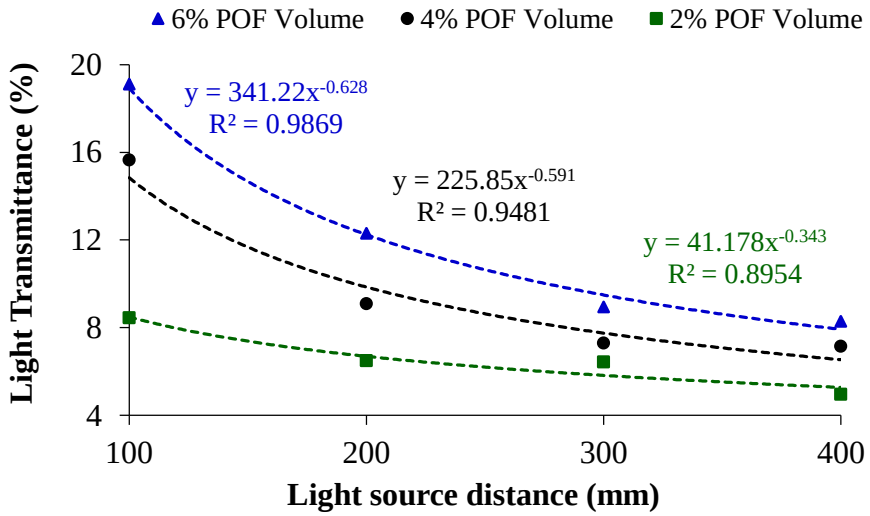

(b) Ø3 mm POF

Figure 4.30 Relationship between light transmittance and light source distance (At 100 mm LDR distance)

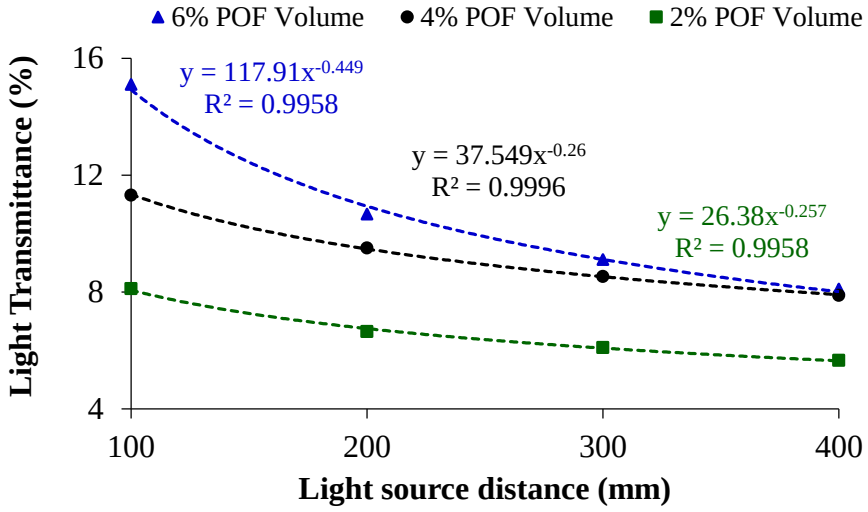

(a) Ø2 mm POF

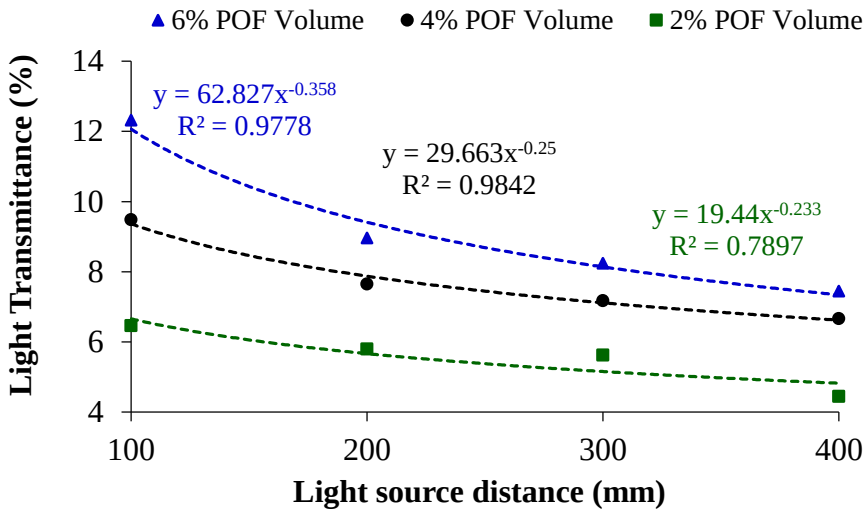

(b) Ø3 mm POF

Figure 4.31 Relationship between light transmittance and light source distance (At 200 mm LDR distance)

4.3.3 Light Transmittance Analysis at varying distances of LDR

The LDR was measuring the transmitted light through the specimens at 100, 200, 300, 400 and 500 mm distances consecutively. Figure 4.32 (a), (b) and Figure 4.33 (a), (b) presents the experimental test results of light transmittance at different distances between LDR and specimen. The results appear to show that as the distance between

the specimen and LDR increased, the amount of light transmitted decreased remarkably. This can be attributed to the fact that light wave diffracted with distance and consequently decreasing the light intensity and wavelength. The finding on the effect of LDR distance was consistent with the results of a study conducted by Li, Li & Guo (2015), who reported that optical power decreases with increasing distance between detector and specimen. Variation in the relative position of fibers on the surface area of concrete affects the intensity of light received by the LDR. The ratio of light transmittance was decreased significantly when the distance between specimen and LDR ranges 100 – 300 mm. However, when the distance exceeds 300 mm, the rate of transmittance decreased gradually. Generally, the LDR and light source distance showed a similar effect on the overall light transmittance of translucent concrete.

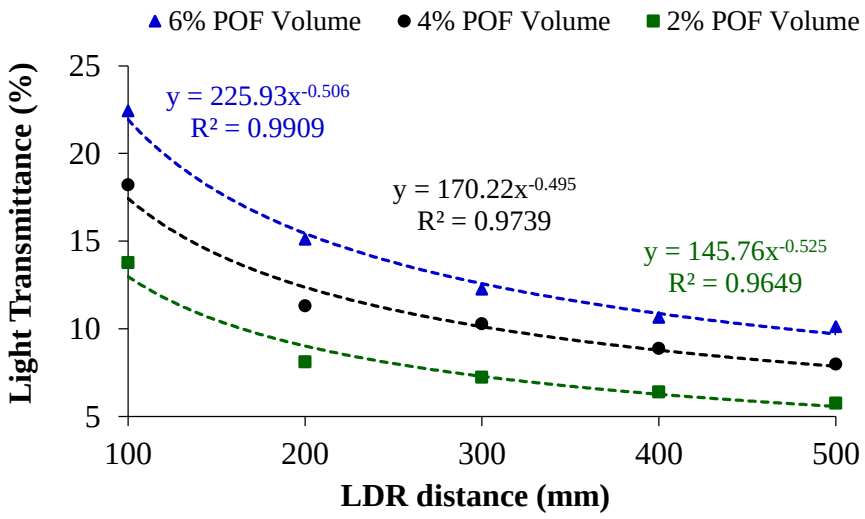

(a) Ø2 mm POF

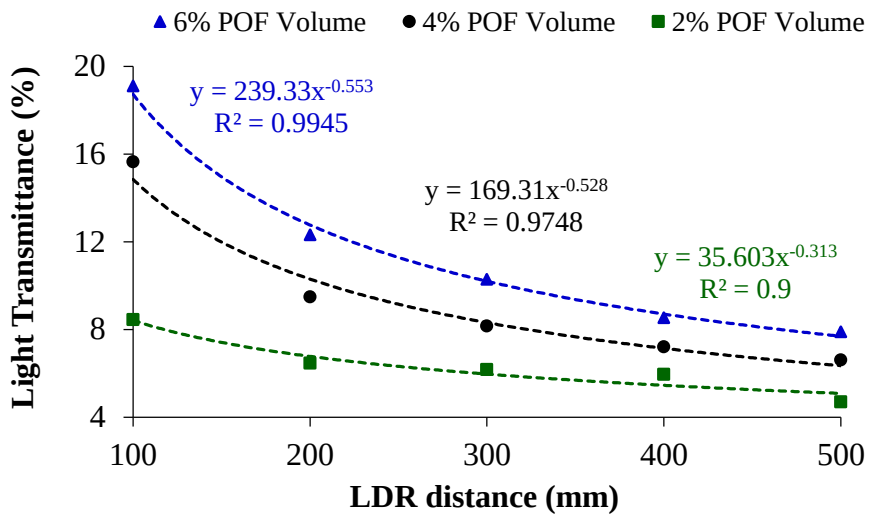

(b) Ø3 mm POF

Figure 4.32 Relationship between light transmittance and LDR distance

(At 100 mm light source distance)

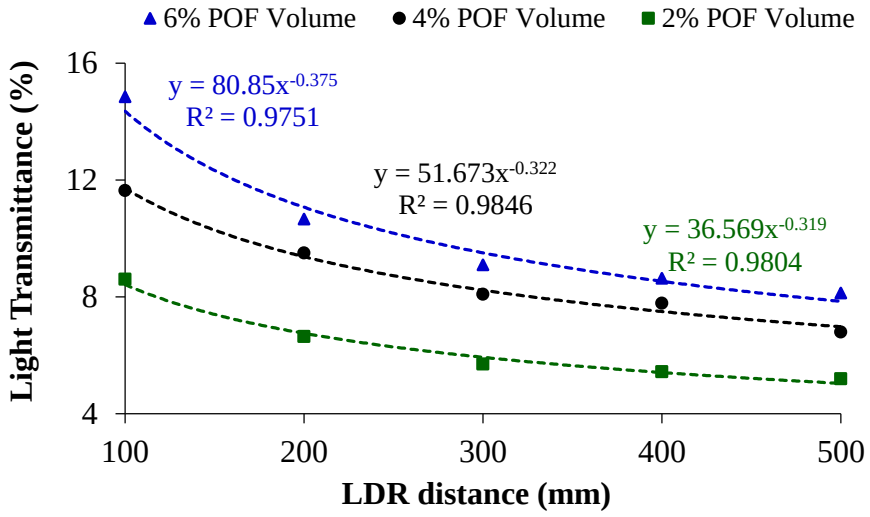

(a) Ø2 mm POF

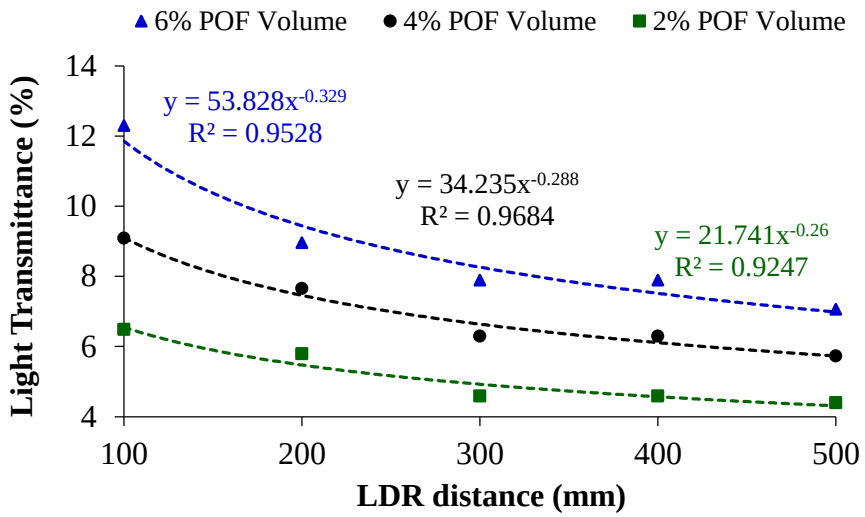

(b) Ø3 mm POF

Figure 4.33 Relationship between light transmittance and LDR distance

(At 200 mm light sources distance)

4.4 Structural Performance of the Translucent Concrete Façade Panels

The primary concern of incorporating POF with concrete matrix was to obtain a new type of concrete material having an ability of light transmittance to reduce the artificial light consumption for lighting purposes in commercial as well as residential buildings and any other civil infrastructures. From section 4.3, sufficient and good light transmittance performance (up to 22% transparency) was obtained using translucent concrete specimens containing 6% of POF volume of 2 mm and 3mm diameters. Thus, the translucent concrete can be successfully used for the production of pre-cast translucent concrete panels/ façades for application in architectural walls of green buildings. The architectural wall (translucent panel) could be a load bearing or non-load bearing integral part of the frame structures. In this section, a worst-case-scenario which is a load-bearing pre-cast translucent concrete panels worth considered and analyzed its structural performance. The translucent concrete panels prepared were designated as TCP-2 and TCP-3 that contains 6% POF volume ratio of 2 mm and 3 mm diameters, respectively. A reference concrete panel designated as RCP was also prepared. The flexural toughness, modulus of rapture, flexural toughness factor, maximum load and moment carrying capacity, bending stress, normal stress and shear stress of the concrete panels were analyzed.

4.4.1 Flexural Toughness of the Translucent Concrete Façade Panels

The load-deflection (P-δ) of the translucent concrete panels as well as the reference concrete panel obtained from the experiment is shown in Figure 4.34. From the experimental investigation, it was observed that the ultimate load in flexure carried by the translucent panel TCP-2 and TCP-3 was 11.38 kN and 11.69 kN, respectively. The ultimate mid-span deflection for TCP-2 and TCP-3 was 1.60 mm and 1.84 mm,

respectively while for the reference concrete panel, the ultimate load taken and ultimate mid-span deflection were 23.23 kN and 1.43 mm, respectively. The results show that the translucent concrete panels containing POF which are TCP-2 and TCP-3 carry 51.02% and 49.66% less ultimate load, respectively than in the reference concrete panel without POF. However, the ultimate mid-span deflection observed in the reference concrete panel (RCP) was 10.64% and 22.22% less compared to TCP-2 and TCP-3, respectively.

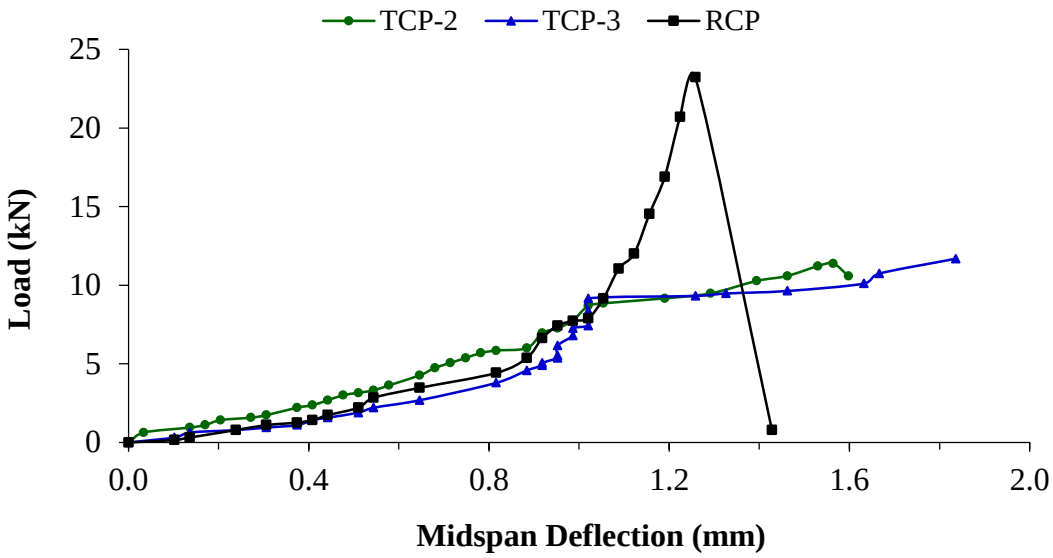

Figure 4.34 Load-deflection (P-δ) graph of the translucent concrete panels and the reference concrete panel

The flexural toughness parameters (flexural toughness factor and flexural toughness) were determined from P-δ plot (Figure 4.34) according to JSCE-SF4 on the basis of serviceability limit or failure criterion. JSCE-SF4 states that reinforced concrete is serviceable up to a deflection $\delta_{tb}=\ell/150$ of the span considering severe serviceability conditions. Based on this philosophy, the flexural toughness of the translucent and reference concrete panels was determined and details are given in Table 4.6. It was clearly noted from the experimental test results that the translucent concrete panels exhibited large deformation without remarkable load drop which indicates better

ductility and energy absorption compared to the reference concrete panel. This decline in brittleness nature of concrete or improvement of ductility was the result of the inclusion of optical fibers (POF). Flexural toughness was 11.01% and 21.15% higher in translucent concrete panels TCP-2 and TCP-3, respectively than in the reference concrete panel (RCP). This finding was consistent with the research outcomes conducted by Salih, Joni & Mohamed (2014b), who reported that inclusion of POF improves the ductility of concrete. The results in Table 4.6 also shows that the panels containing POF exhibited higher flexural toughness factor relative to reference concrete panel. The failure condition in the reference panel (without POF) was sudden once the ultimate load carrying capacity exceeded without showing any crack and warning of failure. While the translucent concrete panels (reinforced with POF) sustains a significant load when the deflection was increasing and showed flexural crack perpendicular to the optical fibers alignment below the neutral axis before failure. The flexural strength of reference panel was 51.02% and 49.66% higher than TRP-2 and TCP-3, respectively.

Table 4.6 Flexural toughness parameters of translucent and reference concrete panels

Panel Designation	Flexural Strength (N/mm^2)	Flexural Toughness (kN.mm)	Flexural Toughness Factor (N/mm^2)
RCP	4.65	8.27	0.55
TCP-2	2.28	9.29	0.62
TCP-3	2.34	10.49	0.70

Figure 4.35 and Figure 3.36 shows the relationship between the flexural toughness and flexural toughness factor with POF, respectively. From the results obtained, it evident that both flexural toughness and flexural toughness factor increased with the inclusion

of POF. A very strong (R^2=0.999) correlation was obtained in an exponential trendline between RCP, TCP-2, and TRP-3 with both toughness parameters.

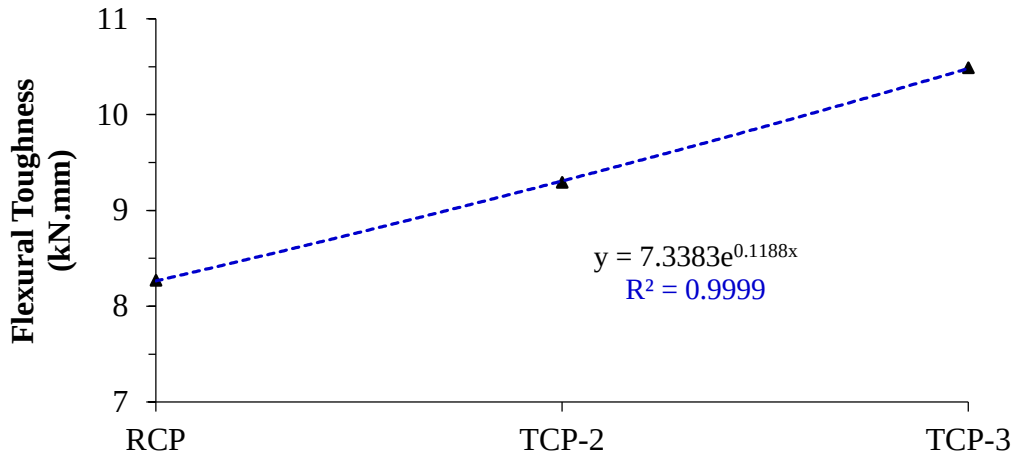

Figure 4.35 Flexural toughness of the reference and the translucent concrete panels

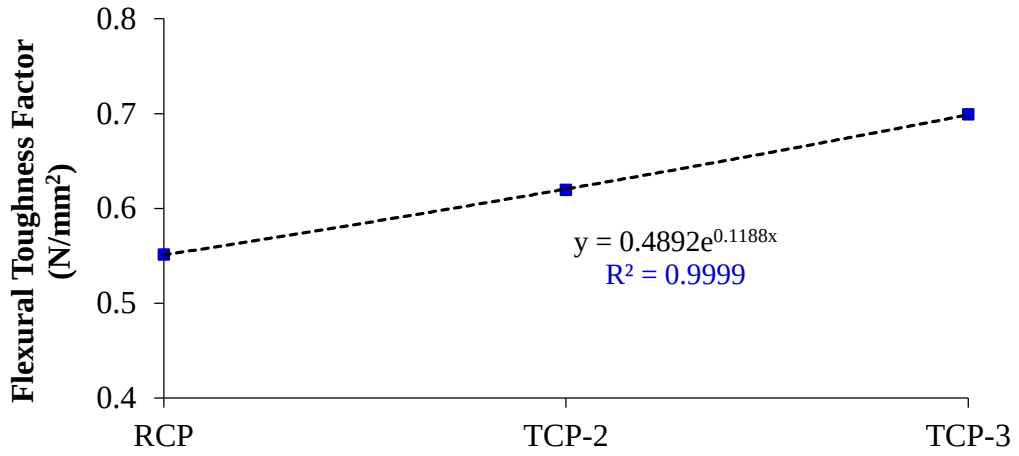

Figure 4.36 Flexural toughness factor of the reference and translucent concrete panels/façades

4.4.2 Experimental Load Analysis of the Translucent Concrete Façade Panels

Results of the experimental load analysis of the translucent and reference concrete panels are presented in Table 4.7. The bending stress-strain, normal stress-strain and shear stress-strain of the POF reinforced concrete and reference concrete panels are shown in Figure 4.37, Figure 4.38 and Figure 4.39, respectively.

Table 4.7 Details of experimental load analysis results of the translucent and reference concrete panels

Experimental Load Analysis Test Results (At failure)	Panel Designation		
	RCP	**TCP-2**	**TCP-3**
28 days Compressive Strength	40.66	36.14	37.01
Mass Density (kg/m^3)	2401.33	2345.33	2320.00
Ultimate Load (kN)	23.23	11.38	11.69
Maximum Deflection (mm)	1.43	1.60	1.84
Maximum Strain (10^{-2} mm/mm)	0.0030	0.0036	0.0034
Ultimate Bending Moment (kN.mm)	1741.95	853.20	876.90
Maximum Support Reaction (kN)	11.61	5.69	5.85
Maximum Bending Stress (N/mm^2)	4.65	2.28	2.34
Maximum Normal Stress (N/mm^2)	1.55	0.76	0.78
Maximum Shear Stress (N/mm^2)	2.32	1.14	1.17
Elasticity of Modulus (GPa)	32.26	29.36	29.23
Shear Modulus (GPa)	15.82	14.39	14.33

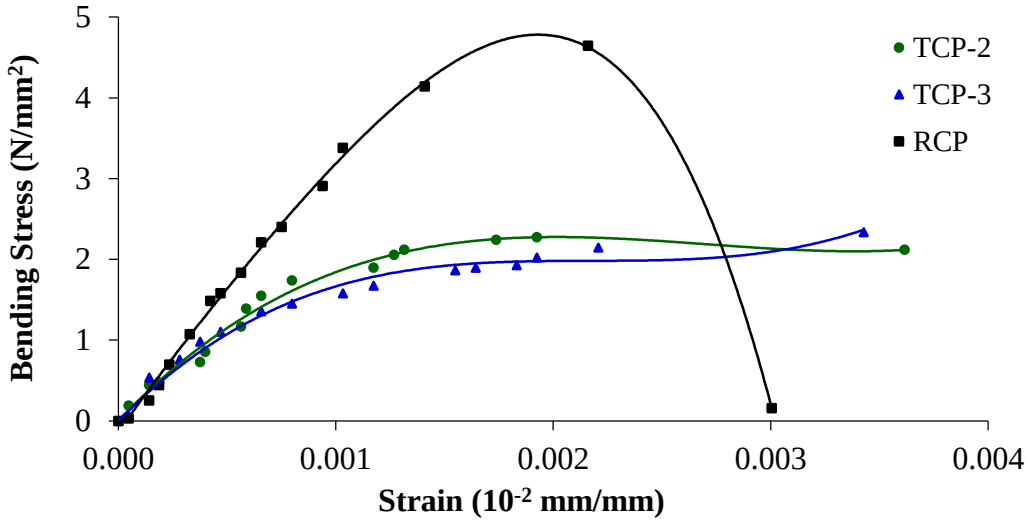

Figure 4.37 Bending stress-strain curve

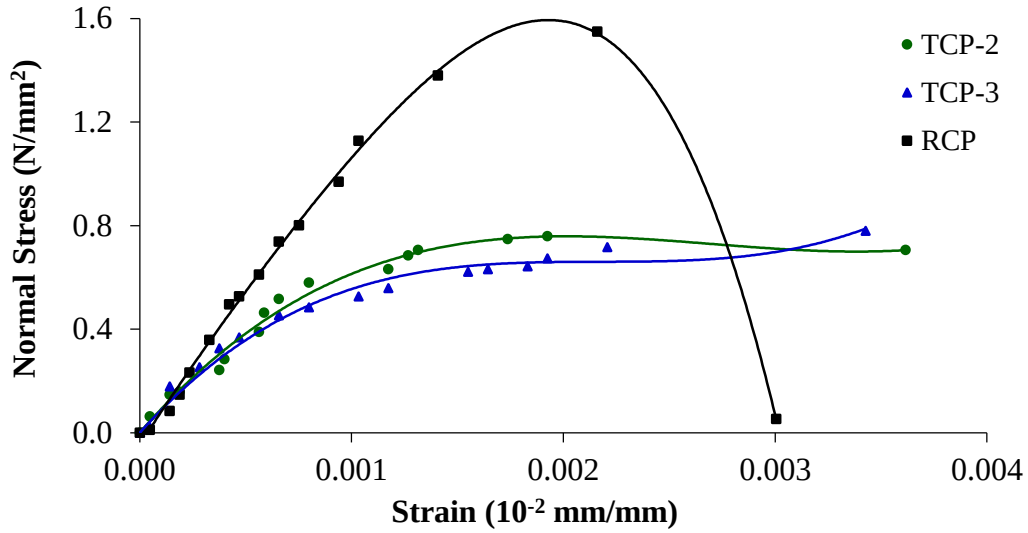

Figure 4.38 Normal stress-strain curve

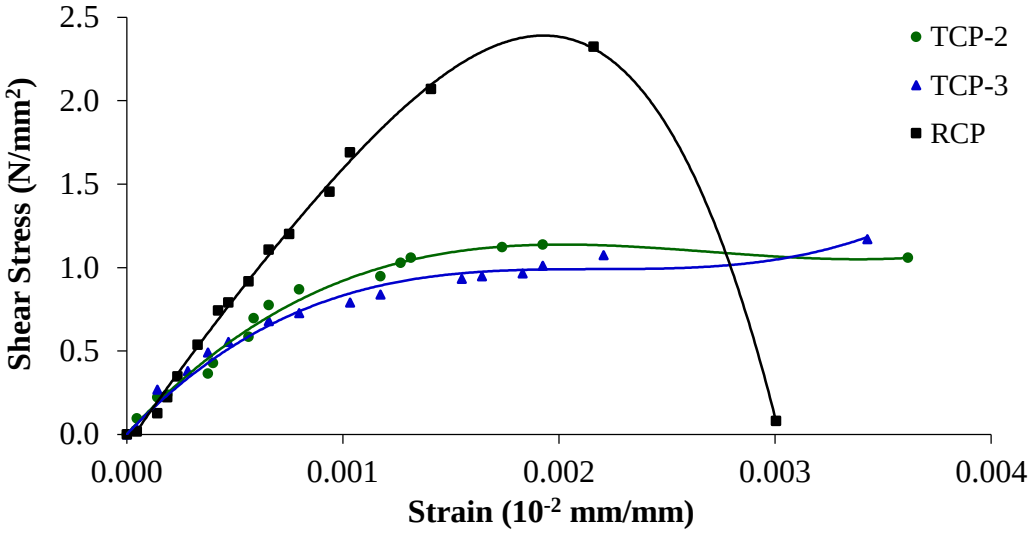

Figure 4.39 Shear stress-strain curve

The results showed that the ultimate bending moment carried by the translucent concrete panels was less than the moment sustained by the reference concrete panel, by 51.02% for TCP-2 and 49.66% for TCP-3. A similar trend was also observed for the support reaction load, bending stress, normal stress and shear stress that the reference panel carried and performs better than those panels reinforced with POF.

However, strains measured experimentally showed that the strain of panels reinforced with POF was higher than that of the panel without POF. It is clear that all façade panels exhibited a maximum lateral strain of magnitude over 0.0030 mm/mm. The strain was 13% – 20% higher for the translucent façade panels than for the reference façade panel. This indicates that despite the load carrying capacity incorporating of POF improves energy dissipation and this allows for warning of failure through large excessive deflection. The ductile nature of the optical fibers attributed to the improved energy dissipation of translucent panels. Furthermore, the failure mode and general response of the façade panels were reliant on the fiber material. The failure of façade panels occurred before reaching the serviceability limit mid-span deflection, $\ell/150$, commonly used for architectural features.

The elasticity modulus and shear modulus of the reference façade panel estimated by ACI 318 was 9% higher than the translucent concrete façade panels. The elasticity and shear modulus lay within the range of 32.2 – 29.2 GPa and 15.8 – 14.3 GPa, respectively. Elasticity modulus and shear modulus are fundamental parameters in designing of concrete structures. Higher elastic modulus indicates that the concrete panel can withstand higher stress but it becomes brittle and sooner cracks appear. While lower elastic modulus indicates the concrete panel can deform and bend easily. On the ground of elasticity modulus, the reference concrete façade panel was more brittle than the translucent concrete façade panels.

CHAPTER FIVE

CONCLUSION AND RECOMMENDATION

5.1 Conclusion

5.1.1 Fresh, Hardened and Durability Properties of SCM-RGA Mixes

Based on the outcomes of the experimental research on the fresh and hardened properties as well as durability of SCM-RGA mixes, the following conclusions were deduced:

1. The slump flow of SCM-RGA mixes decreased and V-funnel flow time increased as the content of glass aggregate increased. At a given water to powder ratio, superplasticizer dosage should be increased as the content of glass aggregate increased to ensure and maintain slump flow and flow time within the acceptable range.
2. The density, compressive strength and flexural strength of SCM-RGA mixes decreased with an increase in glass aggregate content. However, up to 30% RGA replacement ratio, the compressive and flexural strength showed 6.57% and 5.97% of reduction compared to reference SCM respectively.
3. SCM mixes containing glass aggregate exhibited lower water absorption and sorptivity value when compared to the control SCM. Sorptivity and water absorption decreased when the glass aggregate content increased. At 50% RGA replacement ratio, sorptivity of SCM-RGA is 52.3% lower than the reference SCM. This clearly indicates that concrete containing glass aggregates is more durable than conventional concrete.
4. For SCM containing RGA, a good correlation between sorptivity and strength (compressive and flexural values) was observed. The strength of SCM-RGA

decreased due to week interfacial bondage between the binding paste matrix and glass aggregate, and the sorptivity also significantly decreased due to relatively lower water permeability nature of glass.

5. It was observed that as the content of glass aggregate increased, ASR expansion also increased. Nevertheless, all mixes prepared in this study were potentially innocuous in regard to ASR expansion.
6. The experimental evidence showed that glass aggregate can be successfully incorporated in SCM as replacement of fine aggregate without a remarkable effect on workability and strength properties especially up to 30% of glass aggregate content. Thus, contributes towards sustainable solid waste management, saving landfills, conservation of natural resources and environmental protection.

5.1.2 Mechanical Properties of Translucent Concrete

The conclusions to be drawn from the tests results obtained on the mechanical properties of translucent concrete are as follows:

1. The mass density of translucent concrete was found to decrease marginally with increases the volume ratio of plastic optical fibers (POF), regardless of the optical fibers diameter. This decline was the result of the lower density of optical fibers than the cement matrix (occupied by fibers).
2. It was clearly observed that all the translucent concrete specimens exhibited a compressive strength of lower than the reference concrete. On average, the 28 days compressive strength was 8% – 24% lower for the translucent concrete than for the reference concrete. The compressive strength of translucent concrete increased with increasing the volume ratio of optical fibers (POF).

3. There is a directly proportional relationship between the compressive strength values and volume ratio of POF in a quadratic trendline form.
4. The inclusion of POF in concrete was found to significantly decrease the flexural strength. The general trend observed indicate a reduction in flexural strength with increase in POF volume ratio. The 28 days flexural strength was 9% – 24% lower for the translucent concrete than for the reference concrete.
5. There is a linear correlation between the flexural strength and POF volume ratio ($R^2 > 0.95$).

5.1.3 Light Transmittance Performance of Translucent Concrete

According to the experimental results of the light transmittance performance of translucent concrete using electrical circuit set-up with a light dependent resistor (LDR), the following conclusions can be drawn:

1. The light transmittance performance of the translucent concrete significantly depends on the percentage volume of optical fibers incorporated.
2. The experimental results evidently show that plastic optical fibers based translucent concrete with 6% optical fibers volume ratio perform up to 22% of light transmittance. Hence, POF of 6% volume ratio is apt for production of precast translucent concrete panel/façade with sufficient light transmittance for the different architectural wall in green building applications.
3. Translucent concrete can be successfully used as energy efficient construction material for sustainable construction and infrastructure development to reduce artificial light consumption.

5.1.4 Structural Performance of Translucent Concrete Panels

The following conclusions were derived from the experimental work carried out on the structural performance of translucent concrete panels:

1. It was evidently observed from the experimental test results that the translucent concrete panels (containing POF) exhibited large deformation without remarkable load drop which indicates better ductility (toughness behavior) and energy absorption compared to the reference concrete panel (without POF).
2. The flexural toughness and toughness factor were 11% – 22% higher in translucent concrete panels than in the reference concrete panel. Thus, the inclusion of POF improves ductility (toughness) behavior of concrete.
3. The ultimate load, bending moment, shear stress, normal stress and bending stress carrying capacity of the translucent concrete panels were 49% – 51% lower than the reference panel.
4. There is a directly proportional relationship between the flexural toughness as well as toughness factor and POF in an exponential trendline form ($R^2 = 0.999$).
5. The failure mechanism of translucent panels was flexural crack formed along the POF alignment nearest to the mid-span as a result of weakening the interfacial transition zone between the POF surface and paste matrix caused by the crack propagation during the three-point loading.
6. Generally, from serviceability limit state and ductility point of view: translucent panels perform better than the reference panels.

5.2 Recommendation

5.2.1 Recommendation for Application Area

Based on the findings of this research, the following recommendations derived for possible application area:

1. At replacement ratio up to 30%, recycled glass aggregate is viable for production of SCM, SCC and translucent concrete with good workability, sufficient strength, and durability. The SCM-RGA mixes developed in this study are apt for SCC making, grouting, rehabilitation of structures and production of translucent concrete. Due to its lower sorptivity rate, SCM-RGA can also be used in making of SCC for construction of underwater concrete structures and water retaining concrete structures.
2. The translucent concrete panels/ façade developed in this study are apt for application in load bearing and non-load bearing architectural walls of green buildings, underground stations, in structural walls of banks, prisons, and museums to increase security and supervision as well as safety. It can also be used in airports, subways and road marks to add visibility.

5.2.2 Recommendation for Future Work

From this research work, the following recommendations for other researchers could be made:

1. To observe the evolution of strength development of SCM-RGA and translucent concrete, strength tests beyond 28 days could be done also.
2. Other mineral admixtures such as rice husk ash, ceramic powder, sugar-cane bagasse ash, brick powder, quarry dust and so on, can also be used to produce SCM and translucent concrete.
3. Permeability, fire resistance, freeze-thaw resistance, pore structure, performance under high-temperatures and chemical resistance of SCM-RGA and translucent concrete can be evaluated to further understand the durability behavior.
4. Microscopic examination of the bondage between the recycled glass aggregate, cement matrix, and plastic optical fibers can be undertaken to further understand the adhesion properties of SCM-RGA and translucent concrete.
5. It is recommended that further studied be done on the acoustic and thermal insulating properties of translucent concrete.

REFERENCES

ACI 318. (2008). Building code requirements for structural concrete (ACI 318-08) and commentary. *American Concrete Institute*. USA.

Afshinnia, K., & Rangaraju, P. R. (2016). Impact of combined use of ground glass powder and crushed glass aggregate on selected properties of Portland cement concrete. *Construction and Building Materials*, *117*, 263–272.

Al-Kurdi, N., Abdel-Aziz, D., & Alshboul, A. (2014). The impact of using light transmitting concrete on energy saving in office buildings-case of Jordan. *Research Journal of Applied Sciences, Engineering, and Technology*.

Ali, E. E., & Al-Tersawy, S. H. (2012). Recycled glass as a partial replacement for fine aggregate in self-compacting concrete. *Construction and Building Materials*, *35*, 785–791.

Almesfer, N., & Ingham, J. (2014). Effect of Waste Glass on the Properties of Concrete. *Journal of Materials in Civil Engineering*.

Altlomate, A., Alatshan, F., Mashiri, F., & Jadan, M. (2016). Experimental study of light-transmitting concrete. *International Journal of Sustainable Building Technology and Urban Development*, *7*(3–4), 1–7.

ASTM C109. (2007). *Standard test method for compressive strength of hydraulic cement mortars (using 2-in [50] mm cube specimens)*. ASTM International. Pennsylvania, USA.

ASTM C1260. (2007). *Standard test method for potential alkali reactivity of cement-aggregate combinations (Mortar-bar method). ASTM International*. Pennsylvania, USA.

ASTM C33. (2011). *Standard specification for concrete aggregates*. *ASTM International*. Pennsylvania, USA.

ASTM C348. (2002). *Flexural strength of hydraulic-cement mortars*. *ASTM International*. Pennsylvania, USA.

ASTM C349. (2002). *Standard test method for compressive strength of hydraulic-cement mortars (Using portions of prisms broken in flexure)*. *ASTM International*. Pennsylvania, USA.

ASTM C490. (2007). *Standard practice for use of apparatus for the determination of length change of hardened cement paste, mortar, and concrete*. *ASTM International*. Pennsylvania, USA.

ASTM C 1585. (2004). *Standard test method for measurement of the rate of absorption of water by hydraulic-cement concretes*. *ASTM International*. Pennsylvania, USA.

ASTM C 642. (2006). *Standard test method for density, absorption, and voids in the hardened concrete*. *ASTM International*. Pennsylvania, USA.

Australian / New Zealand Standard (AS/NZS 1680.2.1). (2008). *Interior and workplace lighting- Part 2.3: Specific applications— Educational and training*

facilities. Sydney, Australia; Wellington 6020, New Zealand.

Azambuja, A., & Castro, L. (2015). Translucent concrete in architecture prison. *National Journal of Cities Management*, *3*(20), 18–33.

Beeralingegowda, B., & Gundakalle, V. (2013). The effect of addition of limestone powder on the properties of self-compacting concrete. *International Journal of Innovative Research in Sciences, Engineering, and Technology*, *2*(9).

Bentz, D. P., Ferraris, C. F., Jones, S. Z., Lootens, D., & Zunino, F. (2017). Limestone and silica powder replacements for cement: Early-age performance. *Cement and Concrete Composites*, *78*, 43–56.

Billberg, P. (1999). *Self-compacting concrete for civil engineering structures: The Swedish experience*. Cement och Betong Institutet, Stockholm, Sweden.

Boukendakdji, O., Debieb, F., Kadri, E. H., & Benramoul, N. (2016). Effect of viscosity modifying admixtures on the workability and mechanical resistances of self-compacting mortars. *Journal of Materials and Environmental Science*, *7*(2), 558–565.

BS EN 196-1. (1995). *Method of testing cement - Part 1: Determination of strength*. European Committee for Standardization. Brussels, Belgium.

Chandak, S. P. (2010). *Trends in solid waste management : issues, challenges, and opportunities*. *International Consultative Meeting on Expanding Waste Management Services in Developing Countries*. Tokyo, Japan.

Choi, S. Y., Choi, Y. S., & Yang, E. I. (2016). Effects of heavyweight waste glass recycled as a fine aggregate on the mechanical properties of mortar specimens. *Annals of Nuclear Energy*, *99*, 372–382.

Christianto, H. A. (2004). *Effect of chemical and mineral admixtures on the fresh properties of self-compacting mortars*. Middle East Technical University, MSc. Thesis.

Corinaldesi, V., Nardinocchi, A., & Donnini, J. (2016). Reuse of recycled glass in mortar manufacturing. *European Journal of Environmental and Civil Engineering*, *20*, 1–12.

De Castro, S., & De Brito, J. (2013). Evaluation of the durability of concrete made with crushed glass aggregates. *Journal of Cleaner Production*, *41*, 7–14.

Deeb, R. (2013). *Flow of self-compacting flow of self-compacting*. Cardiff University, Ph.D. Thesis.

Dhir, R. K., Dyer, T. D., & Tang, M. C. (2009). Alkali-silica reaction in concrete containing glass. *Materials and Structures/Materiaux et Constructions*, *42*(10), 1451–1462.

Du, H., & Tan, K. H. (2013). Use of waste glass as sand in mortar: Part II - alkali-silica reaction and mitigation methods. *Cement and Concrete Composites*, *35*(1), 118–126.

EFNARC. (2002). *Specification and guidelines for self-compacting concrete*.

European Federation of Specialist Construction Chemicals and Concrete Systems. Norfolk, UK.

EN 197-1. (2000). *Composition, specifications and conformity criteria for common cement*. European Committee for Standardization. Brussels, Belgium.

Energy Information Administration (EIA). (2007). *International emissions data: Energy-Related carbon emissions*. Washington, D.C., United States.

Fischer, U. H. P., Haupt, M., & Joncic, M. (2011). Optical transmission systems using polymeric fibers. *Optoelectronics - Devices and Applications*, 445–468.

Gawatre, D. W., Giri, S. D., & Bande, B. B. (2016). Transparent concrete as an eco-friendly material for building. *International Journal of Engineering Science Invention*, *5*(3).

Georgiadis, A. S., Sideris, K. K., & Anagnostopoulos, N. S. (2009). Properties of SCC produced with limestone filler or viscosity modifying admixture. *Journal of Materials in Civil Engineering*, *22*(4), 352–360.

Halbiniak, J., & Sroka, P. (2015). Translucent concrete as the building material of the 21st century. *TEKA. Commission of Motorization and Energetics in Agriculture*, *15*(1), 23–28.

Hameed, A. (2012). Effect of superplasticizer dosage on the workability of self-compact concrete. *Diyala Journal of Engineering Sciences*, *5*(2), 66–81.

Ismail, Z. Z., & AL-Hashmi, E. A. (2009). Recycling of waste glass as a partial replacement for fine aggregate in concrete. *Waste Management*, *29*(2), 655–659.

Johansson, T. B., Patwardhan, A., Nakicenovic, N., & Gomez-Echeverri, L. (2012). *Global energy assessment - toward a sustainable future*. *Global Energy Assessment (GEA)*.

JSCE-SF4. (1984). *Method of tests for flexural strength and flexural toughness of steel fiber reinforced concrete*. Concrete Library of JSCE, Japan Society of Civil Engineers (JSCE).

Kankriya, S. (2016). Translucent concrete by using optical fibers and glass rods. *International Journal of Scientific*, *6*(10), 625–627.

Karataş, M., Benli, A., & Ergin, A. (2017). Influence of ground pumice powder on the mechanical properties and durability of self-compacting mortars. *Construction and Building Materials*, *150*, 467–479.

Kasozi, A., & Harro, B. Von. (2010). *Solid waste management in Nairobi : A situation analysis*. Integrated Solid Waste Management Plan, UNEP, Environmental & Process Systems Engineering Group, University of Cape Town.

Khaleel, O. R., & Abdul Razak, H. (2012). The effect of powder type on the setting time and self-compactibility of mortar. *Construction and Building Materials*, *36*, 20–26.

Khaleel, O. R., Al-Mishhadani, S. A., & Razak, H. A. (2011). The effect of coarse aggregate on fresh and hardened properties of self-compacting concrete (SCC).

In *The Twelfth East Asia-Pacific Conference on Structural Engineering and Construction* (pp. 805–813). Procedia Engineering.

Khayat, K. H. (2000). Optimization and performance of air-entrained, self-consolidating concrete. *ACI Materials Journal*, *97*(5), 526–535.

Koh, C. J. (2014). *Characterisation of shape of recycled crushed coloured glass and the effect on the properties of structural concrete when used as a fine aggregate replacement*. Ph.D. Thesis, University of Wolverhampton.

Koike, Y., & Asai, M. (2009). The future of plastic optical fiber. *NPG Asia Materials*, *1*(1), 22–28.

Kou, S. C., & Poon, C. S. (2009). Properties of self-compacting concrete prepared with recycled glass aggregate. *Cement and Concrete Composites*, *31*(2), 107–113.

Langer, W., Drew, L., & Sachs, J. (2004). *Aggregate and the Environment*. American Geological Institute (AGI). Alexandria, Virginia, USA.

Li, Y., Li, J., & Guo, H. (2015). Preparation and study of light transmitting properties of sulfoaluminate cement-based materials. *Materials and Design*, *83*, 185–192.

Li, Y., Li, J., Wan, Y., & Xu, Z. (2015). Experimental study of light transmitting cement-based material (LTCM). *Construction and Building Materials*, *96*, 319–325.

Libre, N. A., Khoshnazar, R., & Shekarchi, M. (2010). The relationship between fluidity and stability of self-consolidating mortar incorporating chemical and mineral admixtures. *Construction and Building Materials*.

Limbachiya, M. C. (2009). Bulk engineering and durability properties of washed glass sand concrete. *Construction and Building Materials*, *23*(2), 1078–1083.

Ling, T. C., & Poon, C. S. (2011). Utilization of recycled glass derived from cathode ray tube glass as fine aggregate in cement mortar. *Journal of Hazardous Materials*, *192*(2), 451–456.

Ling, T. C., & Poon, C. S. (2012). A comparative study on the feasible use of recycled beverage and CRT funnel glass as fine aggregate in cement mortar. *Journal of Cleaner Production*, *29*, 46–52.

Ling, T. C., Poon, C. S., & Kou, S. C. (2012). Influence of recycled glass content and curing conditions on the properties of self-compacting concrete after exposure to elevated temperatures. *Cement and Concrete Composites*, *34*(2), 265–272.

Liu, M. (2009). *Wider application of additions in self-compacting concrete*. University College London, Ph.D. Thesis.

Long, J. (2015). Lighting – One size fits all OR design for all ? In *Proceedings 19th Triennial Congress of the IEA. Melbourne, Australia*.

Maraghechi, H., & Al., E. (2012). The role of residual cracks on alkali-silica reactivity of recycled glass aggregates. *Cement and Concrete Composites*, *34*(1), 41–47.

Maraghechi, H., Rajabipour, F., Pantano, C. G., & Burgos, W. D. (2016). Effect of calcium on dissolution and precipitation reactions of amorphous silica at high alkalinity. *Cement and Concrete Research*, *87*, 1–13.

Medina, C., Zhu, W., Howind, T., Sanchez De Rojas, M. I., & Frias, M. (2014). Influence of mixed recycled aggregate on the physical-mechanical properties of recycled concrete. *Journal of Cleaner Production*, *68*, 216–225.

Menéndez, G., Bonavetti, V. L., & Irassar, E. F. (2007). Ternary blend cement concrete. Part II: transport mechanisms. *Materiales de Construcción*, *57*(285), 31–43.

Midorikawa, T., Pelova, G. I. I., & Walraven, J. C. (2009). Application of " The water layer model " to self-compacting mortar with different size distributions of fine aggregate. *Heron*, *54*(2), 73–100.

Mohseni, E., Miyandehi, B. M., Yang, J., & Yazdi, M. A. (2015). Single and combined effects of nano-SiO_2, nano-Al_2O_3, and nano-TiO_2 on the mechanical, rheological and durability properties of self-compacting mortar containing fly ash. *Construction and Building Materials*, *84*, 331–340.

Momin, A. A., Kadiranaikar, R. B., Jagirdar, V., & Inamdar, A. (2014). Study on light transmittance of concrete using optical fibers and glass rods. *IOSR Journal of Mechanical and Civil Engineering*, *2*(2), 67–72.

Monica. (2013). Seeing through concrete. Hungarian success stories. Retrieved from https://hungarian-success-stories.com/2013/03/10/seeing-through-concrete/

Nikhil, K., Farook, U., Ahmed, S., MK, J., Saleem, R., & Omar, S. (2016). Experimental analysis of translucent concrete by using optical fibers. *SSRG International Journal of Civil Engineering (SSRG-IJCE)*, *3*(3), 76–81.

Nunes, S., Matos, A. M., Duarte, T., Figueiras, H., & Sousa-Coutinho, J. (2013). Mixture design of self-compacting glass mortar. *Cement and Concrete Composites*, *43*, 1–11.

Okamura, H., & Ouchi, M. (2003). Self-compacting concrete. *Journal of Advanced Concrete Technology*, *1*(1), 5–15.

Okamura, H., & Ozawa, K. (1995). Mix design of self-compacting concrete. *Concrete Library of JSCE*, *24*(25), 107–120.

Okamura, & Ozawa. (1996). Self-compacting high-performance concrete. *Structural Engineering International*, *6*(4), 269–270.

Okamura, H., Ozawa, K., & Ouchi, M. (2000). Self-Compacting Concrete. *Structural Concrete*, *1*(1), 5–15.

Okrajnov-Bajić, R., & Vasović, D. (2009). Self-compacting concrete and its application in contemporary architectural practice. *Spatium International Review*, (20), 28–34.

Paul, S., & Dutta, A. (2013). Translucent concrete. *International Journal of Scientific and Research Publications*, *3*(10).

Penacho, P., De Brito, J., & Rosário, M. (2014). Physico-mechanical and performance characterization of mortars incorporating fine glass waste aggregate. *Cement and Concrete Composites*, *50*, 47–59.

Philips Lighting Academy. (2008). *Basics of light and lighting*. *Koninklijke Philips Electronics N.V.* Amsterdam, Netherlands.

Phillips. (2015). *The LED lighting revolution - Stimulating socio-economic progress in the 21st century*. *Koninklijke Philips N.V.* Amsterdam, Netherlands.

Rahma, A., El Naber, N., & Issa Ismail, S. (2017). Effect of glass powder on the compression strength and the workability of concrete. *Cogent Engineering*, *4*(1), 1–12.

Rajabipour, F., Maraghechi, H., & Fischer, G. (2010). Investigating the alkali-silica reaction of recycled glass aggregates in concrete materials. *Journal of Materials in Civil Engineering*, *22*(12), 1201–1208.

Rizwan, S. A., & Bier, T. A. (2012). Blends of limestone powder and fly-ash enhance the response of self-compacting mortars. *Construction and Building Materials*, *27*(1), 398–403.

Saccani, A., & Bignozzi, M. C. (2010). ASR expansion behavior of recycled glass fine aggregates in concrete. *Cement and Concrete Research*, *40*(4), 531–536.

Salih, S. A., Joni, H. H., & Mohamed, S. A. (2014a). Effect of Plastic Optical Fiber on some properties of translucent concrete. *Eng. & Tech. Journal*, *32*(12).

Salih, S. A., Joni, H. H., & Mohamed, S. A. (2014b). Effect of Plastic Optical Fibers on properties of translucent concrete boards. In *Proceedings of The First International Conference on Engineering Sciences' Applications, ICESA*.

Sedran, T., & De Larrard, F. (1999). First International RILEM Symposium on Self-Compacting Concrete. In *First International RILEM Symposium on Self-Compacting Concrete, Stockholm, Sweden* (pp. 321–332). RILEM Publications SARL.

Sharifi, Y., Afshoon, I., Firoozjaei, Z., & Momeni, A. (2016). Utilization of waste glass micro-particles in producing self-consolidating concrete mixtures. *International Journal of Concrete Structures and Materials*, *10*(3), 337–353.

Sharifi, Y., Afshoon, I., & Firoozjaie, Z. (2015). Fresh properties of self-compacting concrete containing ground waste glass microparticles as cementing material. *Journal of Advanced Concrete Technology*, *13*(2), 50–66.

Sharifi, Y., Houshiar, M., & Aghebati, B. (2013). Recycled glass replacement as fine aggregate in self-compacting concrete. *Frontiers of Structural and Civil Engineering*, *7*(4), 419–428.

Siad, H., Lachemi, M., Sahmaran, M., Mesbah, H. A., Hossain, K. M. A., & Ozsunar, A. (2017). Potential for using recycled glass sand in engineered cementitious composites. *Magazine of Concrete Research*, *69*(17), 1–14.

Sikora, P., Horszczaruk, E., Skoczylas, K., & Rucinska, T. (2017). Thermal properties of cement mortars containing waste glass aggregate and nano silica. *Procedia Engineering*, *196*, 159–166.

Tan, K. H., & Du, H. (2013). Use of waste glass as sand in mortar: Part I - Fresh, mechanical and durability properties. *Cement and Concrete Composites*, *35*(1), 109–117.

Thorat, P. V., Warulkar, S., & Thombre, P. A. (2014). Plastic optical fiber. *International Journal of Engineering Research and Reviews*, *2*(4), 95–105.

Tironi, A., Scian, A. N., & Irassar, E. F. (2017). Blended cement with limestone filler and kaolinitic calcined clay: Filler and pozzolanic effects. *Journal of Materials in Civil Engineering*, *29*(9), 1–8.

Tiwari, A., & Saharan, P. (2016). Study of behaviour of translucent concrete using rice husk and steel fiber. *SSRG International Journal of Civil Engineering (SSRG-IJCE)*, *3*(7), 130–135.

Topçu, İ. B., & Canbaz, M. (2004). Properties of concrete containing waste glass. *Cement and Concrete Research*, *34*(2), 267–274.

Topçu, İ. B., & Uyğunolu, T. (2010). Influence of mineral additive type on slump-flow and yield stress of self-consolidating mortar. *Scientific Research and Essays*, *5*(12), 1492–1500.

Tutikian, B., & Marquetto, L. (2015). Development of translucent blocks for use in civil construction. *Arquiteturarevista*, *11*(1), 46–54.

Utsi, S. (2008). *Performance-based concrete mix-design: Aggregate and micro mortar optimization applied on self-compacting concrete containing fly ash*. The Luleå University of Technology, Ph.D. Thesis.

Walraven, J. (2003). Structural aspects of self-compacting concrete. In *Proceedings third international symposium Self-compacting concrete, 17-20 August* (pp. 15–22). Reykjavik, Iceland: RILEM Publications SARL.

Wright, J. R., Cartwright, C., Fura, D., & Rajabipour, F. (2014). Fresh and hardened properties of concrete incorporating recycled glass as 100% sand replacement. *Journal of Materials in Civil Engineering*, *26*(10), 1–11.

Yuksel, C., Ahari, R. S., Ahari, B. A., & Ramyar, K. (2013). Evaluation of three test methods for determining the alkali-silica reactivity of glass aggregate. *Cement and Concrete Composites*, *38*, 57–64.

Zhou, Z., Ou, G., Hang, Y., Chen, G., & Ou, J. (2009). Research and development of plastic optical fiber-based smart transparent concrete. *Proc. of SPIE*, *7293*, 1–6.

APPENDICES

Appendix 1: SCM mix design

SCM Laboratory Observation Sheet©2017												
SCM Mix Design												
S/M	**Mortar Volume (m^3)**		**V_W/V_P**	**Paste Volume (m^3)**		**Weight (kg/m^3)**				**W/P**	**W/C**	**S/C**
	Sand Volume **(V_S)**	Paste Volume **(V_{Paste})**		Powder Volume **(V_C)**	Water Volume **(V_W)**	Cement **(W_C)**	Water **(W_W)**	Sand **(W_S)**	Limestone Powder **(W_{LP})**			
50%	0.5	0.5	0.80	0.278	0.222	700.00	222.22	1185.00	155.56	0.26	0.32	1.69
			0.82	0.275	0.225	692.31	225.27		153.85	0.27	0.32	1.71
			0.84	0.272	0.228	684.78	228.26		152.17	0.27	0.33	1.73
			0.86	0.269	0.231	677.42	231.18		150.54	0.28	0.34	1.75
			0.88	0.266	0.234	670.21	234.04		148.94	0.29	0.35	1.77
50%	0.50	0.50	0.90	0.263	0.237	663.16	236.84	1185.00	147.37	0.29	0.36	1.79
			0.94	0.258	0.242	649.48	242.27		144.33	0.30	0.37	1.82
			0.96	0.255	0.245	642.86	244.90		142.86	0.31	0.38	1.84
			0.98	0.253	0.247	636.36	247.47		141.41	0.32	0.39	1.86
			1.00	0.250	0.250	630.00	250.00		140.00	0.32	0.40	1.88
50%	0.50	0.50	**1.02**	**0.248**	**0.252**	**623.76**	**252.48**	1185.00	**138.61**	**0.33**	**0.40**	**1.90**
			1.04	0.245	0.255	617.65	254.90		137.25	0.34	0.41	1.92
			1.06	0.243	0.257	611.65	257.28		135.92	0.34	0.42	1.94
			1.08	0.240	0.260	605.77	259.62		134.62	0.35	0.43	1.96
			1.10	0.238	0.262	600.00	261.90		133.33	0.36	0.44	1.98

Appendix 2: Relationship between slump flow and superplasticiser dosage of SCM mixes

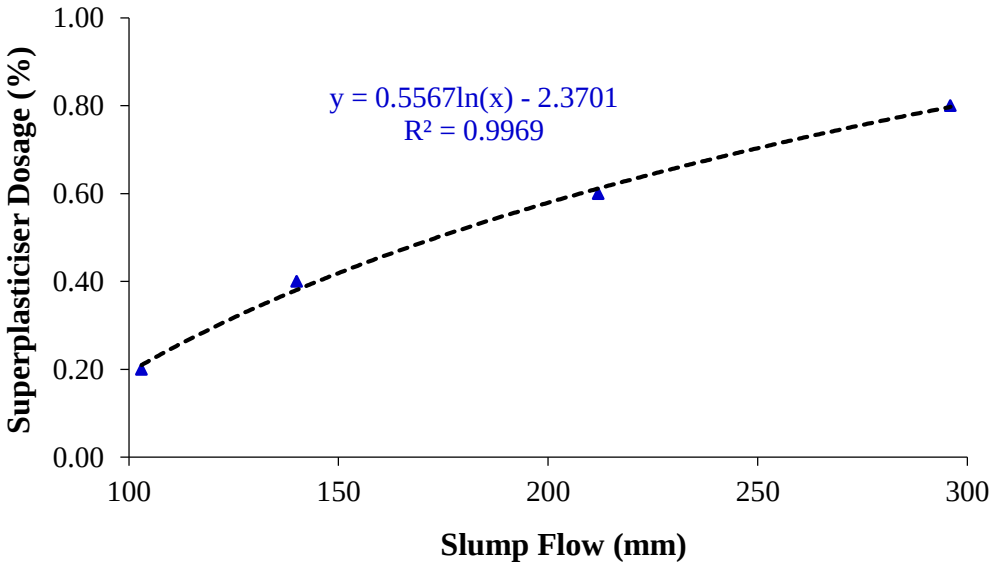

Appendix 3: Relationship between water to powder ratio (W/P) and the V-funnel flow time of SCM mixes

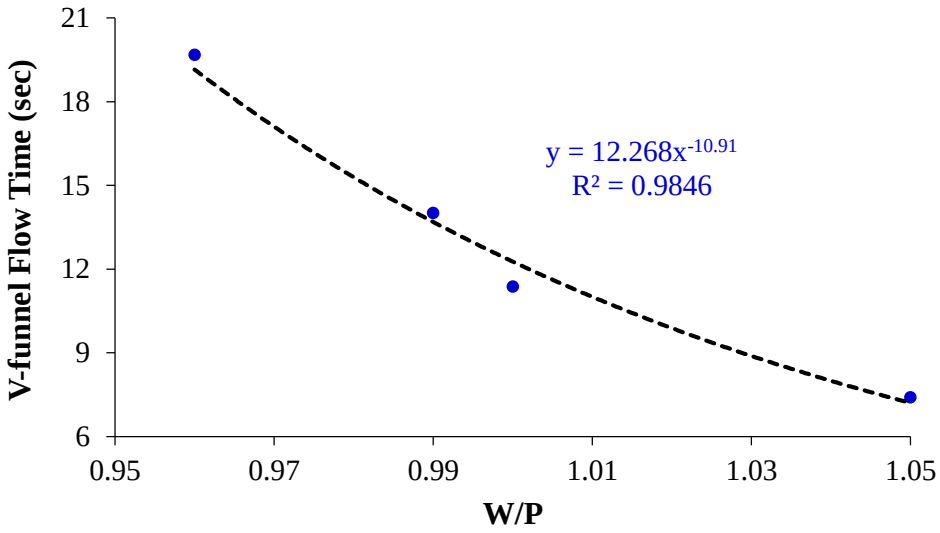

Appendix 4: Bulk density of SCM-RGA mixes

Bulk Density (kg/m^3), 50x50x50 mm^3					
Mix Designation	ID	Surface Dry Mass (g)	Net Volume (cm^3)	Bulk Density (kg/m^3)	Average Bulk Density (kg/m^3)
SCM-RGA0%	[1]	299.19	125.00	2393.52	2385.25
	[2]	300.71	125.00	2405.68	
	[3]	294.57	125.00	2356.56	
SCM-RGA10%	[1]	296.28	125.00	2370.24	2382.43
	[2]	298.84	125.00	2390.72	
	[3]	298.29	125.00	2386.32	
SCM-RGA20%	[1]	297.37	125.00	2378.96	2379.68
	[2]	296.29	125.00	2370.32	
	[3]	298.72	125.00	2389.76	
SCM-RGA30%	[1]	297.28	125.00	2378.24	2372.11
	[2]	295.33	125.00	2362.64	
	[3]	296.93	125.00	2375.44	
SCM-RGA40%	[1]	291.50	125.00	2332.00	2359.31
	[2]	297.76	125.00	2382.08	
	[3]	295.48	125.00	2363.84	
SCM-RGA50%	[1]	294.42	125.00	2355.36	2347.25
	[2]	292.08	125.00	2336.64	
	[3]	293.72	125.00	2349.76	

Appendix 5: Capillary water absorption (sorptivity) of SCM-RGA mixes

Average Water Adsorbed (g)								
Mix Designation	5 min	10 min	30 min	1 h	2 h	3 h	4 h	5 h
SCM-RGA0%	2.47	3.53	6.40	9.10	12.20	13.97	15.13	15.87
SCM-RGA10%	1.75	2.25	4.00	5.70	7.90	9.35	10.45	11.35
SCM-RGA20%	1.60	2.00	3.60	5.10	7.00	8.30	9.30	10.10
SCM-RGA30%	1.50	1.85	3.30	4.80	6.50	7.40	8.15	8.90
SCM-RGA40%	1.60	2.00	3.40	4.60	6.10	7.00	7.60	8.40
SCM-RGA50%	1.50	1.80	3.00	4.20	5.70	6.60	7.30	7.90
$\Delta W/(A*\rho)$, $[g/(cm^2*1g/cm^3)]$, (g/mm^2)								
Mix Designation	5 min	10 min	30 min	1 h	2 h	3 h	4 h	5 h
SCM-RGA0%	0.99	1.41	2.56	3.64	4.88	5.59	6.05	6.35
SCM-RGA10%	0.70	0.90	1.60	2.28	3.16	3.74	4.18	4.54
SCM-RGA20%	0.64	0.80	1.44	2.04	2.80	3.32	3.72	4.04
SCM-RGA30%	0.60	0.74	1.32	1.92	2.60	2.96	3.26	3.56
SCM-RGA40%	0.64	0.80	1.36	1.84	2.44	2.80	3.04	3.36
SCM-RGA50%	0.60	0.72	1.20	1.68	2.28	2.64	2.92	3.16

Appendix 6: Cumulative capillary surface water absorption of SCM-RGA mixes

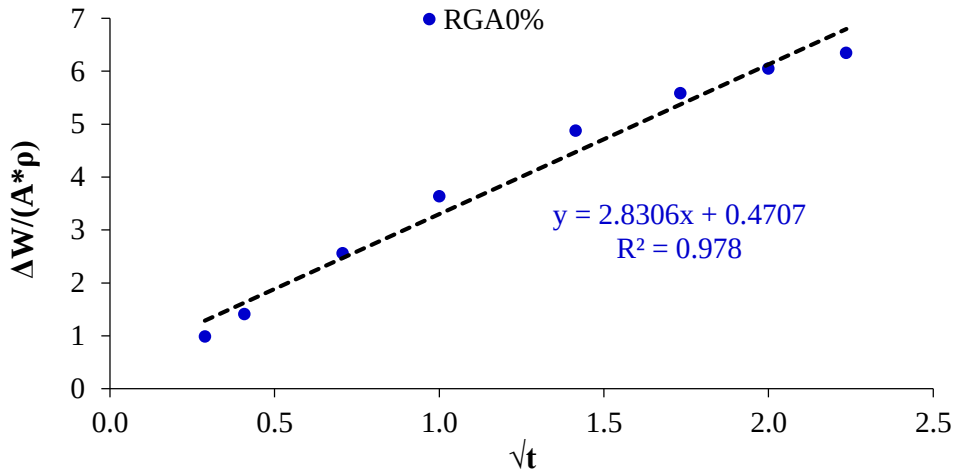

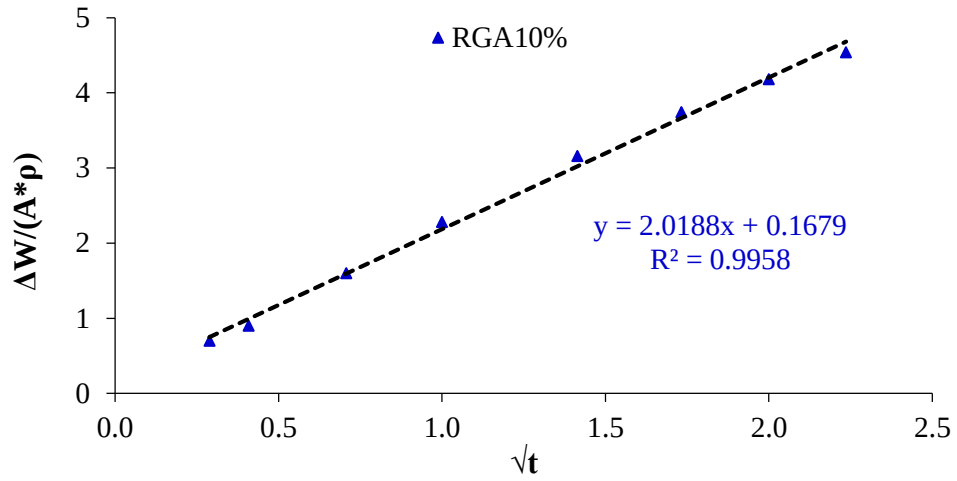

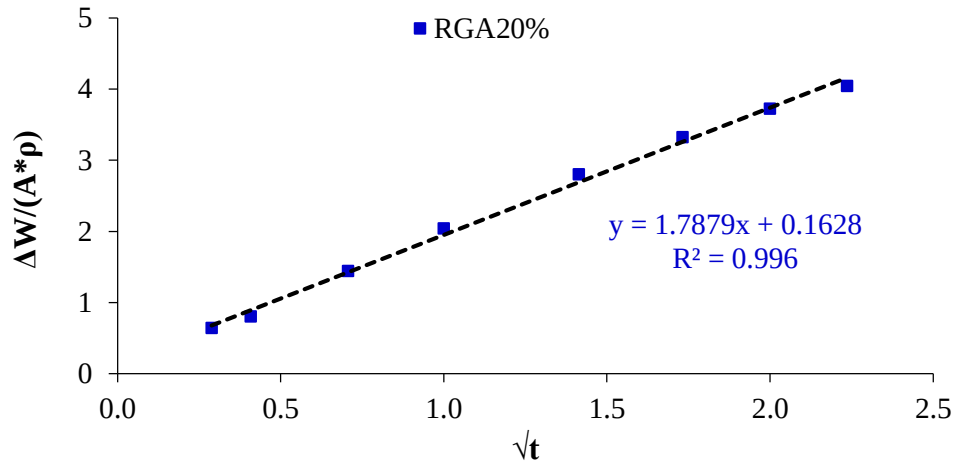

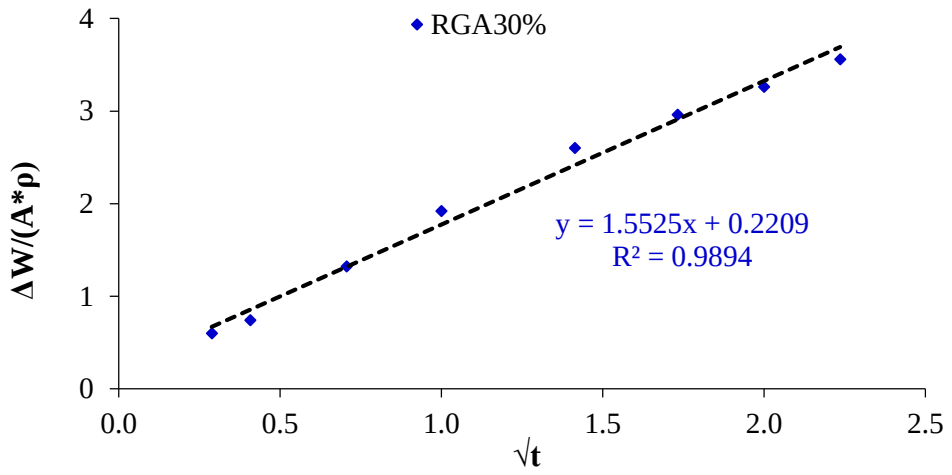
RGA30%
y = 1.5525x + 0.2209
R² = 0.9894
ΔW/(A*ρ)
√t
0
1
2
3
4
0.0
0.5
1.0
1.5
2.0
2.5

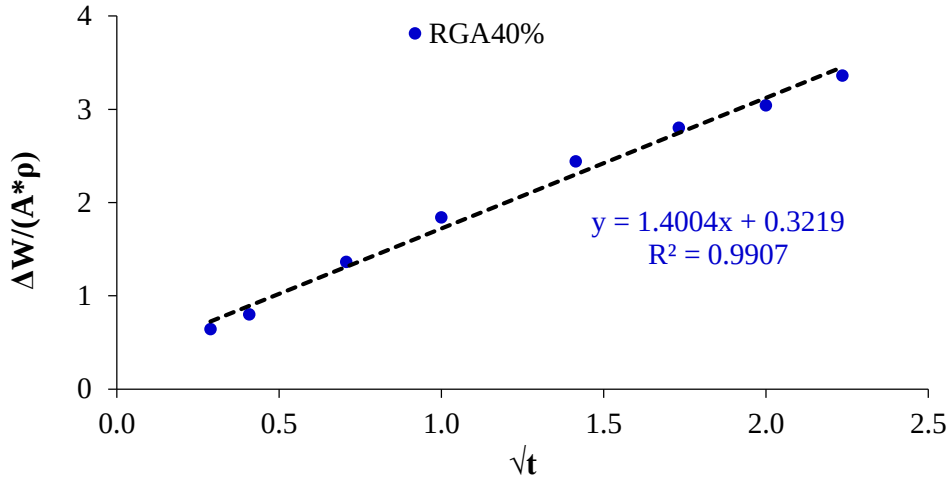
RGA40%
y = 1.4004x + 0.3219
R² = 0.9907
ΔW/(A*ρ)
√t
0
1
2
3
4
0.0
0.5
1.0
1.5
2.0
2.5

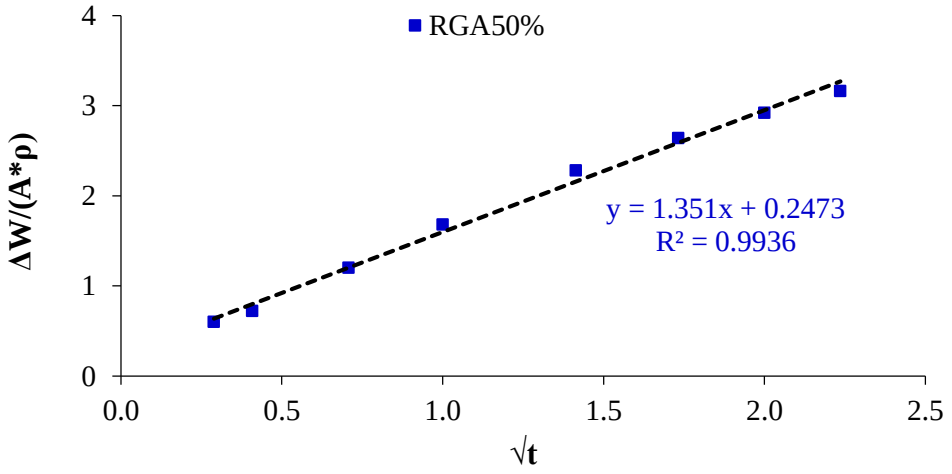
RGA50%
y = 1.351x + 0.2473
R² = 0.9936
ΔW/(A*ρ)
√t
0
1
2
3
4
0.0
0.5
1.0
1.5
2.0
2.5

Appendix 7: POF computation for translucent concrete specimens (Compressive strength test cubes [Ø2 mm POF])

Translucent Concrete Specimens for Compressive Strength Test (Ø2 mm POF)			
Description	2% V/V	4% V/V	6% V/V
Mould Dimension: *50x50x50 mm^3*			
Mould Volume (mm^3)	125,000	125,000	125,000
POF Volume Percentage (%)	2	4	6
POF Volume (mm^3)	2,500	5,000	7,500
POF Diameter (mm)	2	2	2
POF Area (mm^2)	3.14	3.14	3.14
POF Length (mm)	50	50	50
Total Number of POF (#)	16	32	48
Check POF Volume (mm^3)	2,500	5,000	7,500
Peripheral Mould Area (mm^2)	2,500	2,500	2,500
Peripheral POF Area (mm^2)	50	100	150
Number of POF in row (#)	4	6	7
Number of POF in column (#)	4	6	7
Check Total Number of POF (#)	16	32	48
POF Spacing in row (mm)	10	7.1	6.2
POF Spacing in column (mm)	10	7.1	6.2

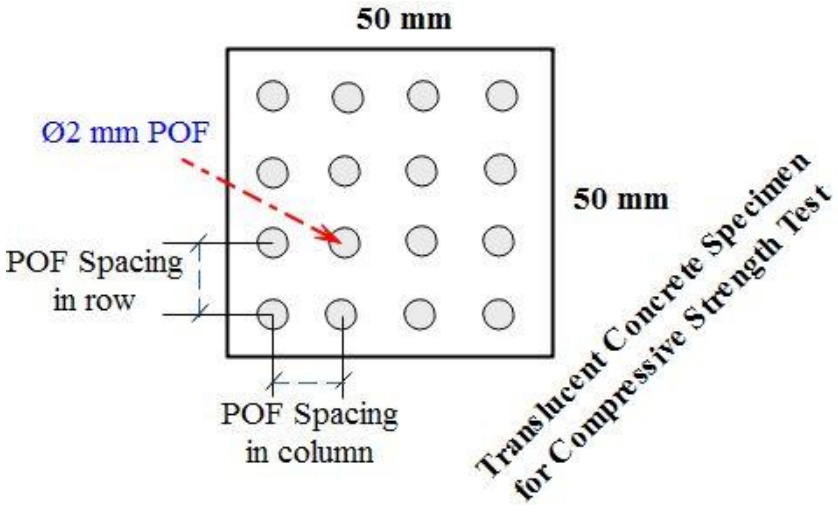

Appendix 8: POF computation for translucent concrete specimens (Compressive strength test cubes [Ø3 mm POF])

Translucent Concrete Specimens for Compressive Strength Test (Ø3 mm POF)			
Description	2% V/V	4% V/V	6% V/V
Mould Dimension: *50x50x50 mm^3*			
Mould Volume (mm^3)	125,000	125,000	125,000
POF Volume Percentage (%)	2	4	6
POF Volume (mm^3)	2,500	5,000	7,500
POF Diameter (mm)	3	3	3
POF Area (mm^2)	7.07	7.07	7.07
POF Length (mm)	50	50	50
Total Number of POF (#)	7	14	21
Check POF Volume (mm^3)	2,500	5,000	7,500
Peripheral Mould Area (mm^2)	2,500	2,500	2,500
Peripheral POF Area (mm^2)	50	100	150
Number of POF in row (#)	3	4	5
Number of POF in column (#)	3	4	5
Check Total Number of POF (#)	7	16	32
POF Spacing in row (mm)	12.5	10	8.3
POF Spacing in column (mm)	12.5	710	8.3

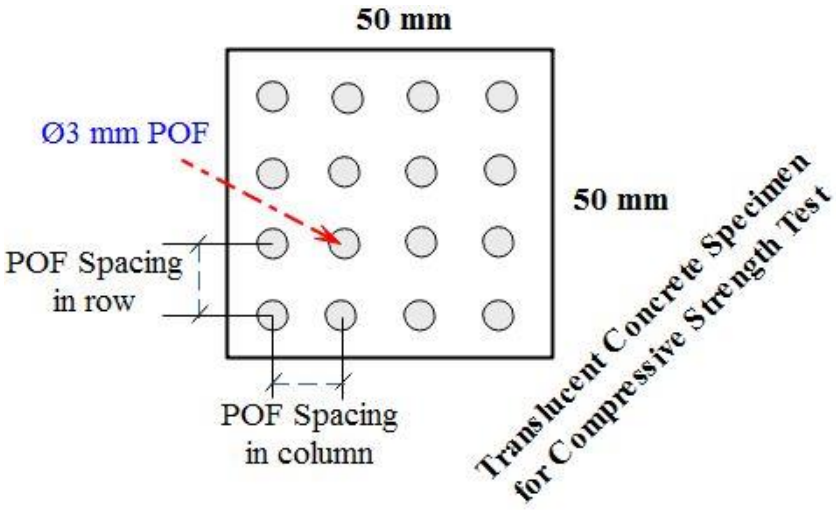

Appendix 9: POF computation for translucent concrete specimens (Flexural strength test cubes [Ø2 mm POF])

Translucent Concrete Specimens for Flexural Strength Test (Ø2 mm POF)			
Description	2% V/V	4% V/V	6% V/V
Mould Dimension: *40x40x160 mm^3*			
Mould Volume (mm^3)	256,000	256,000	256,000
POF Volume Percentage (%)	2	4	6
POF Volume (mm^3)	5,120	10,240	15,360
POF Diameter (mm)	2	2	2
POF Area (mm^2)	3.14	3.14	3.14
POF Length (mm)	40	40	40
Total Number of POF (#)	41	82	122
Check POF Volume (mm^3)	5,120	10,240	15,360
Peripheral Mould Area (mm^2)	6,400	6,400	6,400
Peripheral POF Area (mm^2)	128	256	348
Number of POF in row (#)	3	5	6
Number of POF in column (#)	14	16	20
Check Total Number of POF (#)	41	82	122
POF Spacing in row (mm)	10	6.7	5.7
POF Spacing in column (mm)	11	9.2	7.5

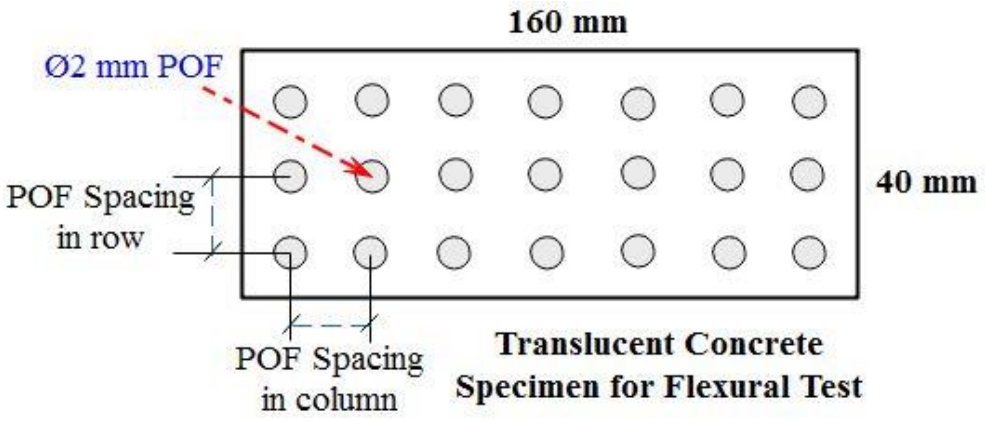

Appendix 10: POF computation for translucent concrete specimens (Flexural strength test cubes [Ø3 mm POF])

Translucent Concrete Specimens for Flexural Strength Test (Ø3 mm POF)			
Description	2% V/V	4% V/V	6% V/V
Mould Dimension: *40x40x160 mm^3*			
Mould Volume (mm^3)	256,000	256,000	256,000
POF Volume Percentage (%)	2	4	6
POF Volume (mm^3)	5,120	10,240	15,360
POF Diameter (mm)	3	3	3
POF Area (mm^2)	7.07	7.07	7.07
POF Length (mm)	40	40	40
Total Number of POF (#)	18	36	54
Check POF Volume (mm^3)	5,120	10,240	15,360
Peripheral Mould Area (mm^2)	6,400	6,400	6,400
Peripheral POF Area (mm^2)	128	256	348
Number of POF in row (#)	2	3	4
Number of POF in column (#)	9	12	14
Check Total Number of POF (#)	18	36	54
POF Spacing in row (mm)	13.3	10	8
POF Spacing in column (mm)	15.9	12.2	11

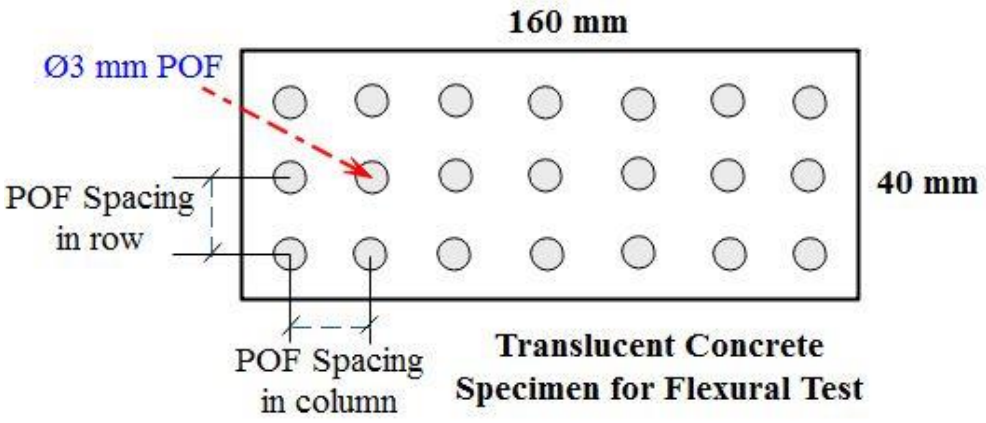

Appendix 11: POF computation for translucent concrete panel (6%v/v)

Translucent Concrete Panel (6%V/V)		
Description	Ø2 mm POF	Ø3 mm POF
Mould Dimension: *300x150x100 mm*^{3}		
Mould Volume (mm^3)	4,500,000	4,500,000
POF Volume Percentage (%)	6	6
POF Volume (mm^3)	270,000	270,000
POF Diameter (mm)	2	3
POF Area (mm^2)	3.14	7.07
POF Length (mm)	100	100
Total Number of POF (#)	860	382
Check POF Volume (mm^3)	270,000	270,000
Peripheral Mould Area (mm^2)	45,000	45,000
Peripheral POF Area (mm^2)	2,700	2,700
Number of POF in row (#)	39	28
Number of POF in column (#)	22	14
Check Total Number of POF (#)	860	382
POF Spacing in row (mm)	7.5	10.3
POF Spacing in column (mm)	6.5	10.2

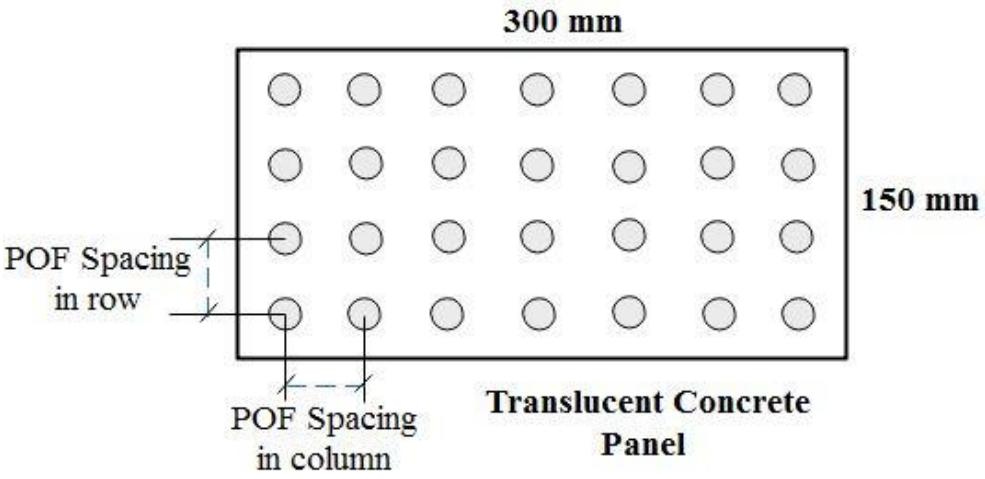

Appendix 12: Light transmittance of translucent concrete (At 300 mm distance of light source and 100 mm distance of LDR)

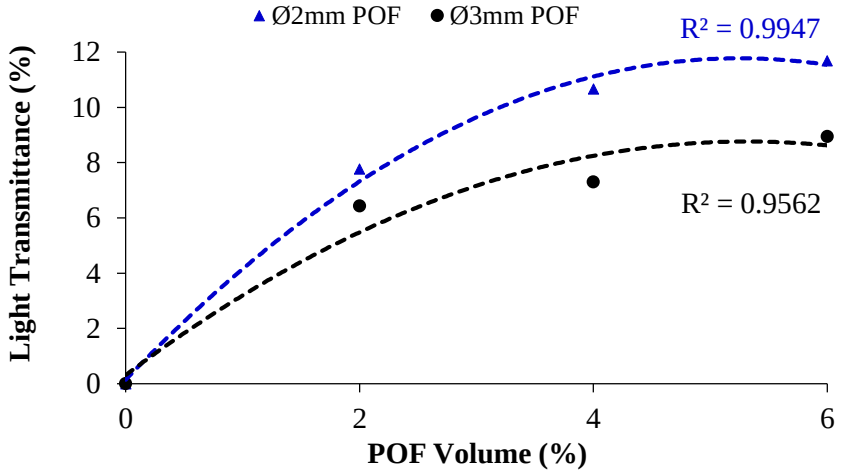

Appendix 13: Light transmittance of translucent concrete (At 300 mm distance of light source and 200 mm distance of LDR)

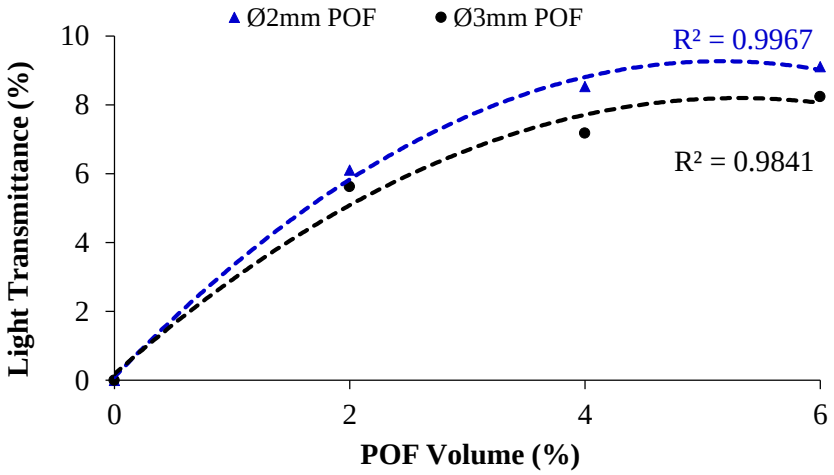

Appendix 14: Light transmittance of translucent concrete (At 300 mm distance of light source and 300 mm distance of LDR)

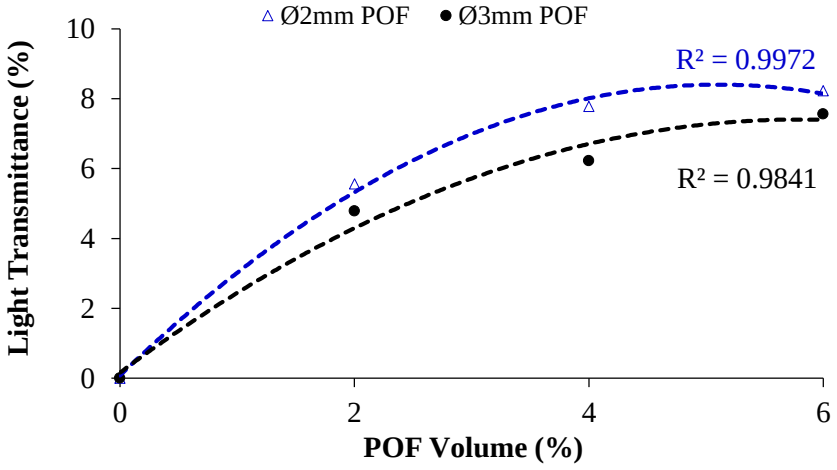

Appendix 15: Light transmittance of translucent concrete (At 300 mm distance of light source and 400 mm distance of LDR)

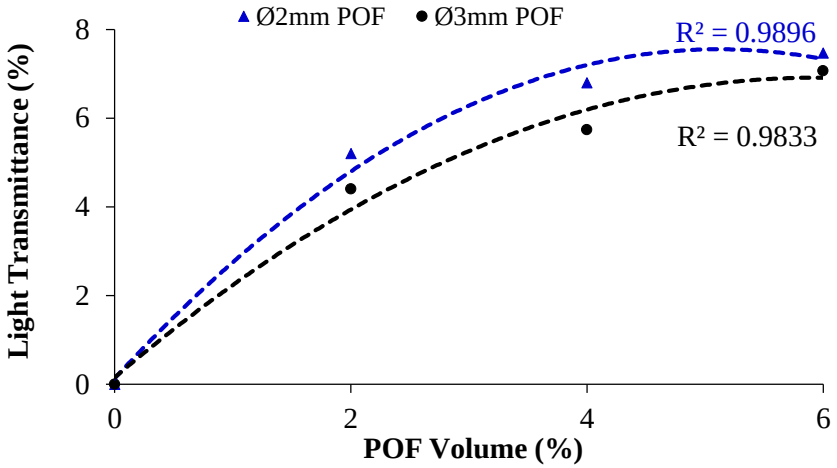

Appendix 16: Light transmittance of translucent concrete (At 300 mm distance of light source and 500 mm distance of LDR)

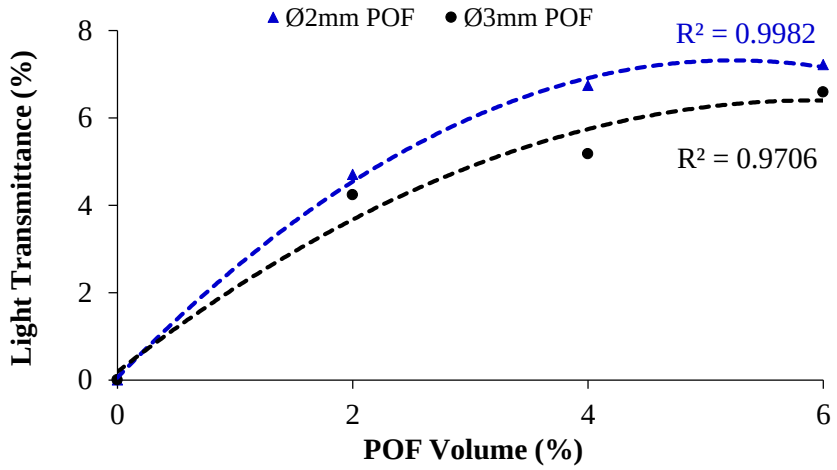

Appendix 17: Light transmittance of translucent concrete (At 400 mm distance of light source and 100 mm distance of LDR)

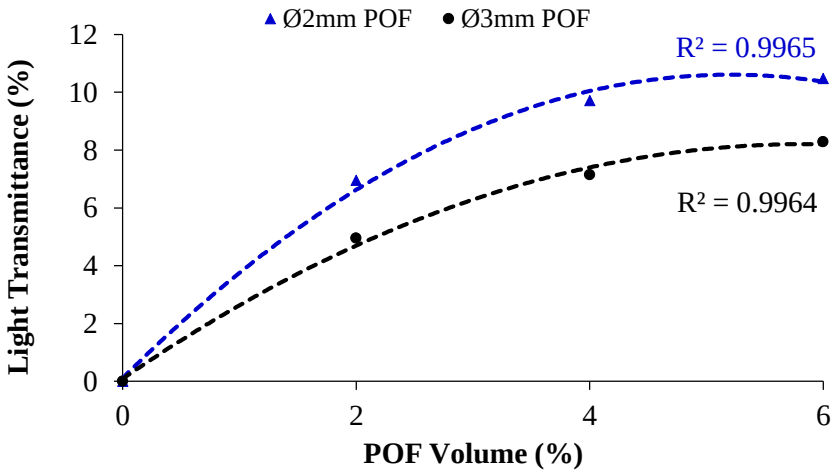

Appendix 18: Light transmittance of translucent concrete (At 400 mm distance of light source and 200 mm distance of LDR)

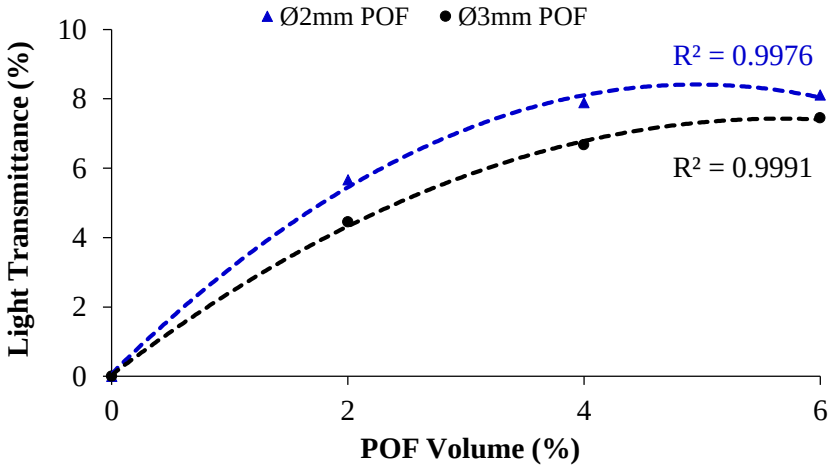

Appendix 19: Light transmittance of translucent concrete (At 400 mm distance of light source and 300 mm distance of LDR)

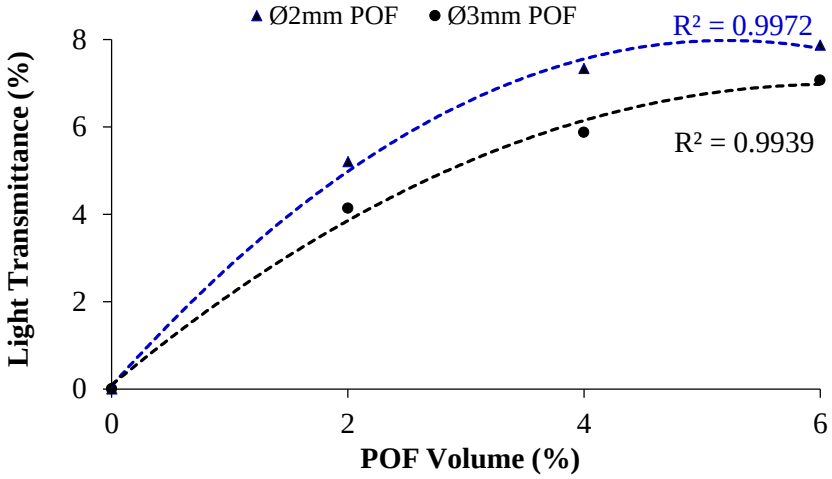

Appendix 20: Light transmittance of translucent concrete (At 400 mm distance of light source and 400 mm distance of LDR)

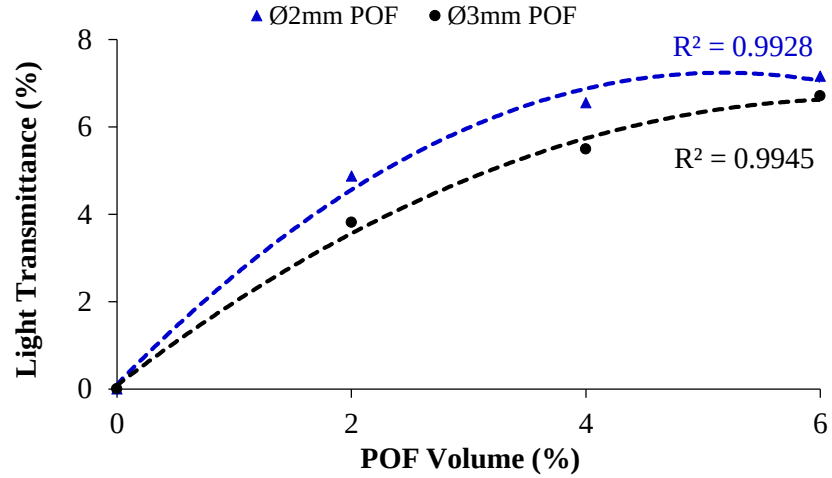

Appendix 21: Light transmittance of translucent concrete (At 400 mm distance of light source and 500 mm distance of LDR)

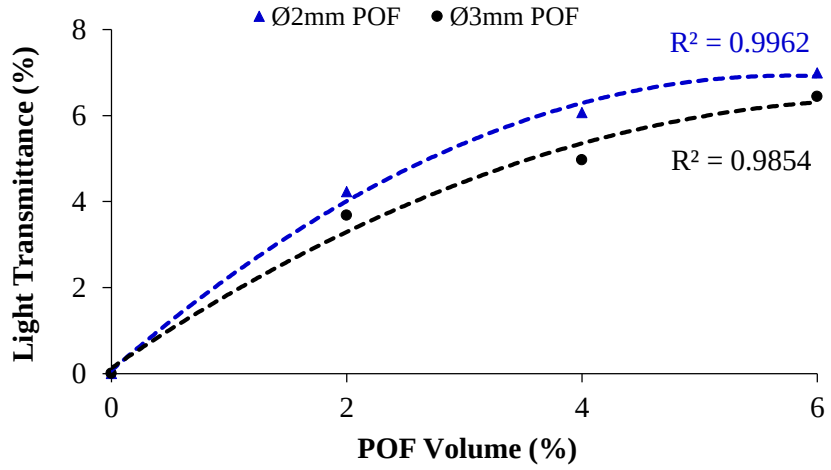

Appendix 22: Light transmittance of translucent concrete (At 100 mm distance of light source and 500 mm distance of LDR)

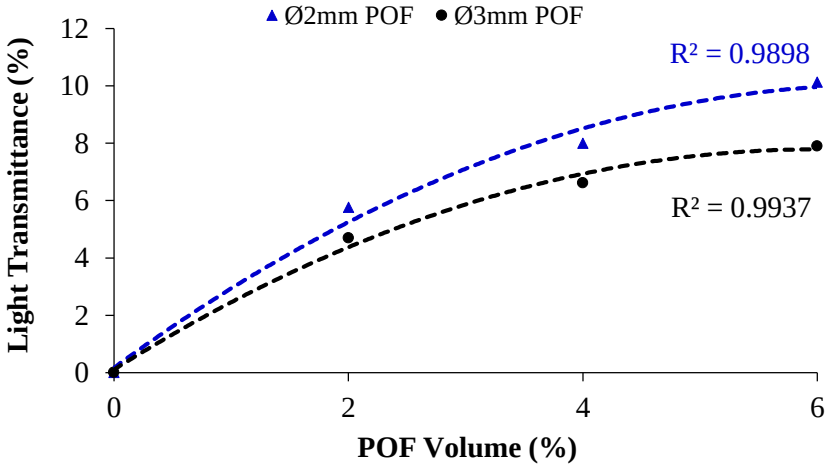

Appendix 23: Light transmittance of translucent concrete (At 200 mm distance of light source and 500 mm distance of LDR)

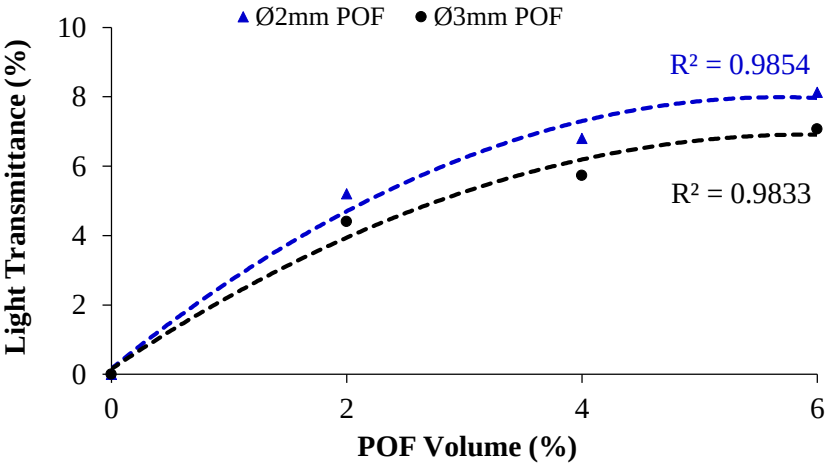

Appendix 24: Relationship between light transmittance of translucent concrete and light source distance (At 300 mm distance of LDR, Ø2 mm POF)

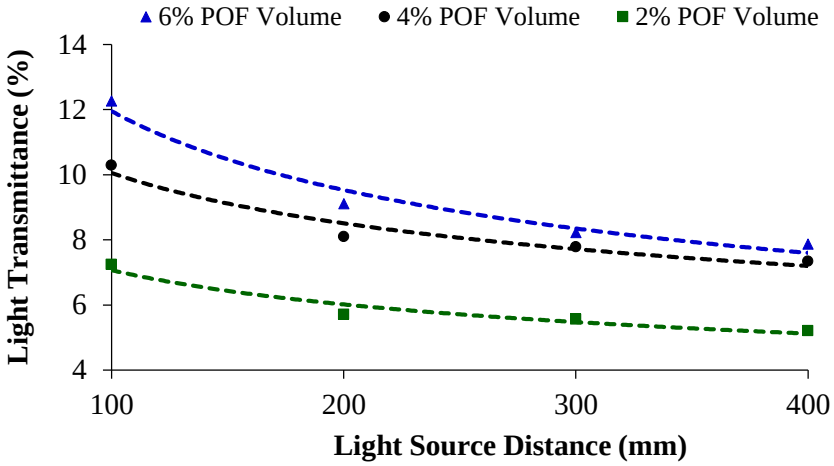

Appendix 25: Relationship between light transmittance of translucent concrete and light source distance (At 300 mm distance of LDR, Ø3 mm POF)

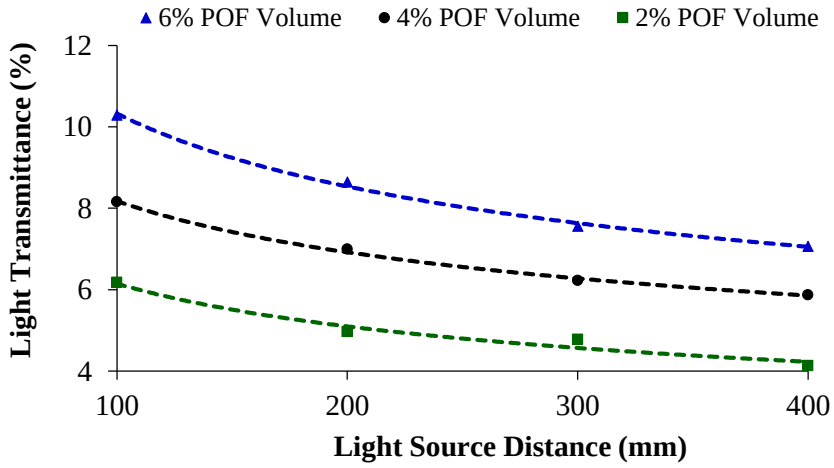

Appendix 26: Relationship between light transmittance of translucent concrete and light source distance (At 400 mm distance of LDR, Ø2 mm POF)

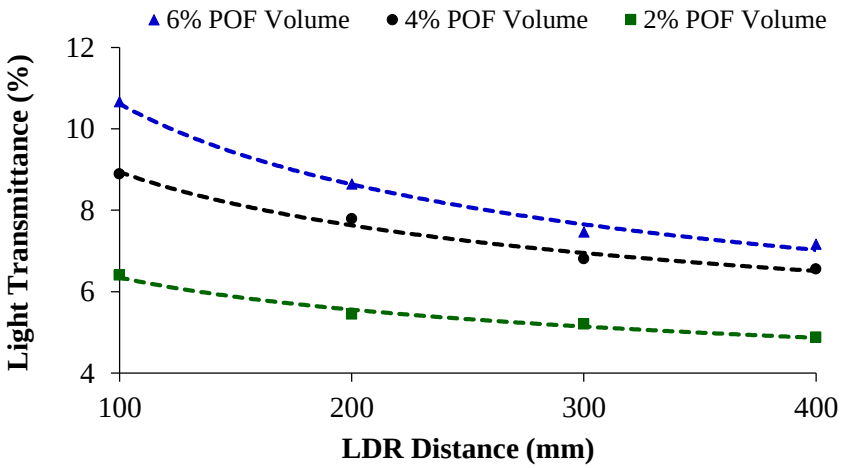

Appendix 27: Relationship between light transmittance of translucent concrete and light source distance (At 400 mm distance of LDR, Ø3 mm POF)

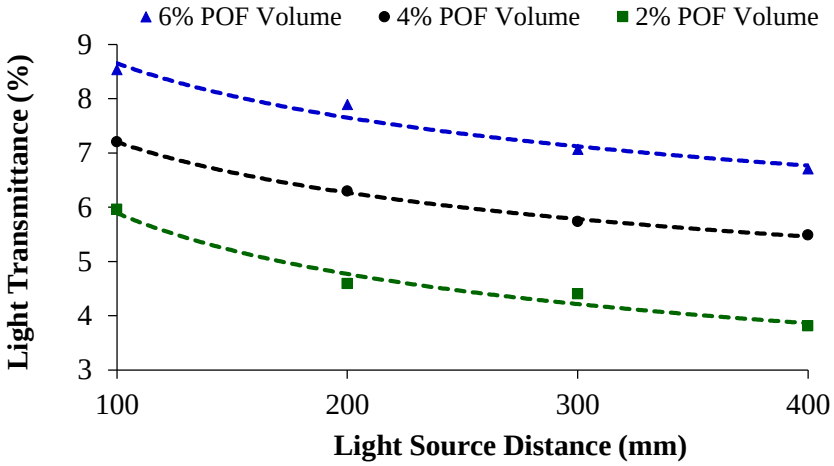

Appendix 28: Relationship between light transmittance of translucent concrete and light source distance (At 500 mm distance of LDR, Ø2 mm POF)

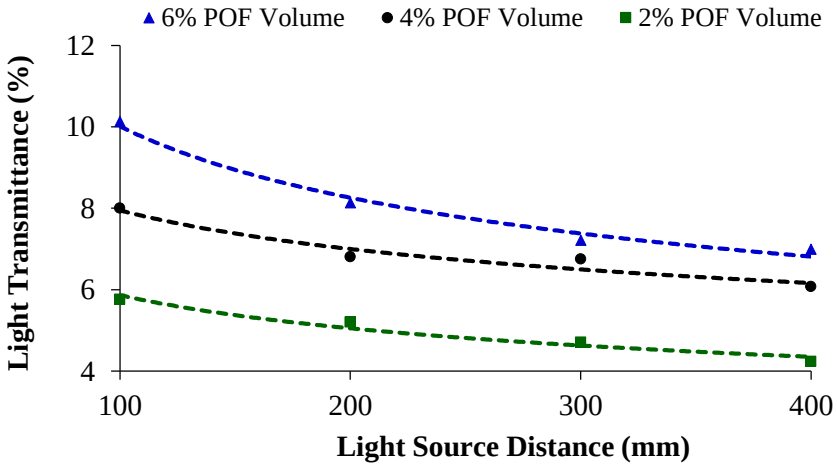

Appendix 29: Relationship between light transmittance of translucent concrete and light source distance (At 500 mm distance of LDR, Ø3 mm POF)

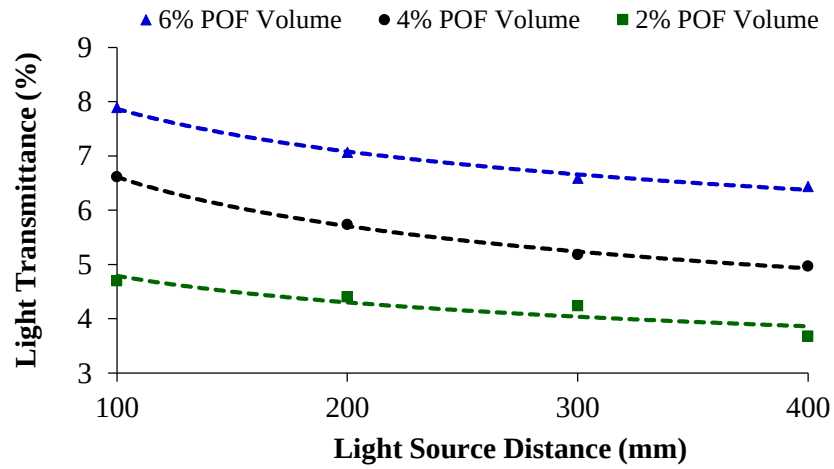

Appendix 30: Relationship between light transmittance of translucent concrete and LDR distance (At 300 mm distance of light source, Ø2 mm POF)

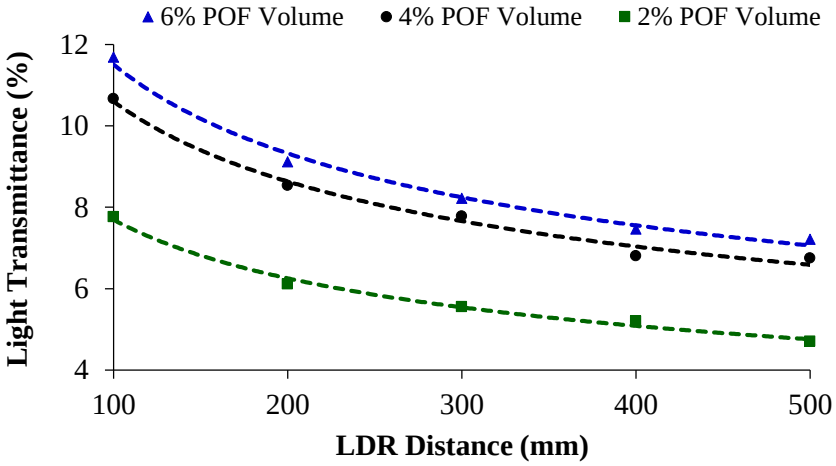

Appendix 31: Relationship between light transmittance of translucent concrete and LDR distance (At 300 mm distance of light source, Ø3 mm POF)

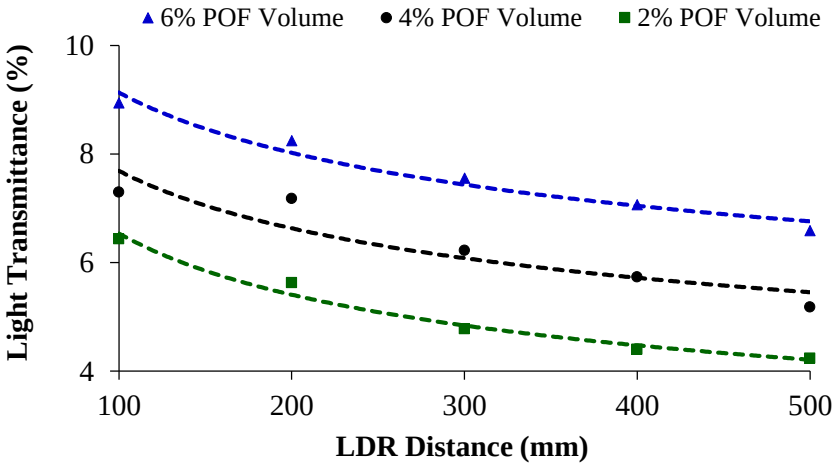

Appendix 32: Relationship between light transmittance of translucent concrete and LDR distance (At 400 mm distance of light source, Ø2 mm POF)

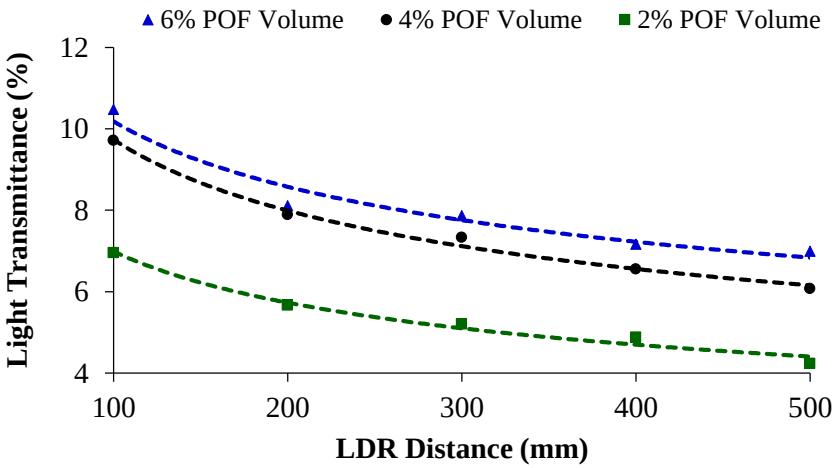

Appendix 33: Relationship between light transmittance of translucent concrete and LDR distance (At 400 mm distance of light source, Ø3 mm POF)

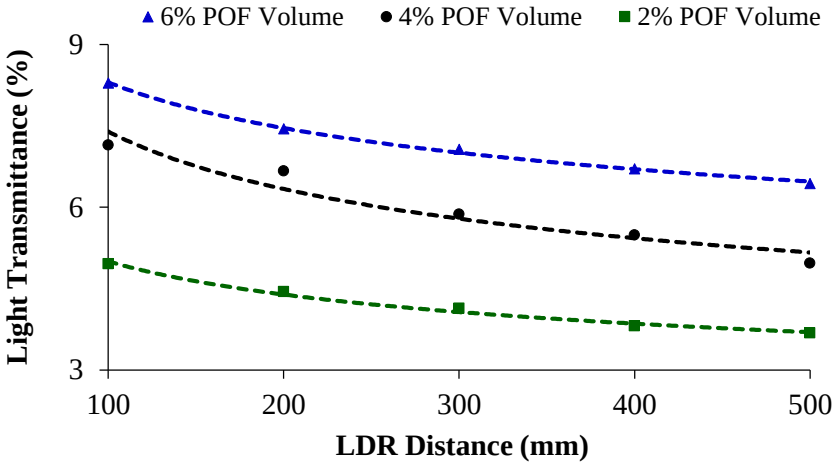

Appendix 34: Experimental load analysis of the reference concrete panel

Load (kN)	*Deflection (mm)*	*Strain (10^{-2}) mm/mm*	*Moment (kN.mm)*	*Reaction (kN)*	*Bending Stress (N/mm^2)*	*Normal Stress (N/mm^2)*	**Shear Stress (N/mm^2)**
0.00	0.00	0.00E+00	0.00	0.00	0.00	0.00	0.00
0.16	0.10	4.69E-05	11.85	0.08	0.03	0.01	0.02
1.26	0.37	1.41E-04	94.80	0.63	0.25	0.08	0.13
2.21	0.51	1.88E-04	165.90	1.11	0.44	0.15	0.22
3.48	0.65	2.35E-04	260.70	1.74	0.70	0.23	0.35
5.37	0.88	3.29E-04	402.90	2.69	1.07	0.36	0.54
7.43	0.95	4.23E-04	556.95	3.71	1.49	0.50	0.74
7.90	1.02	4.69E-04	592.50	3.95	1.58	0.53	0.79
9.16	1.05	5.63E-04	687.30	4.58	1.83	0.61	0.92
11.06	1.09	6.57E-04	829.50	5.53	2.21	0.74	1.11
12.01	1.12	7.51E-04	900.60	6.00	2.40	0.80	1.20
14.54	1.16	9.39E-04	1090.20	7.27	2.91	0.97	1.45
16.91	1.19	1.03E-03	1267.95	8.45	3.38	1.13	1.69
20.70	1.22	1.41E-03	1552.35	10.35	4.14	1.38	2.07
23.23	1.26	2.16E-03	1741.95	11.61	4.65	1.55	2.32
0.79	1.43	3.00E-03	59.25	0.40	0.16	0.05	0.08

Appendix 35: Experimental load analysis of the translucent concrete panel (Ø2 mm, 6% POF)

Load (kN)	*Deflection (mm)*	*Strain (10^{-2}) mm/mm*	*Moment (kN.mm)*	*Reaction (kN)*	*Bending Stress (N/mm^2)*	*Normal Stress (N/mm^2)*	Shear Stress (N/mm^2)
0.00	0.00	0.00E+00	0.00	0.00	0.00	0.00	0.00
0.95	0.14	4.69E-05	71.10	0.47	0.19	0.06	0.09
2.21	0.37	1.41E-04	165.90	1.11	0.44	0.15	0.22
2.37	0.41	1.88E-04	177.75	1.19	0.47	0.16	0.24
3.63	0.58	3.76E-04	272.55	1.82	0.73	0.24	0.36
4.27	0.65	3.99E-04	319.95	2.13	0.85	0.28	0.43
5.85	0.82	5.63E-04	438.45	2.92	1.17	0.39	0.58
6.95	0.92	5.87E-04	521.40	3.48	1.39	0.46	0.70
7.74	0.99	6.57E-04	580.65	3.87	1.55	0.52	0.77
8.69	1.02	7.98E-04	651.75	4.35	1.74	0.58	0.87
9.48	1.29	1.17E-03	711.00	4.74	1.90	0.63	0.95
10.27	1.39	1.27E-03	770.25	5.14	2.05	0.68	1.03
10.59	1.46	1.31E-03	793.95	5.29	2.12	0.71	1.06
11.22	1.53	1.74E-03	841.35	5.61	2.24	0.75	1.12
11.38	1.56	1.92E-03	853.20	5.69	2.28	0.76	1.14
10.59	1.60	3.62E-03	793.95	5.29	2.12	0.71	1.06

Appendix 36: Experimental load analysis of the translucent concrete panel (Ø3 mm, 6% POF)

Load (kN)	Deflection (mm)	Strain (10^{-2}) mm/mm	Moment (kN.mm)	Reaction (kN)	Bending Stress (N/mm^2)	Normal Stress (N/mm^2)	Shear Stress (N/mm^2)
0.00	0.00	0.00E+00	0.00	0.00	0.00	0.00	0.00
0.32	0.10	4.69E-05	23.70	0.16	0.06	0.02	0.03
2.69	0.65	1.41E-04	201.45	1.34	0.54	0.18	0.27
3.79	0.82	2.82E-04	284.40	1.90	0.76	0.25	0.38
4.90	0.92	3.76E-04	367.35	2.45	0.98	0.33	0.49
5.53	0.95	4.69E-04	414.75	2.77	1.11	0.37	0.55
6.79	0.99	6.57E-04	509.55	3.40	1.36	0.45	0.68
7.27	0.99	7.98E-04	545.10	3.63	1.45	0.48	0.73
7.90	1.02	1.03E-03	592.50	3.95	1.58	0.53	0.79
8.37	1.02	1.17E-03	628.05	4.19	1.67	0.56	0.84
9.32	1.26	1.55E-03	699.15	4.66	1.86	0.62	0.93
9.48	1.33	1.64E-03	711.00	4.74	1.90	0.63	0.95
9.64	1.46	1.83E-03	722.85	4.82	1.93	0.64	0.96
10.11	1.63	1.92E-03	758.40	5.06	2.02	0.67	1.01
10.74	1.67	2.21E-03	805.80	5.37	2.15	0.72	1.07
11.69	1.84	3.43E-03	876.90	5.85	2.34	0.78	1.17